Chem Soc Rev

Recent advances on functionalized micro and mesoporous carbon materials: synthesis and applications

Journal:	*Chemical Society Reviews*
Manuscript ID	CS-REV-11-2017-000787.R1
Article Type:	Review Article
Date Submitted by the Author:	09-Feb-2018
Complete List of Authors:	Benzigar, Mercy; a. Future Industries Institute, University of South Australia, Mawson Lakes 5095, Adelaide, South Australia, Australia, Engineering Talapaneni, Siddulu Naidu; The University of Newcastle, Global Innovative Center for Advanced Nanomaterials (GICAN), Faculty of Natural Built Environment and Engineering Joseph, Stalin ; a. Future Industries Institute, University of South Australia, Mawson Lakes 5095, Adelaide, South Australia, Australia, Engineering Ramadass, Kavitha; The University of Newcastle, Global Innovative Center for Advanced Nanomaterials (GICAN), Faculty of Natural Built Environment and Engineering Singh, Gurwinder; University of South Australia, Future Industries Institute Scaranato, Jey; Saudi Basic Industries Corp, SABIC Corporate Research and Development Center at KAUST Ravon, Ugo; Saudi Basic Industries Corporation Al-Bahily, Khalid; Saudi Basic Industries Corporation, SABIC Corporate Research and Development Center at KAUST Vinu, Ajayan; Global Innovative Center for Advanced Materials Faculty of Natural Built Environment and Engineering University of Newcastle

Journal Name

ARTICLE

Recent advances on functionalized micro and mesoporous carbon materials: synthesis and applications

figReceived 00th January 20xx,
Accepted 00th January 20xx

DOI: 10.1039/x0xx00000x

www.rsc.org/

Mercy R. Benzigar,[a†] Siddulu Naidu Talapaneni,[a,b†] Stalin Joseph,[a] Kavitha Ramadass,[a] Gurwinder Singh,[a] Jessica Scaranto,[c] Ugo Ravon,[c] Khalid Al-Bahily,[c] and Ajayan Vinu[a,b]*

Functionalized nanoporous carbon materials have attracted the colossal interest of materials science fraternity owing to their intriguing physical and chemical properties including well-ordered porous structure, exemplary high specific surface areas, electronic and ionic conductivities, excellent accessibility to active sites, and enhanced mass transport and diffusion. These properties make them a special and unique choice for various applications in divergent fields such as energy storage batteries, supercapacitors, energy conversion fuel cells, adsorption/separation of bulky molecules, heterogeneous catalysts, catalyst supports, photocatalysis, carbon capture, gas storage, biomolecule detection, vapour sensing and drug delivery. Because of the anisotropic and synergistic effects arising from the hetero atom doping at the nanoscale, these novel materials show high potential especially in the electrochemical applications such as batteries, supercapacitors and electrocatalysts for the fuel cell applications and water electrolysis. In order to gain the optimal benefit, it is necessary to implement the tailor made functionalities in the porous carbon surfaces as well as in the carbon skeleton through the comprehensive chemistries. These most appealing nanoporous carbon materials can be synthesized through the carbonization of high carbon containing molecular precursors by using soft or hard templating or non-templating pathways. This review encompasses the approaches and the wide range of methodologies that have been employed over the last five years on the preparation and functionalisation of the nanoporous carbon materials via incorporation of metals, non-metal heteroatoms, multiple heteroatoms, anchoring of various surface functional groups that mostly dictate their place in a wide range of practical applications.

1. Introduction

Design of carbon materials with ordered porous structure is one of the hot topics in the area of materials chemistry. The high specific surface area, large pore volume, well-ordered and controllable porous structure, unique morphologies of carbons and their excellent chemical, mechanical and thermal stabilities attract them for various applications including energy storage and conversion, catalysis and sensing.[1-4] Generally, carbon nanotubes, fullerenes and ordered nanoporous (micro and mesoporous) carbons have been widely applied for the energy and environmental applications including as adsorbents for the purification of water and capture of greenhouse gases.[5, 6] However, the complex synthesis methods required for the fabrication of carbon nanotubes or fullerenes put the hurdle in exploiting their full potential in various applications. On the other hand, the preparation of highly ordered nanoporous carbons is quite simple and the properties of these materials are much better than other porous carbon materials owing to their ordered porous structure. Most importantly, the well-ordered porous structures support the addition of new functionalities including organic or inorganic or biomaterials inside the porous channels or on the surface of the carbon walls, which significantly enhance their performances in various applications.

Highly ordered nanoporous carbon materials have been traditionally used for many years in large number of practical applications including catalysis, energy storage and conversion, adsorption and separation and biomedical engineering. The first report on the preparation of highly ordered mesoporous carbon (CMK-1) via nanocasting approach led to a new class of ordered mesoporous carbons (OMCs), with large specific surface areas and tunable pore diameters between 2 and 50 nm.[1, 7] This invention has led to the discovery of many useful porous materials including carbons, polymers, metal oxides, silicas and metals which are considered as potential game changers for various current technologies.[1, 7] The structure of these nanoporous materials can be controlled by varying the structure of the templates used for the synthesis. For example, several mesoporous silica materials with different structures

[a] Future Industries Institute, Division of Information Technology Energy and Environment, University of South Australia, Adelaide, SA 5095, Australia.
[b] Global Innovative Center for Advanced Nanomaterials (GICAN), Faculty of Engineering and Natural Built Environment, The University of Newcastle, Callaghan, NSW 2308, Australia.
E-mail: Ajayan.Vinu@newcastle.edu.au
[c] SABIC Corporate Research and Development Center at KAUST, Saudi Basic Industries Corporation, Thuwal 23955, Saudi Arabia.
[†] These authors contributed equally.

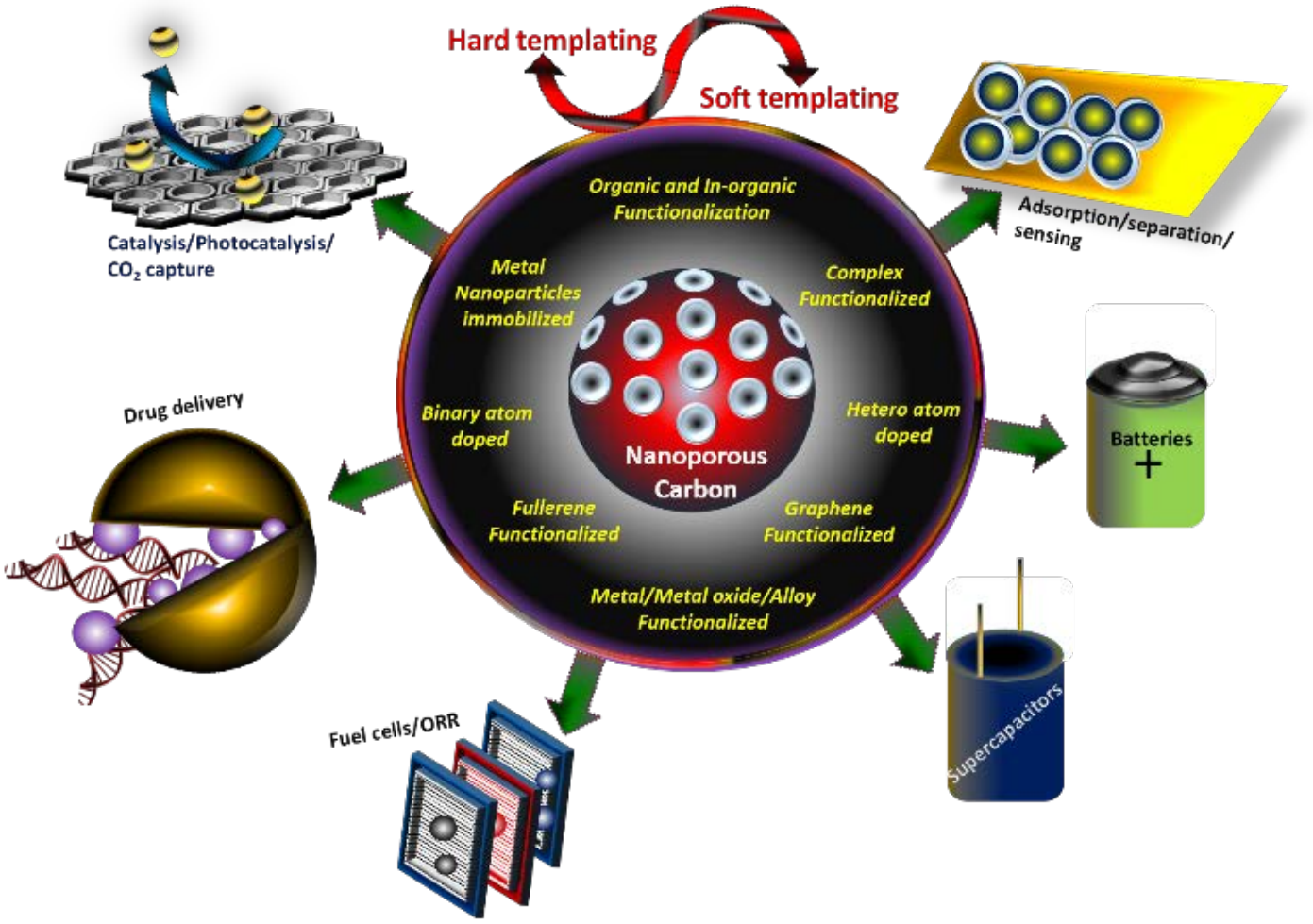

Figure 1 Schematic illustration for the synthesis, functionalisation and the applications of micro and mesoporous carbons.

including MCM-48, SBA-1, SBA-15, SBA-16, KIT-6 and KIT-5 have been used as templates for the fabrication of mesoporous carbon materials (CMK-x) with different mesoporous structures.[8-12] A similar nano-hard templating approach was also used by Hyeon *et al.* for the preparation of ordered porous carbon using phenolic resin as the source of carbon.[13, 14] OMCs having surface areas of more than 2000 $m^2 g^{-1}$, a higher pore volume of up to 3.0 $cm^3 g^{-1}$ and tuneable pore diameters along with high conductivities can be achieved through a nanohard templating approach using mesoporous silica hard-templates. Because of their excellent textural characteristics, physical properties and chemical stability, OMCs have been productively utilized in carbocatalysis, adsorption and separation of toxic molecules, gas storage, selective sensing, energy conversion fuel and solar cells, batteries, super(ultra)capacitors, and biomedical devices.[4, 15-17] The properties and the performance of these OMCs can be controlled with the modification of porous structure with organic or inorganic moieties. For example, the introduction of foreign atoms such as B, N, O, S and P in the carbon framework can tune not only the specific surface area and electronic properties of the materials but also their performance in catalysis or sensing. These factors are critical for various applications including semiconducting, field emission, optical, electronic devices and fuel cells. Therefore, the research on the development of ordered nanoporous carbons with different functional groups is being actively progressed for energy and electrocatalytic applications. Several review articles have been reported on the preparation of pure mesoporous carbons and their applications.[4, 18-21] However, the review papers on the recent development on the preparation, functionalization and applications of nanoporous carbon materials are quite limited.[21] For instance, much progress has been made recently on the conversion of metal organic frameworks (MOFs) in to highly dispersed metal/metal oxide functionalized nanoporous carbons without any external sacrificial templates for energy related applications.[21-23]

In this review, we give an overview on the latest advances in synthesis, structural characteristics, physicochemical properties and the prospects for application of pristine and functionalized OMCs (Table 1). Much emphasis will be given on the relatively new and exciting discoveries on the nanoporous materials with different organic or inorganic functional moieties such as B, N, O, S and P, amines, complexes and hybrid OMCs incorporated with metal nanoparticles, metal oxides, metal chalcogenides and graphene. We also address how these added functionalities may affect the final performance of the materials in various

applications including sensing, drug delivery, carbon capture, energy storage and conversion and adsorption and separation (Fig. 1). New developments on the ways to improve the properties and performance of varieties of functionalized nanoporous carbon reported during the last five years are also described in detail with the aim of demonstrating the uniqueness and the real academic and market potential of these materials. Finally, new directions and the development of these nanostructures and the extension of the application of these materials even in the wide range of applications are described in the conclusion and outlook.

2. Synthesis Methods

OMCs and hetero atom doped OMCs are generally prepared by using templating strategies. Two well-established templating techniques such as hard and soft templating methods are employed for the synthesis of OMCs and hetero atom doped OMCs. In the soft-templating method, the ordered mesoporous framework structure is achieved by the cooperative assembly of amphiphilic surfactant molecules and precursor moieties. In this case, mesoporosity is generated upon removing the surfactants through the calcination process at high temperatures. The nanocasting method is rather a conventional templating process, but the scale of production is in a nanoscale order. In the nano templating approach, highly ordered inorganic mesoporous solid materials are used to replicate their structure into nanoporous carbon materials with well-ordered mesoporosity. There are several review articles outlining the details of these synthetic processes including history, different synthetic strategies, and the formation mechanism for obtaining ordered nanoporous carbons.[2, 4, 7, 15] However, in the present review, we will discuss the recently reported synthesis methods and templating strategies applicable to OMCs from the last five years.

2.1 Hard templating method for OMCs

Hard templating approach is considered as one of the most straightforward ways for synthesizing OMCs.[7] Ordered

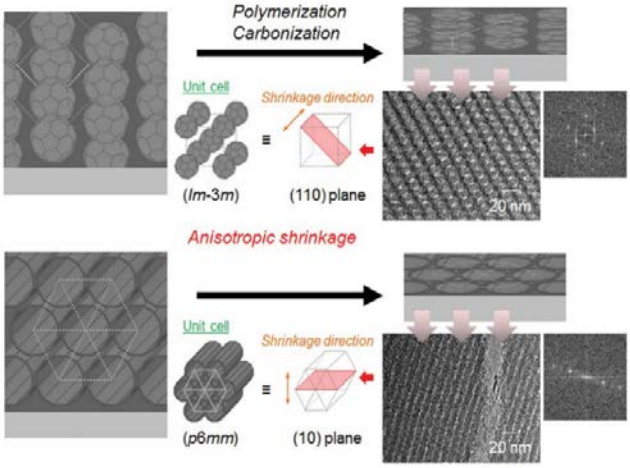

Figure 2 TEM and FFT images of phenol raisin films after carbonisation with their schematic illustration of variation in their mesostructure. Reproduced with permission from ref. 53. Copyright 2013, Royal Society of Chemistry.

mesoporosity in carbon materials can be easily introduced by nanocasting technique using mesoporous inorganic materials such as mesoporous silica and zeolites as hard templates. Various mesoporous carbons with different textural properties have been prepared by using different porous templates through this simple technique and the details of the materials and the structural parameters are given in Table 1. Although many materials have been prepared, the control of structure and morphologies of the materials has been gaining a significant attention owing to the correlation with their final textural parameters. To control the morphology of the final OMCs, it is necessary to control morphology of the template materials. Schuster *et al.* reported that the spherical OMC nanoparticles with bimodal pore size distribution having mean pore sizes centred at 6 and 3.1 nm having 300 nm diameter via nano templating approach can be prepared by using the phenol and formaldehyde mixture precursor and spherical silica as a hard template.[24] The material showed high specific surface areas of 2445 $m^2 g^{-1}$ and the highest inner pore volumes up to 2.32 $cm^3 g^{-1}$. In this case, the shape of silica hard templates has been prepared by using a 400 nm PMMA spheres with close packed opal structure. This unique structure has been replicated into the final nanoporous carbon samples. The typical spherically ordered opal structures of OMCs with large domains of nanoparticles are shown in the TEM images and DLS measurements. Seo *et al.* demonstrated the preparation of OMCs by using furfuryl alcohol (FA) as a carbon source and phosphoric acid or sulfuric acid impregnated acidified mesoporous silica as a precursor.[25] This work has been aimed at preventing the generation of external carbon by selecting a moderately weak acid that would slowly catalyze the polymerization of FA. However, the obtained OMCs exhibited lower surface area than OMCs prepared by using the unmodified mesoporous silicas.

Hard templating approach can also be used to prepare nanoporous carbon in monoliths form. Hierarchical porous carbon monoliths (HPCMs) with both ordered hexagonal mesoporosity and three-dimensionally connected macroporosity, and controlled morphologies have been synthesized via a simple nanocasting pathway by using hierarchically macro/mesoporous silica with tunable morphologies as a hard template and FA and trimethyl benzene (TMB) mixture as a carbon a source. These monoliths exhibit high pore volumes (1.6 $cm^3 g^{-1}$) and specific surface areas (1354 $m^2 g^{-1}$) and a strong hydrophobicity due to the nature of the precursor used in the synthesis.[26] These results reveal that the selection of the precursors is the key to control the surface characteristics of the final carbon materials.

OMCs with various surface areas of 1361 to 3840 $m^2 g^{-1}$ and tunable micropores have been prepared by using zeolite Y and zeolite EMC-2 as sacrificial hard templates and FA as the precursor.[27, 28] Although FA was used as the precursor for zeolite templated porous carbons, the pores of the zeolites are too small to accommodate bulky molecular precursors. Ryoo *et al.* has tackled this problem by using ethanol as a carbon source and hierarchical meso-/microporous zeolite beta as a template for the synthesis of hierarchical nanoporous carbons with

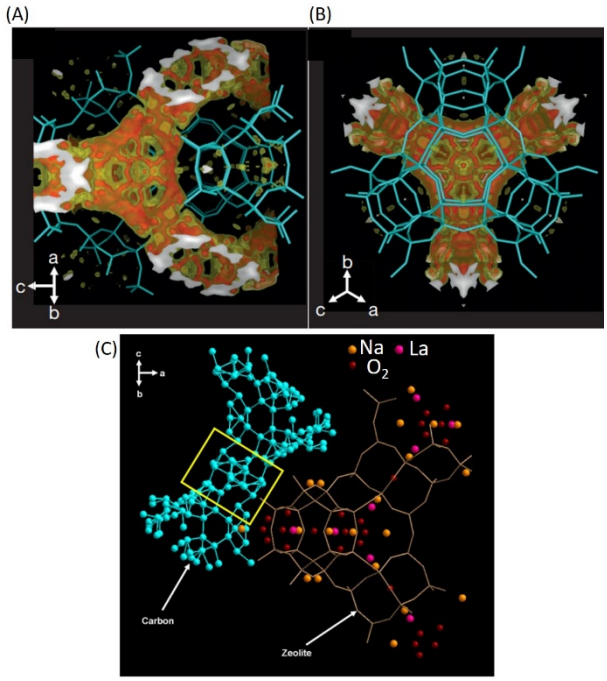

Figure 3 (A and B) Electron-density map of zeolite FAU after carbon deposition. (C) X-ray crystallographic analysis of the carbon structure formed in a single crystal of La3+-ion-exchanged zeolite FAU. Reproduced with permission from ref. 35. Copyright 2016, Nature Publishing Group.

mesopore–micropore hierarchy.[29] The hierarchically porous carbons exhibited a high BET surface area of 2220 $m^2 g^{-1}$, large micropore volume of 0.62 $cm^3 g^{-1}$ and mesopore volume of 1.48 $cm^3 g^{-1}$. The authors concluded that the ethanol precursor is more suitable for the hierarchical carbon synthesis, as compared with propylene or acetylene gas precursors, which is mainly because of the formation of water vapour due to the decomposition of ethanol during the heat treatment. It is also assumed that this process assisted in delaying the deposition of carbons at the exterior. Nueangnoraj *et al.* reported on the formation of cross linked fullerene like three dimensional graphene based ordered microporous carbon with surface area of 2100 $m^2 g^{-1}$ in the confined nanochannels of zeolite Y by using acetylene gas through a pulsed chemical vapour deposition technique.[30]

Mokaya *et al.* introduced an elegant approach to synthesise porous carbons with ultra high surface area of 3332 $m^2 g^{-1}$ and a specific pore volume of 1.66 $cm^3 g^{-1}$ through a simple impregnation of zeolite13X with FA followed by the chemical vapour deposition (CVD) of ethylene gas.[31] This unique double filling approach introduced graphene sheets with a large number of edges within the nanochannels and are responsible for enhancing the specific surface area of the final carbons. The same group also demonstrated a pressure assisted strategy to create microporosity within the porous carbons derived from zeolitic imidazolate framework (ZIF) templates.[32,33, 34] This simple compaction technique can be used as an effective method to either increase or decrease the textural properties of the activated ZIF-templated carbons as it has the potential to create new micropores or decrease the size of the large mesopores into micropores. The properties of the OMCs can also be significantly altered with the external agents such as metal oxides.

Ryoo and his co-workers realized this wonderful opportunity and demonstrated a ground breaking lanthanum-catalysed zeolite templated synthesis process of microporous 3D graphene-like carbon materials using ethylene as a carbon precursor, which have two times higher conductivity than that of CMK-3 (Fig. 3).[35] This is an energy efficient synthesis process as it requires carbonization temperature of only 600°C, whereas the conventional microporous graphene synthesis uses the temperature in the range of 900 to 1000 °C. Noteworthy, microporous carbon deposition in lanthanum modified zeolite Y occurs more than 20 times faster than in an acidic HY zeolite. Acetylene gas can also be used instead of ethylene to construct carbon frameworks by using modified zeolites. As acetylene gas is more reactive than ethylene, carbon deposition can be accomplished even at lower temperatures as low as 340 °C.[35] If the realized microporous carbon materials possess poorly ordered porous structure, it becomes highly ordered nature after heat treatment of 900°C.[36] The same group has also developed a large scale (70 g batch) synthesis of 3D graphene-like ordered microporous carbon with 2770 $m^2 g^{-1}$ BET surface area and 1.32 $cm^3 g^{-1}$ of pore volume by using the cost effective calcium modified zeolite X template and ethylene gas under the same conditions.[37] These zeolite templated carbons (ZTCs) have a higher particle density, and higher surface area (around 3000 $m^2 g^{-1}$) than CMK-3. The gravimetric and volumetric surface areas of ZTCs are the highest among all the carbon materials, therefore they exhibit a superior capacity for energy storage. These approaches demonstrated that the preparation strategy is the key to control the final properties of the OMC which ultimately determine their performances in various applications. Although these materials have interesting properties, the main issue that gives hurdle in the path of their commercialization is the removal of the mesoporous silica and zeolite hard templates by highly toxic HF. Therefore, the researchers found eco and environmentally friendly soft templating approaches to prepare OMCs without compromising the textural parameters.

2.2 Soft templating method for OMCs

A soft-templating approach has been widely applied for the synthesis of various mesoporous materials including zeolites, silica, inorganic metal oxides and mesoporous carbons.[38-44] Preparation procedures for the silica, zeolites and metal oxides have been well established.[45, 46] However, the direct synthesis of OMCs by soft-templating approach is not straightforward. Various factors including the[15] functionalization of templates with the polymeric units, hydrogen bonding between the template and the precursors, organic-organic composites, organic-organic self-assembly, and hydrogen bonding induced organic-organic self-assembly have been optimized to obtain OMCs with excellent textural parameters.[41, 47]

Table 1. Summary of the synthesis conditions, heteroatom contents and textural parameters of the functionalized nanoporous carbons and their application possibilities.

Material	Template and porogen	precursor	T (°C)	Hetero atom content	Structure and morphology	d_{pore} (nm)	SA_{BET} ($m^2 g^{-1}$)	V_{Total} ($cm^3 g^{-1}$)	Applications	Ref.
OMC spheres	Silica inverse opal spheres	Phenol and formaldehyde	900	--	• Spherical shape nanoparticles • 2D-hexagonal mesostructure • *P6mm* symmetry	3.1 6.0	2445	2.63	• Li-S battery	24
TC-Y1	Zeolite Y	Formaldehyde and Propylene	900	--	• *Fd3m* symmetry • Nanoparticles	0.7-4	3519	1.3	• CO_2 adsorption	27
TC-Y2	Zeolite Y	Propylene	900	--	• *Fd3m* symmetry • Nanoparticles	0.7-4	1815	1.8	• CO_2 adsorption	27
TC-EMC	Zeolite EMC-2	Formaldehyde and Propylene	900	--	• *$P6_3/mmc$* symmetry • Retained EMC-2 zeolite morphology	0.7-4	3840	1.8	• CO_2 adsorption	27, 48, 49
HR-ZTC	Hierarchical zeolite beta	Ethanol	600-700		• Nano particles • Zeolite morphology	1.2	2220	2.45	• Supercapacitor	29
P7	Zeolite Y	Acetylene	900		• Core-shell structure	1.0	2100	--	• Supercapacitor	30
FA-ZTC	Zeolite 13X	FA and ethylene	700		• Zeolite particle type morphology	1.2	3332	1.66	• H_2 storage	31
CB-700	ZIF	FA and acetonitrile	700		• Nanoparticles (50-100nm) • ZIF morphology	0.8	970	0.66	• H_2 uptake	32
HPCMs	Hierarchical SBA-15-monolith	Furfuryl alcohol and trimethyl benzene	850	--	• Positive replicas of SBA-15-monolith • Rod shaped morphology	3.36	729-1354	1.6	• Cleaning/recycling spilled oils or organic solvents. • Bilirubin adsorption	26
OMCs	Pluronic F127 and $Fe(NO_3).9H_2O$	Resorcinol and formaldehyde	700-1000	--	• Graphitic tubules morphology • *P6mm* symmetry	4.8	603-808	0.55-0.66	• Supercapacitors	50
OMCs	Pluronic F127, TEOS and $AgNO_3$	Resorcinol and formaldehyde	800	--	• *Fm3m* symmetry • Hexagonal arrangement of pores	10.1-11.0	212-780	0.19-0.65	• Stabilization of Ag nanoparticles	51
Monolithic mesoporous carbons	Pluronic F127 and Citric acid	Resorcinol and formaldehyde	600	--	• 2D hexagonal *p6mm* symmetry	4.7-5.1	675-758	0.14-0.16	• Dehydrogenation of propane to propylene	52
OMC films	Pluronic F127	Phenol and formalin	350-800	--	• Cage type cubic *Im3m* • 2-D hexagonal *p6mm* • Face centered orthorhombic *Fmmm*				• Kr sorption	53
NMC-G	SBA-15	Gelatin	600-1000	N: 4.5 to 14.46 at%	• 2D-hexagonal mesostructure • *P6mm* symmetry • Rod shaped morphology	3.54-6.41	764-846	1.14-1.50	• Sensing of acetic acid • CO_2 adsorption • Electrocatalyst for ORR	54, 55
OMFLC-N	SBA-15	FA and dicyandiamide	1000	N: 8.2 to 10.6 at%	• 2D hexagonal "crystal" • *P6mm* symmetry	1.8-4.0	1580	2.2	• Supercapacitrors	56
NOMC and HNMC	SBA-15	Honey	650-950	N: 1.0 to 3.5 at%	• SBA-15 replicated structure • Rod shaped morphology • *P6mm* symmetry		621-1273	0.73-1.16	• Metal-free catalyst for ORR • Li and Na ion batteries	57, 58
N-OMC and N-OMCNFA	Crab shells and Pluronic F127	Resole and dicyandiamide	750	N: 4.6 to 6.7 at%	• 2D hexagonal • *P6m* symmetry • Nano fibre morphology	4.1-15.0	516-1030	0.3-2.35	• Supercapacitors	59
NONC	SBA-15	Dopamine	800	N: 5 at%	• Successful SBA-15 replication • *P6mm* symmetry • Rod shaped morphology	3.8	1013	1.14	• Supercapacitors	60
G-OMC	Mesoporous NiO	Dopamine	900	N: 1.6 at%	• 2D morphology • Ordered graphitic mesopores	3.5	269	0.35	• Electrochemical double layer capacitors	61
N-HMCs	KIT-6	(1-methyl-1H-pyrrole-2-yl)methanol	850	N: 0.5 to 10.0 at%	• Well-ordered mesopores • Successful transformation of KIT-6 type structure • *Ia3d* symmetry	3.4-4.0	780-1150	0.91-1.02	• Electrocatalyst for ORR towards H_2O_2 production	62
N-HMCSs	Mesoporous silica spheres	polystyrene/polyacrylonitrile	700	N: 3.6 at%	• Hollow structure • Mesopores on the shells	4.1	807	0.87	• Supercapacitors	63, 64
NHPCM	Amine grafted hierarchical porous silica monolith	Furfuryl alcohol	700-1000	N: 1.1 to 1.5 at%	• Carbon rod replicas • Well retention of monolith morphology • Highly regular arrays of branched morphology	3.8	744-796	1.31-1.53	• Electrocatalyst for ORR	65
N-MC	Amine functionalized SBA-15	Sucrose	900	N: 0.6 to 1.5 at%	• Hexagonally ordered cylindrical mesopores • Negative replica of SBA-15	5.14	749-790	0.65-0.86	• Supercapacitors	66
NOMC and C-PY	SBA-15	Pyrrole or aniline	800-1400	N: 0.5 to 10.7 at%	• Inverse replica of the SBA-15 template • Highly ordered mesopores • *P6mm* symmetry	3.7-7.4	591-886	0.52-0.93	• Electrocatalyst for ORR • Supercapacitors	67-69
NOMC	SBA-15	D(+)-glucose and D-glucosamine	900	N: 2.5 to 3.9 at%	• stripe like mesopores • Rod shaped morphology • *P6mm* symmetry	3.9-7.3	352-1152	0.59-0.97	• Supercapacitors	70

N-OMCs	SBA-15	*m*-aminobenzoic acid and *p*-aminobenzoic acid	700	N: 7.8 to 8.3 at%	• Pore channels arranged in a bidimensional ordered array • *P6mm* hexagonal symmetry	5.0	1058-1322	1.0-1.8	• Ibuprofen (drug) release	[71]
HPC-Ns	Hierarchically porous silica monolith	FA, oxalic acid and urea	750-900	N: 1.8-6.4 at.%	• Disordered hierarchical porous structure • Rod shaped morphology	3.5-3.6	1571-2473	1.5-2.2	• Electrocatalyst for ORR	[72]
NHPC-3D	Silica spheres	Dopamine	800	N: 7.4 at%	• Interconnected and layered • Macroporous structure	2.5	1056	2.56	• Supercapacitors	[73]
N-OMCs	SBA-15	Iron phthalocyanine	900	N: 3.5-3.7 at%	• Rugby ball or rice grain-like ellipsoidal shape nanoparticles • Mesopore channels run parallel to the rod shape direction • *P6mm* hexagonal symmetry	3.1	1122-1720	1.6-2.1	• Electrocatalyst for ORR	[74]
N-MCHSs	Silica hollow spheres and Pluronic P123	Dopamine	600-900	N: 2.2-4.5 at%	• Sponge like shells with interconnection of hollow cores • Carbon shells are interconnected by "carbon bridges"	5.0	375-438	0.40-0.43	• Anode for Li-ion batteries	[75]
NMMC	Pluronic F127 and Titanium-carbide	Resol and dicyandiamide	700	N: 4.6-7.8 at%	• 2D hexagonal meso-structure • Highly ordered, stripe-like pores	4.6	1344	0.90	• Supercapacitors	[76]
NMCs	SBA-15	Amino acids	700-900	N: 3.6-9.4 at%	• Ordered nanowire arrays • Rod like "wheats" shape morphology • Ordered and disordered mesoporous structure	4.27-5.72	694-1280	0.89-2.48	• CO_2 Uptake • Electrocatalyst for ORR	[77]
NMC	SBA-15	Resol and cyandiamide	800	N: 5.1-15.1 at%	• 2D Hexagonal mesostructure • Shuttle-like morphology • *P6mm* symmetry	2.4-4.1	1095-1722	0.73-1.81	• Supercapacitors	[78]
NNCM	3D continuous skeleton silica particles	Polyacrylo nitrile (PAN)	900	N: 6.1-6.5 at%	• 3D continuous nano framework • Numerous continuous mesopores	30	391-663	0.9-2.1	• Volumetric capacitors	[79]
meso-BMP 3DOm carbon	Ludox HS40 Slilica spheres	Ionic liquids: BMP-dca EMI-dca EMI-tfsi	900	N: 5.0-17 wt%	• Long-range ordered structure • Pores are less well defined	5-20	320-1380	0.75-3.6	• Electrocatalyst for H_2O_2 production • Electrochemical double-layer capacitors	[80-82]
RF-1 and RF-2	Pluronic F127 and Trimethylbenzene	Resorcinol and hexamethylene tetramine (HMT) Ammonia	350-900	N: 1.1-6.5 at%	• Body-centred cubic (*Im3m*) to 2D hexagonal (*p6m*) structure • Irregular polyhedral particles	3.1-6.7	659-870	0.33-0.49	• Adsorption	[83]
PHMT HMT ACMP-N	--	Resorcinol and hexamethylene tetramine (HMT) Ammonia	600-1000	N: 1.3-6.9 at%	• Interconnected spherical particles • Nitrogen containing microporous carbon	0.6-1.3	528-936	0.19-0.33	• CO_2 capture	[84]
NOMC	Pluronic F127	Resorcinol-melamine-formaldehyde resin	600-800	N: 2.4-2.9 at%	• Body-centred cubic *Im3m* symmetry • Irregular polyhedral particles	2.71-3.02	583-631	0.30-0.33	• CO_2 adsorption	[85]
Nitrogen-enriched OMCs	Pluronic F127	Resorcinol formaldehyde NH_3 gas	700-850	N: 7.1-9.1 at%	• Highly ordered mesoporous structure • *P6m* symmetry	6.6-7.0	643-1415	0.57-1.2	• Supercapacitors	[86]
H-NMC C-NMC	Pluronic F127	Resol and dicyandiamide	600	N: 0.09 to 13.1 wt%	• Tunable mesostructures (*p6m* and *Im3m* symmetry) • Mesostructure formed in a layer-by-layer fashion	3.1-17.6	494-586	0.14-0.17	• CO_2 capture • Supercapacitors	[87]
N-OMCs	Pluronic F127 and Na_2CO_3	Resorcinol formaldehyde dicyandiamide	600	N: 0.23 to 4.2 wt%	• Parallel mesoporous channels • Well retention of mesoporous structure • 2D *P6mm* hexagonal symmetry	5.5-9.3	376-718	0.42-0.78	• Dehydrochlorination of 1,2-dichloroethane	[88-90]
N-OMCs	Pluronic F127	Urea-phenol-formaldehyde	600	N: 0.38 to 1.41 wt%	• Spherical morphology • Cubic *Im3m* mesostructure	2.1	446-566	0.24-0.31	• Adsorbent for acidic gases • Electrochemical capacitors	[91-93]

om- MR	Pluronic F127	Phenolic-functionalized melamine resin	400	N: 18.16 wt%	• Ordered mesostructured of *Im3m* symmetry • Polyhedron shape morphology	2.9	385.9	0.17	• CO_2 Adsorption • Supercapacitors	94, 95
NPGC	Pluronic F127 TEOS, nickel nitrate	Glucose and melamine	800-1000	N: 2.9-6.96 wt%	• Nanosheet-like structure • Interconnected nanoporous structure	4.8 - 6.3	579-1116	0.38-0.79	• Supercapacitors	96
N-doped OMC	Pluronic F127 TEOS	Resol and dicyandiamide	700	N: 5.74-8.1 wt%	• Hexagonal pore arrangement • Stripelike 2D mesostructure	5.1 - 7.4	631-1374	0.4-1.5	• Supercapacitors	97
NMNC	--	Glucose and NH_3	800-1000	N: 2.6-4.7 wt%	• Sphere structure • Network-like morphology	2.3 - 2.8	1154-2588	0.67-1.71	• Electrocatalyst for ORR	98
NMC5	Pluronic F127 and Fluorocarbon	Resorcinol formaldehyde Melamine	700-1000	N: 5.5-25.7 wt%	• Sphere shape morphology • Ordered porous structure	5.0	307-484	0.30-0.41	• Electrocatalyst for ORR	99
NOMC	Pluronic F127	3-aminophenol hexamethylene tetramine (HMT) Ammonia	800	N: 3.4-5.4 wt%	• Polyhedral crystal like morphology • Rhombic dodecahedron shape • *m3m* symmetry	3.6 - 5.4	72-1159	0.05-0.72	• Supercapacitors	100
NMC	Pluronic P123 Sodium silicate	Melamine-formaldehyde resin	600-900	N: 5.5-27.1 wt%	• Disordered porous structure	5.0	252-794	0.31-1.15	• Electrocatalyst for ORR	101
NHCSs	Pluronic P123 Sodium oleate	2,4-dihydroxybenzoic acid and hexamethylene tetramine (HMT)	800-1000	N: 3.6-7.8 at%	• Ruptured spherical particles • Hollow spherical structures	3.9	738-820	0.5-0.56	• Electrocatalyst for ORR	102
BOMCs	SBA-15	sucrose and 4-hydroxyphenylboronicacid	900	B: 0.64-2.11 at%	• 2D hexagonal mesoporous structure • *P6mm* symmetry • Rod-like particles	6.4 - 7.2	778-1040	1.18-1.52	• Electrocatalyst for ORR	103, 104
Mesoporous CB film	Pluronic F127	Phenol, formalin and boric acid	400-700	B: 3.6 at%	• 2D hexagonal mesoporous structure	3.6 - 4.1	475-551	0.45-0.53	• Proton exchange membrane fuel cells	105
Hierarchical carbons with boron	Pluronic F127	Resorcinol and boric acid	800	B: 0.42-2.37 at%	• Hierarchical mesoporous structure • Ordered pores	5.0	547-643	0.49-0.73	• Supercapacitors	106
POMCs	SBA-15	Phenol and triphenylphosphine	900	P: 1.36 at%	• Spherical carbon microstructures • Highly ordered uniform pore distribution	3.5	814-1182	1.4-1.87	• Electrocatalyst for ORR	107
POMCs	SBA-15	Glucose and triphenylphosphine	900	P: 0.64 at%	• Rod shape morphology • *P6mm* symmetry	3.8 - 4.3	1117-1338	1.24-1.37	• Pt nanoparticles stabilization • Methanol electrooxidation	108
SN-OMCs	SBA-15	Thiophene and pyrimidine	700	N: 6.2at% S: 0.25 to 0.68 at%	• 2D hexagonal mesoporous structure • Rod like morphology • *P6mm* symmetry	3.5	750-1100	0.53-0.83	• Electrocatalyst for ORR	109
NSOMC	SBA-15	Pyrrole and H_2SO_4	650-950	N: 4.8 to 10.0 at% S: 1.7 to 2.6 at%	• 2D hexagonal mesoporous structure • Rod like morphology • *P6mm* symmetry	3.24	978-1021	1.1-1.2	• Electrochemical double-layer capacitor	110
SNOMC	SBA-15	Pyrrole and thiophene	800	N: 1.2 to 5.7 at% S: 5.6 to 8.7 at%	• 2D hexagonal mesoporous structure • Rod like morphology • *P6mm* symmetry	6.2	601	1.0	• Electrocatalyst for ORR	111
SN-OMC	SBA-15	Diphenylthiocarbazone	800-1000	N: 3.2 at% S: 0.8 at%	• 2D hexagonal mesoporous structure • Rod like morphology • *P6mm* symmetry	5.1	647-816	0.5-0.75	• Electrocatalyst for ORR	112
OMC-S	SBA-15	Sucrose and benzyl disulfide	900	S: 1.4 to 1.5 at%	• 2D hexagonal mesoporous structure • Rod like morphology • *P6mm* symmetry	4.5 - 5.4	1099-1244	1.37-1.61	• Electrocatalyst for ORR	113
HTBP	Pluronic F127	Resorcinol, boric acid and phosphoric acid	600	B: 0.8 to 1.6 at% P: 2.3 to 3.6 at% O: 8.1 to 10.0 at%	• Ordered mesostructured	6.2	590-659	0.59-0.67	• Supercapacitors	114

Among these strategies, the direct synthesis of OMCs using organic–organic self-assembly involving the combination of polymerizable precursors and block copolymer templates is expected to be more flexible than other soft templating methods and the traditional hard templating nanocasting methods.[47] Li *et al.* reported a series of hexagonally ordered mesoporous carbons (OMC-Ts) by adjusting the pyrolysis temperature of resorcinol and formaldehyde mixture via a soft templating and catalytic graphitization approach by using the Pluronic F127, $EO_{106}PO_{70}EO_{20}$ triblock copolymer as the template and $Fe(NO_3).9H_2O$ as a catalyst.[50] The structure of OMC-Ts has a two-dimensional hexagonal (p6mm) mesostructure with tubule like morphology. The OMC-700 sample synthesized at 700 ˚C showed a high specific surface area of 808 $m^2\ g^{-1}$, and pore volume of 0.55 $cm^3\ g^{-1}$ with a uniform mean pore size of 4.8 nm.

Sterk *et al.* described a soft-templating synthesis procedure to prepare OMCs with BET surface area up to 780 $m^2\ g^{-1}$ using triblock copolymer F127 and phenolic resin precursors in the presence of tetraethyl orthosilicate (TEOS). In this case, silver nitrate was added in the synthesis mixture to increase the microporosity as well the metal nanoparticles in the porous channels of OMCs.[51] Monolithic mesoporous carbons were also prepared from resorcinol–formaldehyde resin through a simple autoclaving method using citric acid as a catalyst and triblock copolymer F127 as a structure directing agent. The obtained mesoporous carbons have a hexagonal pore system, uniform pore size of ~5.0 nm and a high BET surface area of ~758 $m^2\ g^{-1}$.[52] Similar strategy was also adopted to make highly ordered OMC films with controllable mesostructures and highly accessible surfaces. A simple direct carbonization of phenolic resin and the conventional Pluronic F127 and $EO_{106}PO_{70}EO_{20}$ triblock copolymer as a template afforded the highly ordered OMC films (Fig. 2).[53] The structure of the films can be controlled by adjusting the amount of the surfactant in the synthesis mixture. Unique concept of mesostructural transformation of cage-type to tubular frameworks via anisotropic shrinkage upon increasing the carbonization temperature was also demonstrated.[40] Anisotropic shrinkage upon increasing the carbonization temperature has been observed for thin film samples and the process changes the space group of the obtained films. On the other hand, only unit cell parameters were reduced for the powder samples upon alteration of carbonization temperature while keeping the original space groups by isotropic shrinkage with condensation of the framework. This unique approach involving a simple adjustment of the preparation conditions, the amounts of Pluronic F12, and the carbonization temperature is found to be the effective tool for controlling structure of the OMC films.

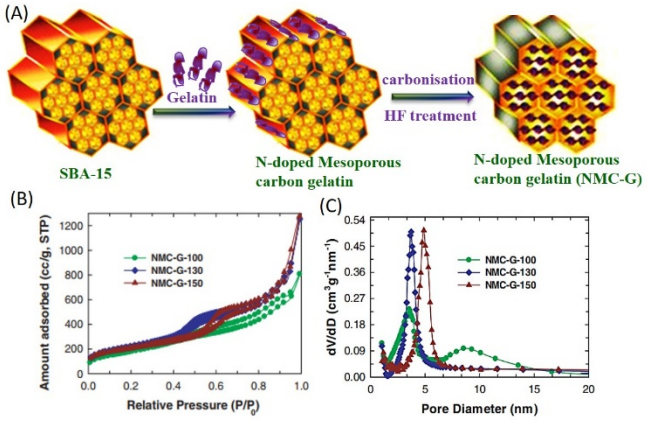

Figure 4 (A) Synthesis scheme for the fabrication of ordered mesoporous carbon with nitrogen (NMC-G) prepared through nano templating approach. (B) N_2 adsorption-desorption patterns of NMC-G samples replicated form SBA-15-x templates: a) NMC-G-100, b) NMC-G-130, and c) Pore size distribution of the same. Reproduced with permission from ref. 54. Copyright 2012, Wiley-VCH Verlag GmbH & Co. KGaA, Weinheim.

3. Hetero atom doped OMCs

Heteroatom doping is the replacement of some of the carbon atoms in the uniform graphitic carbon structure with other foreign atoms which significantly changes the electronic, electrical and surface charge properties of the final materials. The introduction of heteroatoms such as boron, nitrogen, sulphur, and phosphorus into the OMCs could cause electron modulation due to their different electronegativity. This also tunes their charge distribution, optoelectronic properties and/or defect induced chemical functionalities, which are useful for many technological applications.[115, 116] Heteroatom-doped OMCs can be prepared either by in-situ doping during the preparation of nanoporous carbon materials or through post-treatment of preformed carbon nanomaterials with heteroatom-containing precursors.[117] Post treatment procedure often leads to only surface functionalization without altering their bulk properties whereas the in-situ doping of hetero atoms can help to homogeneously incorporate the heteroatoms into the entire nanoporous carbon matrix.

3.1 Nitrogen doped OMCs

Nitrogen is one of the neighbour elements next to carbon in the periodic table and it has an atomic radius similar to that of carbon but has different electronic configuration and electronegativity.[117] Thus, nitrogen doping into the OMCs could change their electronic structures while minimizing the lattice mismatch, leading to unique electronic properties. Great efforts have been paid to introduce nitrogen atoms into OMCs as the incorporation of nitrogen atoms into the nanoporous carbon matrix can significantly enhance their conducting, field emission, catalytic, and energy storage properties.[118-132]

3.1.1 Hard templating approach

The precursors containing N atoms including polymeric compounds, acetonitrile, urea, aromatic or aliphatic amines are generally used in combination with the hard-templating method for the incorporation of nitrogen in the carbon framework of OMCs.[133, 134] Recently, Vinu *et al.* demonstrated the synthesis of highly ordered nitrogen-containing mesoporous carbon (NMC-G) with well-ordered mesopores and various pore diameters and also high basicity using a low-cost, naturally occurring gelatin biomolecule as a single-molecule precursor and 2D hexagonal SBA-15 with different pore

diameters prepared at different hydrothermal temperatures were used as the hard templates (Fig. 4).[54, 55]

The realized NMC-G materials have excellent textural properties such as high specific surface areas (764-804 $m^2 g^{-1}$), huge pore volumes (1.14-1.40 $cm^3 g^{-1}$), and mesoporous diameters (3.54-4.89 nm). Recently, Huang *et al.* made the ground breaking discovery on synthesis of self-supported N-doped ordered mesoporous few-layer carbon (OMFLC-N) super structures catalysed by Ni catalyst through chemical vapour deposition using a simple and environmentally friendly precursors such as FA and dicyandiamide (DCDA) and mesoporous SBA-15 silica as the template.[56] OMFLC-N sample exhibited a high conductivity (360 S cm^{-1}) with mesoscopically ordered few-layers and also possessed the largest surface area (1580 $m^2 g^{-1}$), a high total pore volume (2.20 $cm^3 g^{-1}$), the smallest average pore width (2.25 nm), and the most prominent pores smaller than 2 nm. Graphene-like structure with ≤5 layers and minimum number of defects in OMFLC-N were verified by Raman spectroscopy. The introduction of transition metal ions helps the formation of highly graphitic structure along the walls whereas the N doping changes the electronic structure of the formed carbons. The combination of these factors significantly enhances the conductivity of the final materials.

Natural biomass honey which contains 80–85% of carbohydrates, 15–17% water, 0.3% proteins, 0.2% ashes and minor quantities of amino acids and vitamins have also been utilized as the source of nitrogen and carbon for the fabrication of nitrogen-doped ordered mesoporous carbons (NOMCs). Guo *et al.* and Xiao *et al.* have independently demonstrated the synthesis of NOMCs by nanocasting method using SBA-15 as the template and natural honey as a source for nitrogen and carbon (Fig. 5). The structure of NOMCs exhibited two-dimensional hexagonal mesoporous framework, composed of ordered nitrogen doped carbon nano rods. The BET specific surface areas of NOMCs were in the range of 600 to 1100 $m^2 g^{-1}$ but varied significantly with the change of carbonization temperature. It should be noted that the pore size of NOMCs is 4.0 nm, which is less than half of the mesoporous silica template

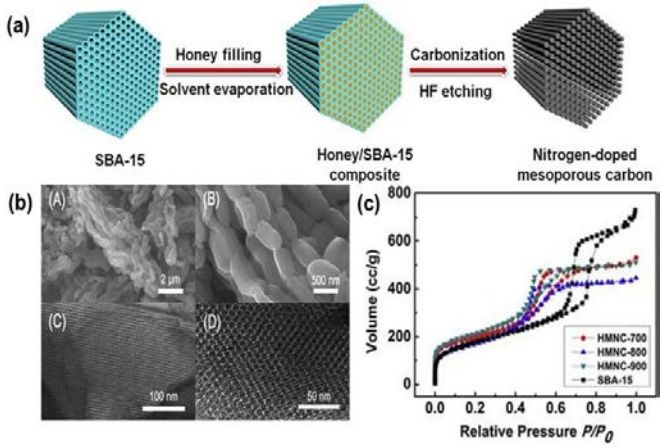

Figure 5 (a) Schematic illustration for the synthesis procedure of NOMCs prepared from honey and SBA-15. (b) FESEM and HRTEM images of NOMCs synthesized at 800 °C. (c) Nitrogen sorption isotherms of NOMCs prepared at different temperatures along with mesoporous silica SBA-15 hard template. Reproduced with permission from ref. 58. Copyright 2016, Elsevier.

SBA-15 (9.1 nm) but similar to the wall thickness, revealing the transformation of silica walls into pores and the pores of the templates into N-doped carbon walls.[57, 58] NOMC nanofiber array was prepared by a combination of a soft templating method in combination of hard-templating approach using a well-mixed solution of calcined crab shells, Pluronic F127, dicyandiamide (DCDA) and resole.[59] NOMC nanofiber arrays possessed four resolved SAXS scattering peaks, which were indexed as the 100, 110, 200, and 210 planes of a 2D hexagonal mesostructure with a space group of *p6m*. The obtained NOMC nanofiber material also exhibited a high surface area (1030 $m^2 g^{-1}$) and a large pore volume (2.35 $cm^3 g^{-1}$), with uniform mesopores of ca. 15.0 nm which was much larger than that of CMK-3s, OMFLC-N, and NOMCs.[1, 56-58] These reports clearly reveal that the natural biomasses are the unique and low cost sources for the in-situ introduction of nitrogen atoms in the carbon framework of OMCs which could offer exciting electronic properties.

Although natural biomasses used for the heteroatom doped nanoporous carbons are cost effective, the control of the degree of polymerization is highly difficult. This has been addressed by the judicious choice of easily polymerisable precursors. A facile synthesis route has been developed to prepare nitrogen-doped ordered nanoporous carbons (NONCs) by Wu *et al.* based on in situ polydopamine coating onto the SBA-15 pore surface.[60] The dopamine was quickly self-polymerized onto the pore wall of SBA-15, forming polydopamine/silica nanocomposites in the presence of tris-buffer solution. The carbonization of the polydopamine/silica nanocomposite in N_2 and then removal of the silica template eventually led to the formation of NONC material with a BET surface area of 1013 $m^2 g^{-1}$. However, these materials suffered from poor crystallinity which suppress the conductivity of the materials. This was overcome by the discovery of Yuan *et al.* who reported the synthesis of nitrogenated graphitic ordered mesoporous carbon (G-OMC) by using mesoporous nickel oxide as a template as well as the catalyst and dopamine as a precursor. The results revealed that G-OMC materials had a higher degree of graphitization than those prepared from dopamine and pure SBA-15 as the template, which was mainly because of the catalytic graphitization induced by the nickel oxide catalyst. The I_D/I_G value of the G-OMC was 0.69, which was much less than that of the I_D/I_G value of CMK-3 (0.84), revealing the high graphitic nature of G-OMC.[61]

For many applications, not only the conductivity but also the amount of nitrogen doping in the carbon framework is also crucial as it sometimes dictates the final performance of the materials. For instance, Park *et al.* demonstrated the synthesis of mesoporous nitrogen-doped carbon with tunable nitrogen content with a simple adjustment of the amount of the precursor, (1-methyl-1H-pyrrole-2-yl) methanol (MPM), which is structurally similar to FA, using 3D body centred cubic KIT-6 as a template. The nitrogen content of the resulting carbon was controlled in the range of 0−10 at. % and all prepared samples had well-ordered mesopores with diameters of 3.4−4.0 nm with BET specific surface areas of 780−1150 $m^2 g^{-1}$.[62]

Nitrogen atoms have also been doped with OMCs with different morphologies using different techniques. For example, monodispersed nitrogen-doped hollow mesoporous carbon spheres (N-HMCSs) have been synthesized using a novel "dissolution-capture" method wherein the polystyrene/polyacrylonitrile composite nanospheres (PS@PAN) were used as the carbon and nitrogen resource, which were uniformly coated by a layer of mesoporous silica. After organic solvent treatment, the PS@PAN were dissolved and then captured in the confined nanospace of mesoporous silica shell. The N-HMCSs with the surface area and pore volume of 807 m^2 g^{-1} and 0.87 cm^3 g^{-1} were produced after the carbonization followed by the removal of the template through HF etching.[63, 64] The orientation of the formed carbon nanorods can be controlled with the simple modification of the surface of the sacrificial template. Wang *et al.* reported an in situ source-template-interface reaction route to prepare 3D N-doped hierarchical porous carbon monolith (NHPCM) composed of branched mesoporous rods by nanocasting method with the amine functionalized hierarchical porous silica monolith (NHPSM) scavenger and FA as the carbon source.[65] It has been demonstrated that this unique approach helped to anchor a high density of N atoms on the surface of the NHPCM as a simple solid-solid interface reaction between the carbon precursors and amine functionalized NHPSM favoured the doping on the surface. Asefa *et al.* also described the NOMC synthesis by using the amine groups functionalized mesoporous silica SBA-15 but glucose was used instead of FA as a carbon precursor.[66] By varying the nature of the solvents (polar or non-polar) used for grafting amines on the surface of the templates, the amount of N doping on the final NOMC was controlled.

Liang and Tsiakaras *et al.* reported a novel impregnation method, namely vaporization-capillary condensation process to synthesize NOMC via nano hard templating method using SBA-15 as the template and pyrrole as the precursor in the presence of $FeCl_3$ catalyst. This new impregnation method yielded a much larger surface area (661 m^2 g^{-1}) and pore volume than the wet incipient method (292 m^2 g^{-1}).[67, 68] With the adjustment of the pore diameter of SBA-15 template and the carbonization temperature, the textural parameters and nitrogen content of NOMCs prepared from pyrrole precursor were controlled, respectively.[69] NOMCs have also been synthesized by using a mixture of D(+)-glucose and D-glucosamine hydrochloride as carbon precursors and SBA-15 as the template. The as-prepared products showed a large pore volume (0.59–0.97 cm^3 g^{-1}), high surface areas (352.72–1152.67 m^2 g^{-1}) and rational nitrogen content (ca. 2.5–3.9 wt.%).[70] In another study, Sanchez *et al.* demonstrated the NOMCs synthesis by using SBA-15 and two aromatic polyaramids namely, m-aminobenzoic acid (MABA) and p-aminobenzoic acid (PABA) as the precursors for C and N.[71] NOMCs with different morphologies and a nitrogen content of 3.5–3.7 at.% were also prepared by Yu *et al.* through the pyrolysis of iron phthalocyanine infiltrated in SBA-15 with different mesochannel lengths. The BET surface area was found to be decreased with increasing the mesopore channel length of the SBA-15.[74] Transition metal containing precursors not only act as the source for the porous carbons, but also act as a catalysts in improving the graphitic nature and conductivity in the resulting materials.

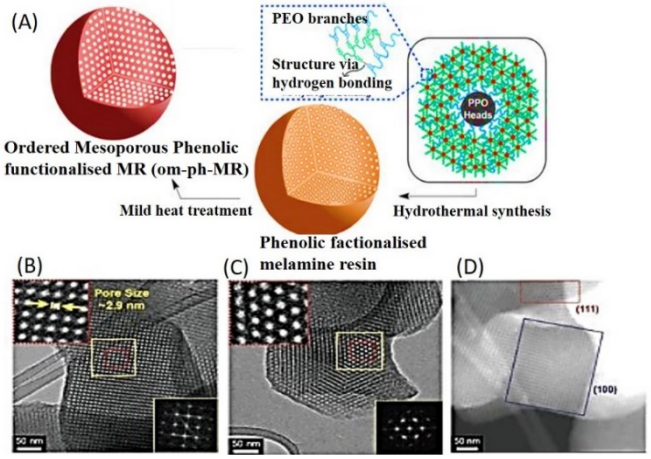

Figure 6 (A) Synthesis of mesoporous nitrogen doped carbon (MNC) with various percentages of mixture of precursors. (B-D) HRTEM images of MNCs of different compositions of precursors. Reproduced with permission from ref. 94. Copyright 2015, American Chemical Society.

Aniline, pyrrole and phenanthroline, were also independently used as nitrogenated carbon precursors to synthesize NOMCs by the nanocasting method with SBA-15 template. The NOMC materials derived from pyrrole (C-PY-900: 765 m^2 g^{-1}) and phenanthroline (C-Phen-900: 746 m^2 g^{-1}) exhibited higher specific surface areas than the aniline analogue but the nitrogen content of these samples was almost constant (3.1–3.3 at%) for the three carbon sources, except for a slight difference in the nitrogen configuration.[135] NOMC catalyst was directly synthesized using SBA-15 as a hard template, sucrose as a carbon source and urea as the nitrogen source, respectively. A 3.6 wt% of nitrogen doping in the NOMC was achieved with more than 70% of the nitrogen incorporated as quaternary nitrogen species.[136] This is one of the best ways of controlling nature of the nitrogen species on the wall structure of the NOMCs.

Nitrogen doping was also tried in porous carbons with different pore diameters. Chen *et al.* reported on the synthesis of nitrogen-doped micro-mesoporous carbon material with surface area of 789-1367 m^2 g^{-1} by employing urea-formaldehyde resin as carbon and nitrogen sources, zinc chloride as a porogen and SBA-15 as a hard template.[137] Nitrogen doped three dimensionally ordered microporous carbon (N-ZTC) was also synthesized by using aqueous acetonitrile as a nitrogen-containing carbon source, and zeolite beta as a template. The obtained materials possess nitrogen content of approximately 4 wt%, a large surface area and pore volumes of 1860 m^2 g^{-1} and 1.4 cm^3 g^{-1}, respectively.[138] Ling *et al.* reported on hard-templating synthesis of pristine and functionalized CMK-3 materials having BET surface areas in the range of 1152 to 1760 m^2 g^{-1} with various functionalities, including micropore development, nitrogen doping by using SBA-15 as the mesopore template, and silicate oligomer as the micropore template, low-molecular-weight phenolic resins as the carbon precursors and nitrogen-rich hexamethoxymethylmelamine (HMMM) as a nitrogen precursor.[139]

Ahn *et al.* synthesized a series of ladder type nitrogen-doped mesoporous carbons (CPANs), which was found to have a high stability, by using SBA-15 and in situ polymerization of polyacrylonitrile (PAN) inside the mesochannels of template at different carbonization temperatures. Among the materials prepared, CPAN-800, synthesized at the carbonization temperature of 800°C, was found to be the best one with many desirable properties such as high specific surface area (1182 $m^2 g^{-1}$) and pore volume (1.54 $cm^3 g^{-1}$), moderate nitrogen content of 9.52%, and highly ordered mesoporous structure with uniform pore sizes of 4.34 nm.[140] Zhao *et al.* adopted a similar strategy but used a low molecular weight phenolic resin (resol) as a carbon source and a high nitrogen-containing cyanamide as the nitrogen dopant. The prepared NOMCs exhibited a high surface area of 1741 $m^2 g^{-1}$ and nitrogen content up to 15 wt% by nanocasting approach. It was also demonstrated that the BET surface area (1397–1741 $m^2 g^{-1}$), pore size (3.6–4.1 nm) and pore volume (1.05–1.81 $cm^3 g^{-1}$) were easily tailored by controlling cyanamide-to-resol mass ratio or the carbonization temperature in the range of 600–900°C.[78] Yang *et al.* used silica gel template with 3D continuous skeleton and PAN in DMF solution for the synthesis of nitrogen-doped mesoporous carbon (NNCM) with the tunable pore volume of (1.22 to 2.11 $cm^3 g^{-1}$) but a fixed pore size in order to control the coating density for miniaturized energy devices. This was achieved by the simple adjustment of the quantity of PAN in DMF in the mesochannels of the 3D template.[79] 3D NOMCs having BET surface area up to 1131 $m^2 g^{-1}$ have been carried out using three dimensionally ordered silica as the template and FA and oxalic acid as the carbon source and an acid catalyst, respectively under ammonia pyrolysis.[141]

Nitrogen doped hierarchically porous carbon materials (HPC-Ns) has been successfully synthesized by Shi *et al.* by applying a simple N-doping procedure using FA, oxalic acid and urea mixture in ethanol solution as a carbon and nitrogen precursor and hierarchically macro/mesoporous silica as a template. The synthesized HPC-N samples demonstrated 3D connected ordered mesoporosity with extremely large specific surface area (2473 $m^2 g^{-1}$) and relatively high content of pyridinic N.[72] It was clear that when the nitrogen precursor was combined with organic polar solvent, the specific surface area was significantly enhanced.

3D interconnected nitrogen-doped hierarchical porous carbons (NHPC-3D) were also prepared via a hard-templating method with colloidal silica spheres (80 nm) and dopamine as the template and precursor, respectively. One of the interesting features of this study was the use of dopamine as the nitrogen precursor and the utilization of large sized colloidal silica nanoparticles as templates. Dopamine has several advantages such as self and low temperature polymerization, easy interaction with the surface of any templates and the final total carbon yield after carbonization. In addition, the templates with large nanoparticles offered a 3D structure with macropores. The obtained NHPC-3D also exhibited a high surface area of 1056 $m^2 g^{-1}$, a large pore volume of 2.56 $cm^3 g^{-1}$, and a high nitrogen content of 8.2 wt%, which also revealed the presence of large quantity of micropores in the samples.[73] Huo *et al.* also used dopamine precursor and mesoporous silica hollow spheres template to prepare nitrogen doped mesoporous carbon hollow spheres (NMCHSs) with specific surface area of 411.6 $m^2 g^{-1}$.[75] Tang *et al.* developed an innovative method of the sublimation and capillary condensation assisted nanocasting method for the fabrication of Fe and N dual-doped mesoporous carbon catalyst with 988 $m^2 g^{-1}$ BET surface area and 0.87 $cm^3 g^{-1}$ pore volume. Easily sublimmable iron phthalocyanine was used as the sources of iron, nitrogen and carbon, while mesoporous silica SBA-15 has been used as the hard template.[142]

Nitrogen-doped mesoporous carbon spheres (NMCS) were prepared by a nanocasting route using benzoxazine resins as the precursor of nitrogen and carbon, and ordered mesoporous silica spheres as the hard template. The prepared NMCS exhibited amorphous spherical nanoparticles with worm-like mesoporous channels, the specific surface area, pore volume and nitrogen contents were 634 $m^2 g^{-1}$, 0.91 $cm^3 g^{-1}$ and 3.50 (wt%),respectively.[143] Nitrogen-doped hierarchical mesoporous/microporous carbon (NMMC) was also prepared by using nitrogen-doped mesoporous titanium-carbide/carbon composite, followed by removal of carbides with chlorination. The obtained NMMC gave a high surface area of 1344 $m^2 g^{-1}$ and exhibited micropores that were drilled on the mesopore walls with the size of 0.70, 0.97 and 1.61 nm.[76]

Although the solvents play an important role in controlling the pore filling which is critical not only to control the nitrogen content but also structural order of the materials but sometimes it significantly increases the total cost of the production of the materials. Gao *et al.* described the synthesis of NOMCs with improved yields of up to 25% by direct heating of amino acids in inside porous channels of SBA-15 without using any solvent and metal catalysts. The diverse types of amino acids, their variable interactions with SBA-15 and different pyrolytic behaviours led to nitrogen-doped mesoporous carbons with tunable surface areas (700–1400 $m^2 g^{-1}$), pore volumes (0.9–2.5 $cm^3 g^{-1}$), and pore sizes of 4.3–10 nm.[77]

Nitrogen doped mesoporous carbon (meso-BMP) was synthesized by Hasche *et al.* with the pyrolysis of high nitrogen (17 Wt%) containing N -butyl- 3-methylpyridinium dicyanamide (BMP-dca) and commercial silica nanoparticles (Ludox HS40) as a template. The N_2 adsorption derived BET surface area of the meso-BMP is around 320 m^2 g^{-1} and the total pore volume derived from NLDFT method is 0.749 cm^3 g^{-1}.[80] NOMC with 2D hexagonal symmetry structure was synthesized *via* a facile solid–solid grinding/templating route, in which the ionic liquids (ILs) of 1-cyanoethyl-3-methylimidazolium chloride and SBA-15 were employed as the precursor and hard template, respectively. As-synthesized NOMC features with a uniform mesoporous size (3.5 nm), ropes-like morphology (0.4–1 µm in length) and high surface area (803 m^2 g^{-1}) with the nitrogen content of 5.5 at%.[82] Mesoporous nitrogen doped carbon with surface area up to 325 m^2 g^{-1} was produced through the nano hard template method using resorcinol, melamine, and formaldehyde as the carbon precursors catalyzed by the alkaline medium and mesoporous silica as a hard template.[144-147] It was believed that the nitrogen doping sometimes collapse the pore structure of the final porous carbons or creates a lot of defects. Stein *et al.* used an elegant approach in which a novel ionic liquid (IL) 1-ethyl-3-methylimidazolium dicyanoamide (EMI-DCA) based precursor which not only acts as a nitrogen source but also provides structural stabilization was used. In this approach, silica spheres were used as templates which generated NOMC with a high specific surface area and a large pore volume of 1393 m^2 g^{-1} and 4.5 cm^3 g^{-1}, respectively.[81, 148, 149] Ionic liquid based precursors are found to be the best sources for stabilising the porous structures of NOMC which resulted a high specific pore volume owing to their good affinity and adhesion on silica surfaces.[150-155]

Most of these fabricated materials were made in the form of powder, which may not be useful for making devices for electrochemical sensing applications. Therefore, researchers turned their attention to fabricate these NOMCs in a film form. For instance, free-standing nitrogen-doped mesoporous carbon films were prepared by Peng *et al.* by carbonization of gelatin/HKUST-1 composite films, which were fabricated from gelatin/copper hydroxide nanostrands composite films. Gelatin provided the sources of both carbon and nitrogen whereas the copper hydroxides offered porosity. The formation of HKUST-1 crystals expanded the gelatin matrix and produced porous structures which were retained during the carbonization process.[156]

3.1.2 Soft templating approach

As hard templating procedures requires the removal of the inorganic materials using toxic acids or strong bases, there has been a significant attention on the development of NOMCs using methods other than hard templating. Soft-templating is considered as one of the viable options to avoid this complex and toxic procedure involved in hard templating. In the soft-templating synthesis of NOMCs, two key issues should be kept in mind for the generation of ordered mesoporous frameworks. The first and the most important point to consider before using the soft templating approach is the interactions between the structure directing agents and the nitrogenated precursor as it is a key parameter which supports the formation of highly ordered structures. The other factor is the

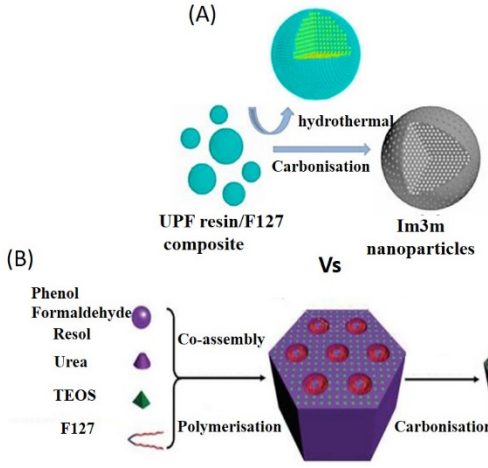

Figure 7 (A) Schematic representation of the N-OMC nanospheres synthesis from aqueous-phase approach. Reproduced with permission from ref. 91. Copyright 2014, Elsevier. (B) Schematic diagram for preparation of the NOMC/SiO_2 nanocomposite using organic-organic polymer co-assembly followed by polymerization. Reproduced with permission from ref. 93. Copyright 2015, Royal society of Chemistry.

condensation/polymerization kinetics of intermolecular precursor species. It has been realized that phenolic resins, nitrogen precursors, and polyethylene oxide (PEO)-containing block copolymers, which serve as the carbon sources and structure directing soft templates, respectively, is considered as the good combination for the direct self-assembly synthesis of NOMCs. For example, Liu *et al.* reported a one-pot route to prepare NOMCs having *Ia3d* and *p6m* symmetry with BET surface areas in the range of 500 to 870 m^2 g^{-1} in an aqueous media by dissolving the resorcinol, hexamethylenetetramine (HMT) and Pluronic F127 into a dilute aqueous ammonia. It is worth to mention that the symmetry of NOMCs changed from *Ia3d* to *P6m* upon increasing of the carbonization temperature and also by the simple introduction of trimethylbenzene (TMB) during the synthesis.[83-85, 157]

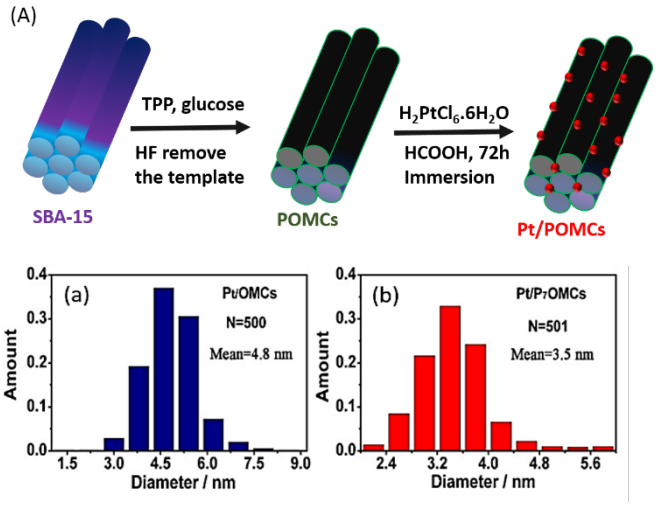

Figure 8 (A) Schematic representation of the synthesis of Pt/POMCs. Histograms on particle size distribution of (a) Pt/OMCs and (b) Pt/P_7 OMCs. Reproduced with permission from ref. 108. Copyright 2014, Elsevier.

Direct synthesis of NOMCs with a high nitrogen content through the soft templating approach remains a significant challenge due to the limited availability of nitrogen precursors capable of co-polymerizing with phenolic resins without deterioration of the order of mesostructural arrangement and a significant diminishment of nitrogen content during carbonization. Dai *et al.* reported on the direct synthesis of NOMCs through the self-assembly of phenolic resins and a Pluronic block copolymer via the soft-template method under pyrolysis of ammonia.[86] This approach did not require any nitrogen-containing carbon precursors or post-treatment, but had the advantage of the preferential reaction and/or replacement of oxygen with nitrogen species, generated by decomposition of ammonia at elevated temperatures, in oxygen-rich polymers during pyrolysis. This method used different steps including carbonization, nitrogen functionalization, and activation into a simple one step process and generated NOMCs with a uniform pore size, large surface area (up to 1400 $m^2 g^{-1}$), and a high nitrogen content (up to 9.3 at%). The nitrogen atoms are mostly bound in the form of pyridinic and pyrrolic forms.

Evaporation-induced self-assembly (EISA) process has also been tried for the preparation of NOMCs. Zhao *et al.* made tremendous contribution on the direct synthesis of NOMSc and established different methods for producing the same. Recently, this group has reported a controllable one-pot method to synthesize NOMC with a high N content up to 13.1 wt% by using F127, resol and dicyandiamide as a soft template, a carbon, and a nitrogen source, respectively. It was assumed that the resol molecules not only assisted the coordination of the template and the nitrogen precursors through a simple hydrogen bonding and electrostatic interactions but also provided the stability to the final ONMCs. The obtained NOMCs possess tunable mesostructures (*p6m* and *Im3m* symmetry) and pore size (3.1–17.6 nm), high surface areas of 494–586 $m^2 g^{-1}$.[87] Later, NOMCs were prepared via a two-step approach by using resorcinol (R), formaldehyde (F) and dicyandiamide (DCD) mixture as the precursor. In this approach, dicyandiamide, formaldehyde and resorcinol were pre-polymerized in the presence of Na_2CO_3 base catalyst to produce DCD-RF resol. The DCD-RF resol was mixed with a solution of triblock copolymer Pluronic F127 followed by the addition of 2 M aqueous HCl solution to facilitate the self-assembly and condensation in the second step.[88-90] Soluble precursors such as urea–phenol–formaldehyde resin has been used as nitrogen source for the preparation of NOMC spheres with the mean diameter of 240 nm and *Im*3*m* symmetry through a simple co-assembly with the polymeric surfactants under highly acidic conditions (Fig. 7B). By adjusting the ratio of urea to phenol, the nitrogen content of the NOMCs was controlled.[91-93]

An aqueous cooperative assembly route has been also employed for the fabrication of NOMC with the body centred cubic *Im3m* symmetry using resorcinol and hexamethylenetetramine (HMT) precursors, copolymer F127 as soft template.[158] Xue *et al.* and Choi *et al.* separately reported on a co-assembly approach based on Pluronic F127 mediated micelle to turn non-porous melamine and phenolic resin to a highly ordered mesoporous polymeric network (space group: *Im3̄m*) with a high nitrogen content of 18 at% (Fig. 7A).[94, 95] Amino-acids based cooperative assembly route has been introduced by Liu *et al.* In this process, basic amino acids such as L-lysine and L-arginine, as polymerization catalysts, two phenol derivatives, resorcinol and 3-aminophenol, were used as carbon and nitrogen sources and block copolymers F127 and P123 as the soft templates. The NOMCs exhibited a BET surface area up to 256 $m^2 g^{-1}$ with cubic *Im3m* and hexagonal *p6m* symmetry depends on the template used in the synthesis process.[159]

Yang *et al.* prepared nitrogen-doped carbon aerogels (NCAs) by direct chemical synthesis by using an organic sol–gel process with different mole ratio of tripolycyanamide (T) and resorcinol (R). Then, the organic aerogels were pyrolyzed to obtain NCAs. The N_2 adsorption isotherms of the NCAs exhibit a typical type IV isotherm with an obvious hysteresis loop at high relative pressure, which indicates that the prepared material has the mean pore diameter of 12.6 nm.[160] The pore diameter of the NCAs was controlled by tuning the concentration of the N precursors with a concomitant increase of the mesoporous

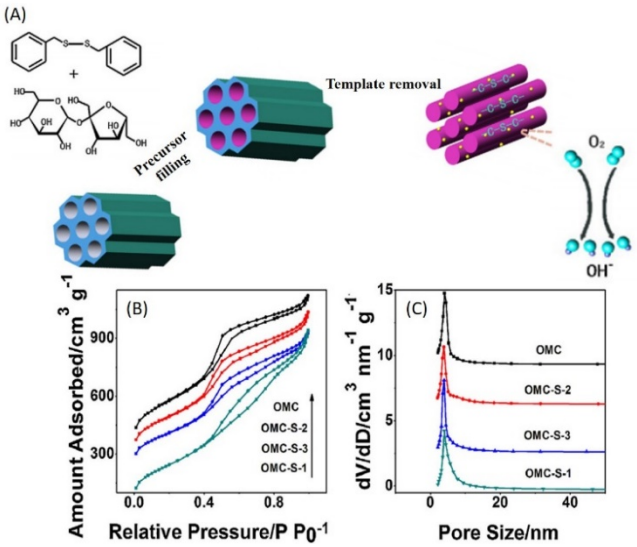

Figure 9 (A) Schematic presentation for the preparation of metal free OMC-S catalyst. The N_2 sorption analysis (B) isotherms of OMC and (C) their pore size distribution. Reproduced with permission from ref. 113. Copyright 2013, Elsevier.

fraction. Mesoporous carbon aerogels with 0-4% nitrogen content and surface area of 798 $m^2 g^{-1}$ were also prepared from 3D resorcinol (R) – melamine (M) – formaldehyde (F) aerogels by tuning the M/R ratio during the polymerization process.[161]

Dual soft templating technique, the combination of inorganic and organic template, has been recently receiving much attention for the synthesis of NOMcs with tunable morphologies and pore diameters. Qiao *et al.* demonstrated the synthesis of a series of nitrogen-doped mesoporous carbon spheres (NMCs) synthesis *via* a facile dual soft-templating procedure using a resorcinol-formaldehyde resin and melamine as carbon and nitrogen precursors, and a mixture of Pluronic F127 and Fluorocarbon (FC4) surfactants at different carbonization temperatures. The surface area (307-483 $m^2 g^{-1}$), pore volume (0.3-0.4 $cm^3 g^{-1}$), conductivity, and nitrogen-

doping (25-5.5 Wt%) concentration of the synthesized NMC were tuned by adjusting the nitrogen content and pyrolysis temperature.[99] Porogens combined with the Ni metal catalyst, melamine were added to control the graphitic nature and the porosity of the nitrogen doped porous graphitic carbon (NPGC) with a high surface area of 1027 $m^2 g^{-1}$ and a nitrogen content of 7.7 wt%.[96] On the other hand, Xia *et al.* used resol and dicyandiamide as the carbon and nitrogen precursor together with the porogen, TEOS to increase the specific surface area and the pore size of the NOMC to 1374 $m^2 g^{-1}$ and 7.4 nm, respectively.[97]

The polyhedraloligosilsesquioxanes (POSS) were also used as carbon source and assembled into hierarchically porous carbon structures by a block copolymer-assisted method using Pluronic P123 and F127 as the soft templates. The structure of the materials was tuned from hexagonal to cubic by changing the nature of the templates. The prepared NOMCs from POSS exhibited the specific surface area of over 2000 $m^2 g^{-1}$ and a large pore volume of 1.19 $cm^3 g^{-1}$.[162] Nitrogen-doped mesoporous carbon microfibers (NMCMFs) having surface area of 230 $m^2 g^{-1}$ were prepared via an evaporation-induced tri-consistent assembly of a triblock copolymer F127, resols and prehydrolyzed tetraethoxysilane on natural silk followed by pyrolysis.[163] Nitrogen-doped hollow mesoporous carbon spheres (NHCSs) were also prepared from 2,4-dihydroxybenzoic acid and hexamethylenetetramine as precursors and a mixture of Pluronic P123 and sodium oleate as a template, followed by thermal treatment at 650°C in ammonia atmosphere and subsequent high temperature annealing at 800-1000°C in nitrogen.[102] Instead of POSS, TiO_2 nanostructures were also used as inorganic templates in order to ease the synthesis process and obtaining the hierarchical micro/mesoporous framework. Nitrogen-doped hierarchical micro/mesoporous carbon nets were fabricated via supramolecular assemblies of block copolymer P123 with the assistance of dicyandiamide and TiO_2 nanostructures. The as-obtained carbon nets had the combination of both micro and mesopores that gave the specific surface area of approximately 2144 $m^2 g^{-1}$ and a high-level nitrogen doping with a nitrogen content of approximately 8.25 wt.[164]

Microwave technique which is considered as eco-friendly and energy saving approach for the preparation of nanomaterials has been used for the synthesis of NOMCs. Hung *et al.* used this technique and prepared NOMCs with a high specific surface area (794 $m^2 g^{-1}$ from carbon–silicate (C–Si) composites via co-condensation method using a melamine-formaldehyde resin oligomer as the precursor, and P123 triblock copolymer surfactant and sodium silicate as the soft and hard template, respectively.[101] Although the technique proposed was eco-friendly, it was found to be not suitable to obtain NOMCs with excellent textural parameters which are needed for enhancing the performance of these materials in many applications including energy storage and conversion.

NOMC with a cubic Im3m symmetry and rhombic dodecahedral single-crystal morphology was also prepared via organic–organic self-assembly of triblock copolymer F127, 3-aminophenol, and hexamethylenetetramine (HMTA) in aqueous base solution which had the specific surface area up to 1159 $m^2 g^{-1}$.[100] Guo *et al.* demonstrated the preparation of nitrogen-doped mesoporous network-like carbon (NMNC) via hydrothermal reaction of glucose solution followed by pyrolysis under ammonia atmosphere without using any external template. In this work, self-polymerization reaction of glucose molecules in aqueous solution occurred under hydrothermal conditions at 200°C. During this step, carbonaceous spheres were produced *via* aromatization and carbonization of glucose, due to abundant functional groups (such as -OH, -CHO, -COOH, etc) on their surfaces. These spheres were colluded to form colloidal network-like carbonaceous spheres through intermolecular dehydration and cross-linking with the dehydration reaction among the carbonaceous spheres. The obtained NMNC sample synthesized at 1000°C (NMNC-1000) exhibited extremely high specific surface area (2588 $m^2 g^{-1}$), well defined spherical shape morphology and mesoporous structure which are critical for mass transport and electrochemical applications.[98] This elegant approach presents a unique way of improving the specific surface area and the functional groups of the porous carbon materials. It can be expected that different combinations of the carbon precursors with inorganic metal or metal oxides will offer a new families of porous carbon nanostructures.

3.2 B doped ordered mesoporous carbons

Boron is one of the interesting element which can not only change the electronic and electrical properties of the carbon nanostructures but also the thermal stability under nitrogen or air after the substitution in the graphitic framework. Boron-doped ordered mesoporous carbons (B-OMCs) were prepared using an in-situ approach via organic-inorganic co-assembly, in which, boron-modified phenolic resins were used as the carbon precursor, tetraethyl orthosilicate as the inorganic precursor and reverse amphiphilic triblock copolymer ($PO_{97}EO_{186}PO_{97}$) as the soft template. B-OMCs with the BET surface areas of 1040 to 1255 $m^2 g^{-1}$ and pore volume of 1.55 $cm^3 g^{-1}$ were also prepared by co-impregnation and carbonization of sucrose and 4-hydroxyphenylboronic acid into SBA-15 silica template.[103, 104] EISA method has also been used for the preparation of B-OMCs in which resorcinol and boric acid were used as the precursors and Pluronic F127 as the soft template by combining the soft-templating and hydrothermal techniques.[106] The contents of boron was easily tuned with a simple adjustment of the boric acid to resorcinol ratio. A dense, continuous and amorphous boron-containing ordered mesoporous carbon (CB) films were also synthesized by using resols as a precursor for carbon, boric acid as a heteroatom precursor, and amphiphilic triblock copolymer F127 as a template. In this case, evaporation-induced triconstituent co-assembly method was used to obtain highly uniform films which was found to have high chemical inertness. This unique property of these films made them attractive for corrosion resistance applications.[105]

3.3 P doped ordered mesoporous carbons

Phosphorus belongs to the group V in the periodic table and has the same number of valence electrons as nitrogen atom.

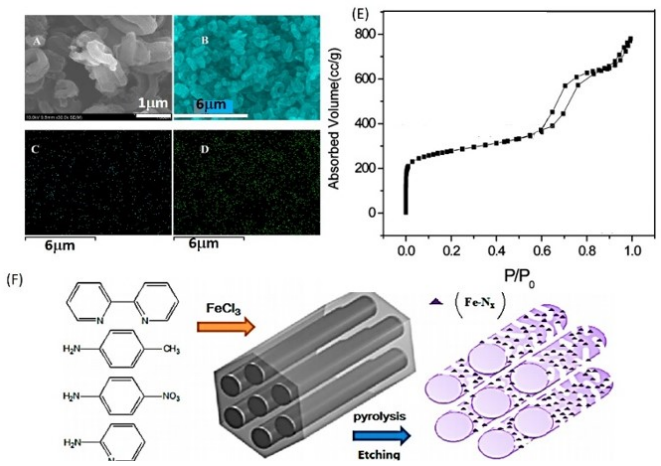

Figure 10 (A) SEM image of Fe-N-GC-900. (B) EDS for Fe, N, C, cl and O. (C and D) Elemental mapping of Fe and N respectively. (E) The nitrogen adsorption-desorption isotherm of Fe-N-GC-900 and (F) Schematic illustration of the synthesis of micro and mesoporous Fe-N-GC with ordered structure. Reproduced with permission from ref. 182. Copyright 2014, American Chemical society.

Although it has lower electronegativity than the N atoms, it exhibits almost similar chemical and electronic properties. However, phosphorous has a larger atomic radius and higher electron releasing ability than nitrogen, which make it as an excellent choice of dopant for carbon materials. Yu *et al.* reported on the first synthesis of micron sized phosphorus-doped ordered mesoporous carbons (POMCs) with different lengths through nanocasting method using SBA-15 mesoporous silica with different sizes, triphenylphosphine, and phenol as the templates, phosphorus and carbon sources, respectively. The realized POMCs exhibited a high BET specific surface area of 1182 $m^2 g^{-1}$, a large pore volume of 1.87 $cm^3 g^{-1}$ with a mean pore diameter centred at 3.4 nm.[107] The content of the P in POMCs by tuning the amount of triphenylphosphine. The amount of P in the carbon nanostructures also control the micropores in the samples. The specific surface area of the POMCs can be increased to 1338.8 $m^2 g^{-1}$ with a simple adjustment of the P content as it creates a lot of micropores in the walls (Fig. 8).[108] Through a careful adjustment of the P in the synthesis mixture, porous carbons with different pore parameters and tunable electronic properties could be obtained.

4. Binary atoms doped OMC

4.1 N and S co-doped ordered mesoporous carbons

Incorporation of dual heteroatoms in the OMCs provides unique chemical and electronic properties due to creation of defects and uneven charge distribution in the carbon framework structure. This will also change the hydrophobic or hydrophilic nature of the surface of the framework. In this section, we will show the methods used for different types of OMCs with dual heteroatoms dopants and their effect on the structure and properties of the materials. Guan *et al.* reported sulfur and nitrogen doped ordered mesoporous carbons (SN-OMCs) by using SBA-15 as a scavenger under CVD conditions with the ferrocene, pyrimidine and thiophene precursors. After etching away the iron metal and SBA-15 silica template, the resulting SN-OMC material featured distinctive bimodal mesoporous structure with a high BET specific surface area (~1100 $m^2 g^{-1}$) and uniform distribution of sulfur and nitrogen dopants.[109] Different mixed precursors such as pyrole-sulfuric acid and polythiophene-polypyrrole (PPy) were also used for the preparation of SN-OMC which had well-ordered porous structure and tunable N and S contents.[110] Instead of dual precursor, a single molecular precursor that contains both S and N was also used for the synthesis of SN-OMC. For example, SN-OMC were synthesized by nano-casting method using novel fluidic precursor – acrylonitrile telomer (ANT) and mesoporous silica SBA-15 as a hard template. SN-OMC contained both nitrogen and sulfur atom dopants with 4 and 0.6 at.% and also a high specific surface area of 1012 $m^2 g^{-1}$.[165] One step nanocasting technique in which diphenylthiocarbazone was used as a precursor for carbon, sulphur and nitrogen and SBA-15 as a nano hard template was also developed for the synthesis of SN-OMC.[112] Sulfur-doped ordered mesoporous carbons (OMC-S) with 1.5 wt% of sulphur and BET surface area up to 1261 $m^2 g^{-1}$ was prepared by using SBA-15 as the template and different amounts of sucrose and benzyl disulphide as the carbon and sulfur sources, respectively (Fig. 9).[113]

4.2 N and O co-doped ordered mesoporous carbons

Polyamides have been used as precursors for the synthesis of nitrogen- and oxygen- doped ordered mesoporous carbons (NOOMCs) by applying 3-aminobenzoic acid (MABA) and SBA-15 mesoporous silica as a precursor and template through liquid infiltration and thermal polymerization method. The obtained NOOMCs showed specific surface area up to 1084 $m^2 g^{-1}$ with a narrow pore size distributions and a mean pore diameter centred at 4.0 nm and nitrogen and oxygen contents as large as 6 and 6.4–11.5 wt.%, respectively.[166, 167] A mixture of molten fructose and urea, which are low cost and environmentally friendly precursor, has also been used for the fabrication of NOOMCs with 3D porous structure using mesoporous silica KIT-6 as a template. The obtained NOOMCs exhibited enhanced surface polarity and a high specific surface area and pore volume of 1197 $m^2 g^{-1}$ and 1.16 $cm^3 g^{-1}$ and heteroatom (O, N) contents of up to 19.1 wt.-%. However, the content of the dopants can be varied by tuning the quantity of the precursors.[168]

4.3 Ordered mesoporous carbons with B, P and/or N doping

The combination of P and B doping is another interesting dual dopant which afforded interesting structural and chemical properties. Hydrothermal doping strategy has been applied for the doping of boron and phosphorus into OMCs (HTBP) *via* a facile aqueous self-assembly using resorcinol as the carbon source, boric acid, and phosphoric acid as the heteroatom source. In this method, Pluronic F127 was employed as the soft template structure-directing agent. By varying the hydrothermal synthesis temperature, the concentration of B and P introduced in the OMCs can be controlled from 0.8 to 1.6 wt% and from 2.3 to 3.6 wt%, respectively.[52] This was due to different interaction of B and P with C precursors at a high

hydrothermal temperature. Triple hetero atom doping was also carried on the OMCs. N, B, and P-doped ordered mesoporous carbons with surface area up to 550 m^2 g^{-1} were prepared by applying SBA-15 as a nano hard template, a mixture of aniline, triphenylborane and triphenylphosphine as precursors through nano templating approach.[169] First nitrogen was introduced into the carbon matrix using aniline at 900 °C using Fe as a catalyst but the B and P atoms were incorporated into the N doped carbon matrix during the carbonization step.

4.4 Ordered mesoporous carbons with N and P doping

N and P co-doped 3D cubic ordered mesoporous carbons (NP-OMC) with bimodal mesoporosity and surface area of 1968 m^2 g^{-1} using saccharide as a carbon source along with urea and phytic acid (PA) as precursors for N, P and carbon, respectively, and cubic ordered Ia3d mesoporous silica KIT-6 as a hard template.[170] 2D N and P doped ordered mesoporous carbons (NP-OMCs) were also prepared by using sucrose, cyanamide and phosphoric acid mixtures and SBA-15 as the template. The prepared materials had a high BET surface area (1300 m^2 g^{-1}) and a large total pore volume of 1.64 cm^3 g^{-1}.[171]

5. Functionalised nanoporous carbon

The functionalization of the porous structures with organic molecules or inorganic metal or metal oxide nanoparticles can introduce new properties to the parent materials. This will expand the application potential of the OMCs in various fields including adsorption, separation, sensing, energy storage and conversion, and catalysis. The highly ordered porous structure with uniform pores and high specific surface area will provide enough space for the decoration of the surface with different functionalities which will enhance the properties that will be helpful for various applications. However, the fabrication of these functionalities inside the mesochannels without any agglomeration is quite challenging as the uniform distribution of these functionalities is the key to elevate the performance of these materials in several specific applications. Several reports have been published in the literature on metal, metal oxides, alloys, metal complexes, graphene, metal chalcogenides, and amines or amine complexes, and proteins functionalized OMCs. In this section, we will highlight on the different methods used for the immobilization of these functionalities in OMCs and how these functionalities create new properties to the final materials.

5.1 Metal nano particles immobilized nanoporous carbons

Li *et al.* described the immobilization of ultra-small size Pd nanoparticles (PdNPs) of 3.0 to 5.0 nm in size having uniform shape and without agglomeration in OMCs. In this method, nitrogen doped OMCs was used in order to provide anchoring support that would avoid the agglomeration of the small sized PdNPs. The incorporation of PdNPs in the OMC-N was performed in a two-step process, immobilization followed by reduction using aqueous solution of $NaBH_4$. The OMC-N of used in this study had 8.6 wt% of nitrogen which was introduced by post-synthesis treatment either with NH_3 or melamine over FDU type OMC materials.[172] Pd supported on CMK-3 (Pd/CMK-3) and

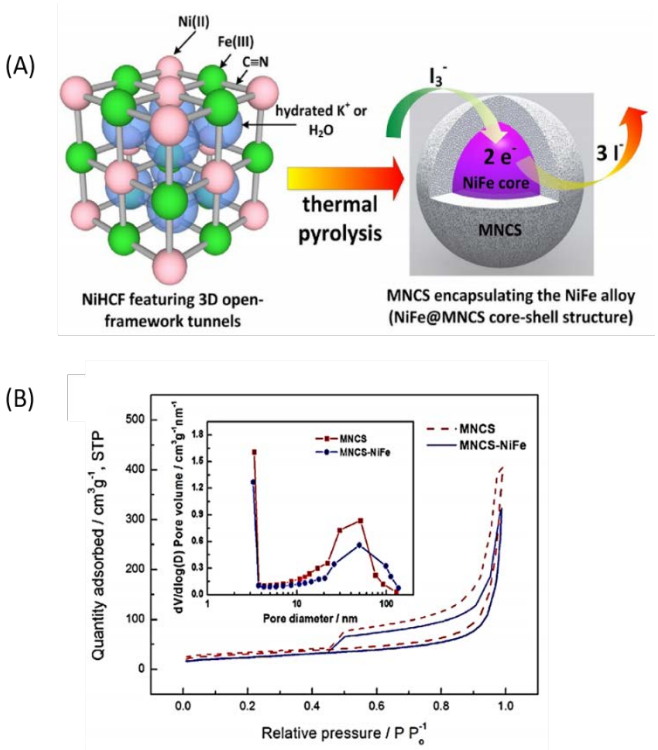

Figure 11 (A) schematic representation of core shell structure of NiFe@MNCS prepared by pyrolysis. (B) N_2 sorption isotherms of MNCS and MNCS-NiFe. (Insert), shows their pore size distribution. Reproduced with permission from ref. 190. Copyright 2016, Elsevier.

N-doped CMK-3 (Pd/N-CMK-3) materials were also prepared by impregnating CMK-3 powder with aqueous solutions of 1,10-phenanthroline and H_2PdCl_4 in two steps via ultrasound-assisted impregnation strategy followed by reduction using 30 vol% H_2/N_2 carrier gas at 200°C.[173] The N_2 sorption analysis of Pd/CMK-3 and Pd/NCMK- 3 showed typical type IV isotherms with clear hysteresis loops of H1-type, indicating that the mesoporous structure and the relatively uniform mesopores of CMK-3 were still preserved in Pd/CMK-3 and Pd/N-CMK-3 samples. Mesoporous carbon (MC-8) and nitrogen doped mesoporous carbon (NMC-8) which were prepared by Zr-SBA-15 as the template were also used as supports to get the Pd NPs of 4.0 and 2.5 nm. NMC-8 and MC-8 supports with surface areas of 1054 m^2 g^{-1} and 1489 m^2 g^{-1} were prepared by carbonization of mixture of xylene/furfuryl alcohol/oxalic acid with and without ammonia gas nitridation and the hard template method using large pore Zr-SBA-15. Zr atoms were introduced into the template to obtain large pore size in the template which would be beneficial for the decoration of highly dispersed Pd nanoparticles which were prepared by wet-chemical reduction method.[174]

As the post-synthetic approach was considered as a time consuming process, Ye *et al.* used a one-step co-calcination approach to prepare Pd NPs budded on NOMC (Pd/N-MCN) by using phenol, formaldehyde, melamine, and $PdCl_2$ as precursors for C, N and Pd and F127 through soft templating method.[175] In-situ synthesis approach was also adopted for the preparation of Pd NPs supported on nitrogen doped mesoporous carbon

(Pd/N-C) by direct pyrolysis of palladium dimethylglyoximate complex at 400°C under 10% hydrogen gas.[176] However, the obtained Pd/N-c exhibited relatively low surface area and pore volume of 124.1 $m^2 g^{-1}$ 0.158 $cm^3 g^{-1}$. An in-situ spray-drying method followed by the calcination route was used to fabricate the 3.8 to 4.5 nm sized Pt nanoparticles supported on nitrogen-doped porous carbon microspheres (Pt/C_N). This study showed that the size of the Pt NPs and N-doping into conventional carbon black were simultaneously controlled via spray-drying method and also by adjusting the precursor pH using ammonium hydroxide.[177] Nano-Sn/mesoporous carbon parasitic composite was prepared by Duan *et al.* using immobilization of Sn^{2+} solution and followed by H_2 gas assisted reduction.[178] Mesoporous carbon used to anchor Sn nano particles has an open porous structure with less than 10 nm filmy pore walls, and the pore diameter is about 30–70 nm, which has been prepared using sucrose and $CaCO_3$ template. The open porous structure of mesoporous carbon was highly favourable for the filling of tin nanoparticles of 10–30 nm which were uniformly distributed in the pores of carbon matrix.

Cobalt and iron doped NOMCs (C–N–Co and C–N–Fe) with tunable nitrogen content (up to 9.5%) was prepared from direct carbonization of vitamin B12 and the polyaniline-Fe (PANI-Fe) complex,[179] respectively and silica nanoparticles, SBA-15, and montmorillonite were used as templates. The specific surface areas of these C–N–Co samples obtained by using the silica nanoparticles, SBA-15, and montmorillonite were 568, 387, and 239 $m^2 g^{-1}$, respectively. These values were much higher than that of VB12/C (134 $m^2 g^{-1}$). The mesopore size distributions of the above samples were centred at 12.0, 3.5, and 4.5 nm, respectively, according to the BJH model.[180] Mesoporous C-N-Fe material was also prepared by using poly(4- vinylpyridine) and iron chloride as the precursors and SBA-15 as a template.[181]

The mixture of metal and hetero atom doping provides much better chemical and electrical properties than that of OMCs doped with either heteroatom or metal nanoparticles. A series of $Fe–N_x$ doped ordered hierarchically micro- and mesoporous carbon (Fe–N–GC) materials were prepared through the nanomoulding synthesis procedures by direct pyrolysis of the various nitrogen containing heterocyclic compounds such as 2,2-bipyridine, p-aminotoluene, p-nitroaniline, and 2-amino pyridine, respectively, and iron chlorides in the confined mesoporous channels of SBA-15 (Fig. 10).[182] Fe–N–GC had a high specific surface area of up to 929 $m^2 g^{-1}$, which was composed of mesopore surface area of 499 $m^2 g^{-1}$ and micropore surface area of 430 $m^2 g^{-1}$, corresponding to their narrow mesopore size distributions centred at 6.3 nm and micropore size centred at 0.37 nm. Li *et al.* used "task-specific" approach by using ferrocene-based ionic liquid $[FcN][NTf_2]$ (Fe-IL) as a metal-containing feedstock with a nitrogen-enriched ionic liquid $[MCNIm][N(CN)_2]$ (N-IL) as a compatible nitrogen content modulator and SBA-15 template to prepare mesoporous iron-nitrogen-doped carbon (Fe^X@NOMC).[183] Fe^X@NOMC had a nitrogen content up to 11.9 wt% and highly ordered mesoporous structure, a high surface area (411–506 $m^2 g^{-1}$), pore volumes (0.71–1.05 $cm^3 g^{-1}$) and pore size distribution was highly uniform centred at 5.6 nm.

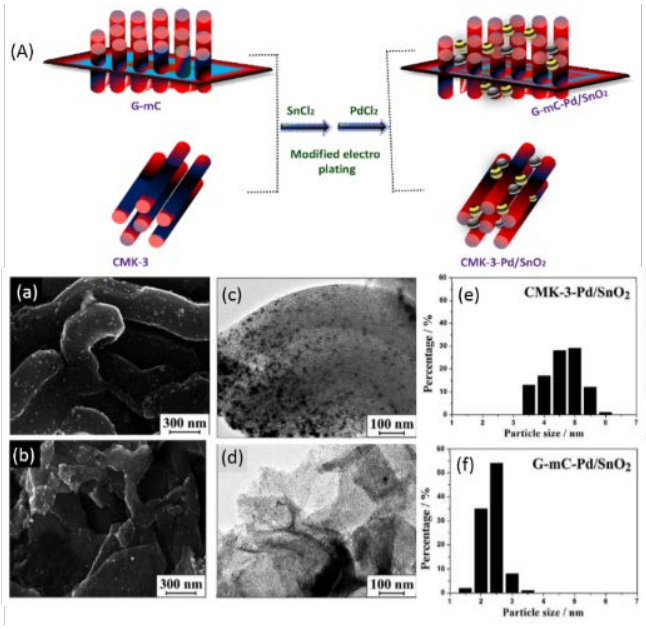

Figure 12 (A) Schematic representation for the synthesis of CMK-3-pd/SnO_2 and G-mc-pd/SnO_2. (a and C) High resolution SEM and TEM images and (e and f) Histograms of particle size distribution of CMK-3-pd/SnO_2 and G-mc-pd/SnO_2 respectively. Reproduced with permission from ref. 204. Copyright 2016, Royal society of Chemistry.

Ordered hierarchically porous carbon co-doped with N and Fe (Fe-NOHPC) was prepared by Deng *et al.* through an EISA process followed by carbonization under ammonia by using resol, F127 and $FeSO_4$ as carbon precursor, soft template and iron source, respectively.[184] Fe-NOHPC possessed N and Fe concentrations of 3.54 and 0.18 at%, with an ordered hierarchically porous structure, a high surface area (1172.5 $m^2 g^{-1}$) and pore volume of 1.03 $cm^3 g^{-1}$. Ahn *et al.* reported on the preparation of well dispersed Fe nanoparticles within N-doped mesoporous carbon nanofibers (Fe-NMCNF) with surface area and pore volume up to 468.9 $m^2 g^{-1}$ and 0.95 $cm^3 g^{-1}$ from polyacrylonitrile (PAN) and iron(II) phthalocyanine mixture using electrospinning followed by reduction of H_2 gas.[185]

Cobalt nano particles of 6.7 to 12.8 nm in size were immobilized on the OMC-N materials through excessive wetness impregnation method using $Co(NO_3)_2$ precursor by auto reduction process without using any external reductant. The size of the Co nano particles was reduced from 12.8 to 6.7 nm with an increase in the nitrogen content in the NOMC samples from 5.8 to 10.4 wt%. However, the size of the particles was increased to 19.4 nm when OMC without any N dopant was used, confirming the anchoring role of N functionalities in OMCs.[186] Soft-templating method was also used for the in-situ preparation of Co nanoparticles in NOMCs. A 3D cobalt-nitrogen-doped ordered macro-/mesoporous carbons (Co-N-OMMCs) with 9.64 wt% of nitrogen and 1.52 wt% of Co were prepared from a mixture of resol/dicyandiamide (DCDA)/$Co(NO_3)_2$ through a dual-templating approach using opal colloidal silica spheres as a macroporous mold and triblock copolymer Pluronic F127 as a mesoporous template. In the synthesis process, an aqueous/ethanolic solution containing resol, DCDA, $Co(NO_3)_2 \cdot 6H_2O$ and F127 was infiltrated into the void spaces of the silica opal template, and the mesostructure was formed during an EISA process.[187] The nitrogen adsorption/desorption isotherms of Co-N-OMMCs samples

were of type IV with a high specific surface area and a total pore volume of 679 m^2 g^{-1} and 1.71 cm^3 g^{-1}, respectively, with an average pore size centred at 11.2 nm. Direct polymerization of a reverse copolymer PPO-PEO-PPO/$[Ni(H_2O)_6](NO_3)_2$/phenolic resin self-assembled in ethanol medium yielded highly decorated Ni nanoparticles in the OMCs. During the pyrolysis process, Ni^{2+} was reduced into metallic Ni nanoparticle which were uniformly distributed onto the surface of OMCs.

5.2 Alloy nano particles incorporated nanoporous carbons

The combination of metals can introduce unique electrical and electronic properties as it tunes the electronic structure of the nanoparticles. In addition, the alloy system has also been employed in many catalytic systems owing to their ability to lower the activation barrier system. Most importantly, the concept of alloying can also significantly reduce the cost of the materials. By decorating these alloys system on highly ordered support system, the active specific surface area or the

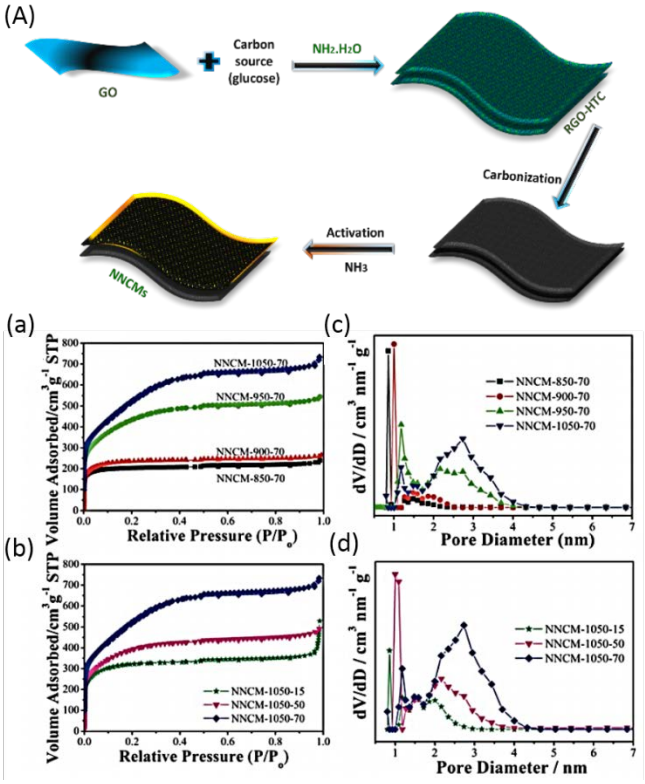

Figure 13 (A) Schematic representation of the synthesis method of NNCMs. (a and b) The N_2 adsorption-desorption isotherms of NNCMs and (c and d) the pore size distribution of NNCMs. Reproduced with permission from ref. 209. Copyright 2016, Royal Society of Chemistry.

properties of the alloy nanoparticles can be significantly altered. In this section, we will summarise different methods employed for the fabrication of various alloys or bimetallic doped OMCs and how these nanoparticles affect the properties and of the final materials.

Maiyalagan *et al.* reported on the deposition of Pt-Ru alloy nanoparticles of 3.8 nm size with atomic ratio Pt/Ru (1:1) and 20 wt% of metal loading (Pt-Ru) in the highly ordered mesoporous carbon CMK-8 by using sodium borohydride based wet chemical reduction method.[188] The noble metals were co-doped with transition metal nanoparticles inside the mesochannels of OMCs in order to reduce the total cost of these catalytic systems. Wang *et al.* described the synthesis of PtCo bimetallic nanoparticles with a molar ratio of Pt:Co of about 1:1.1 supported on the NOMC framework with ultrafine dispersion and uniform particle size distribution (ca. 1.5 nm) through the wet impregnation method followed by the reduction at 500°C in a flow of 5% H_2 in Ar.[189] The surface area, pore volume and pore size of PtCo/NOMC were 507 m^2 g^{-1}, 0.41 cm^3 g^{-1} and 6.5 nm, respectively. NiFe alloy nanoparticle encapsulated in mesoporous nitrogen-doped carbon sphere (MNCS) were also synthesized using direct thermal pyrolysis of nickel hexacyanoferrate at 500°C without using any external template (Fig. 11).[190] Pd_3Cu alloy nanoparticles were also encapsulated inside the mesochannels of NOMCs using $PdCl_2$ and cupric acetate as precursors for Pd and Cu, and sodium citrate as a reducing agent *via* wet chemistry method.[191]

5.3 Metal oxides and metal chalcogenides functionalized nanoporous carbons

Metal oxide nanoparticles have been widely used in various applications. However, the textural properties of these oxides are the limiting factors which affect the final performance of the materials in different applications. On the other hand, metal chalcogenides are unique semiconducting materials and they complement semi metallic graphene. They are widely employed in electronic and optoelectronic applications owing to their small energy band gap. By functionalizing these metal chalcogenide or metal oxides nanostructures inside the mesochannels of OMCs, new advanced porous materials with improved properties can be realized. Shen *et al.* reported on the synthesis of mesoporous $Li_4Ti_5O_{12}$/C nanocomposite by post functionalization of acid treated CMK-3 through the sintering of lithium acetate and tetra butyl titanate precursors at 750°C for 6 h in a nitrogen atmosphere.[192] The small $Li_4Ti_5O_{11}$ nanocrystals were nicely interconnected in the mesochannels of OMCs which significantly increased the ionic and electronic conductivity of the composite system. These factors are critical for energy storage applications, especially in battery. A significant reduction of the specific surface area from 1138 m^2 g^{-1} to 127 m^2 g^{-1} confirmed the formation of these $Li_4Ti_5O_{12}$ nanocrystals inside the mesochannels of the OMCs.

Meso-porous C–TiO_2 nanocomposites with anatase TiO_2 whose contents ranging from 40wt% to 87wt was prepared through EISA strategy by using $TiCl_4$ and/or $Ti(OC_4H_9)_4$ as titanium sources, phenolic resin as the carbon source, and triblock copolymer F127 or P123 as the structure-direct agent.[193] Nitrogen-doped urchin-like Fe_3O_4@C-N composites were prepared by a simple hydrothermal carbonization of hydroxyferric oxide (α-FeOOH) coated with polydopamine (PDA) at 400 °C under Ar atmosphere.[194] Cobalt oxide particles of 30-50 nm encapsulated in nitrogen co-doped carbon (Co–N/C) bi-catalysts were prepared *via* a one-pot approach by using dopamine hydrochloride (DA) and formaldehyde (F) as a nitrogen containing carbon sources, P123 as a soft template and cobalt acetate as a precursor for Co.[195] Iron sulphides ($Fe_{1-x}S$) embedded in nitrogen and sulfur dual-doped mesoporous

graphitic carbon spheres ($Fe_{1-x}S$/N, S-MGCSs) were synthesized via a two-step pyrolysis followed by acid leaching process. The preparation of $Fe_{1-x}S$/N, S-MGCSs involved the coordination of Fe^{2+} with PDA followed by carbonization and leaching of iron oxides and finally vulcanization under thiourea. The prepared $Fe_{1-x}S$/N, S-MGCS materials had the specific surface area and pore volume up to 371.4 $m^2 g^{-1}$ and 0.41 $cm^3 g^{-1}$, respectively.[196]

N-doped mesoporous carbon capped with MoO_2 nanobelts (MoO_2@NC), a core–shell-structured nanocomposite comprising a MoO_2 nanobelts core and an N-doped mesoporous carbon shell was prepared by *in situ* thermal reduction of MoO_3 nanobelts, accompanied with the N-doped carbon from the polypyrrole precursor *via* one-step annealing process.[197] Sun *et al.* described a facile melt–impregnation method for the confinement of Se_2S_6 ultra small nano crystals into the nitrogen-doped mesoporous carbons (Se_2S_6/NMCs).[198] In the synthesis of Se_2S_6/NMCs, selenium and sulphur melts are miscible with each other at 500°C and then infiltrated into the mesopores of NMCs. The composite Se_2S_6/NMCs had a considerable amount of mesoporosity with a specific surface area of 159 $m^2 g^{-1}$ and pore volume of 0.8 $cm^3 g^{-1}$.

5.4 Graphene functionalised nanoporous carbon

Graphene, a two-dimensional form of carbon layers with crystalline honeycomb lattice and their layers are connected by relatively weak forces, has received substantial importance due to the open porous structure accrued from the stacking. This typical behaviour of graphene tends to exhibit exclusive physical and chemical properties due to its ease in stacking to form graphite and can be rolled to form nanotubes or spherical fullerenes. Although graphene is a fascinating material with an effective surface area, the undeveloped porous structure limits the opportunity in developing the graphene into useful multi-dimensional flexible materials. Recently, various constructive ideas have been executed to build the graphene with nanoporous structures and to utilize their surface defects originated from imperfections of the crystal lattice, for immobilisations and anchoring various nanoparticles or by fabricating hybrid graphene materials. Noteworthy, the chemically synthesised graphene through coupling reactions are usually said to be nanographene and nanoporous graphene which is the hot topic in the development of new generation materials.

Despite of graphene being one of the highest surface area materials, the graphene derived materials pronounce a very low surface area when compared with the single layer graphene especially due to the π stacking exhibited by the graphene sheets. Therefore, it is wise to implement porosity on the graphene based materials to increase the specific surface area and so far, there are four effective ways to do the purpose namely: exfoliation technique, templating methods, stacking/aggregation and reduction of graphene oxide to form core or hydrogels and finally integrating graphene using spacers. In this section, we will focus on the functionalization of graphene on the mesoporous channels of OMCs.

Porous and non-porous carbon nanofibers (PCNF and CNF) were prepared and used as spacers to synthesise high surface area 2D graphene (G) prepared at 900 ˚C.[199] In the typical synthesis, graphite powder was chemically modified through acidification in two steps to get oxidized graphite and on exfoliation and lyophilisation through ultra-sonication process, the graphene oxide (GO) powder was obtained. The resulted GO

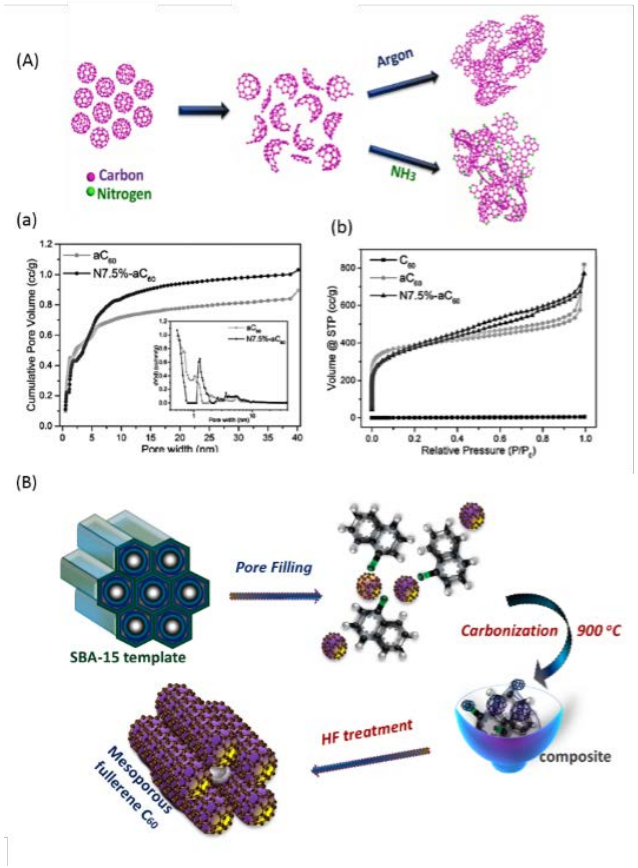

Figure 14 (A) Schematic illustration of KOH activation on fullerene C_{60} molecules. (a) Pore size distribution of C_{60}, aC_{60} and N7.5% aC_{60}. (c) N_2 adsorption-desorption isotherms of C_{60}, aC_{60} and N7.5% aC_{60} and (B) Schematic representation for the first successful synthesis of polymerised highly ordered nanoporous fullerene C_{60} with crystalline wall structures. Reproduced with permission from ref. 213 and 214. Copyright 2016 and 2017, Wiley-VCH Verlag GnbH & Co. KGaA, Weinheim.

powder was mixed with the PCNF and CNF to obtain G-PCNF and G-CNF. The 2D graphene sheets were further functionalised by Pt to form Pt/G-PCNF and Pt/GNF through magnetic stirring and the Pt was reduced by refluxing, following the polyol reduction method. The difference between the porous and non-porous 2D graphene materials were demonstrated through the FESEM, where the G/PCNF showed mesoporous structure and the rough surface of the porous material provided more active sites for the catalyst deposition. Like spacers, other bridging molecules were also used to bridge the graphene sheets. For example, the synthesis of porous carbon nanosheets by using asparagine, which is an amino acid and used as a bridging molecule to connect the GO and the electrostatically connected GO served as the structure directing agent to form porous nanosheets was reported.[200] The GO was also exfoliated into discrete sheets through ultrasound and the individual sheets were then converted into 3D graphene composite (GN) by depositing Au nanoparticles and reduced by using PEG. Thus,

prepared 3D-AuNPsGN increased the active surface area for electrochemical sensing of the antibodies.[201]

It is well known that, the multilayer graphene (MLG) has higher mechanical strength and at the same time, has lesser properties compared to that of single layer graphene. With the objective of allowing wide range applications of MLGs, the MLG was combined with porous carbon (PC) through CVD process to form hybrid MLG/PC core shell films, where their structure was controlled by nickel gauze which was used as the template and their pore sizes were controlled by the CVD reaction time and tuning the methane feeding rate. Since the hybrid MLG has the characteristics of graphene and porous carbon, the film could maintain the structure that fetched a huge advantage containing MLG shell and PC core, with the nanoporous.[59] PC have shown tremendous advantage owing to their excellent structural and textural properties and ones again porous carbon microspheres (PCs) in combination with graphene to forge hybrid film was reported by Hongbo *et al.*[202] They followed three conventional steps namely reduction, leavening and compression to fabricate the hybrid flexible porous film. The porous carbon microspheres moved between the pore walls of the flexible graphene nano sheet (GNS), prevented the stacking of the GNS and kept the open porous system in confinement facilitating electrochemical performance.

Although porous carbons are fascinating, they relatively have poor electrical conductivity. For example, CMK-3 has a poor electrical conductivity and cyclability compared to the graphene. To combine the bright side of porous carbon (CMK-3) and graphene, in 2015 Nan *et al.* synthesised graphene based 2D porous carbon which was used as a support for the functionalization of Pt nanoparticles.[203] In the following year, the same group has demonstrated the functionalization of graphene based mesoporous carbon with Pd and SnO_2 nanoparticles as shown in Fig. 12. They used the SBA-15 silica template and graphene to prepare graphene mesoporous carbon (G-mc).[204] By following the electroless plating method, Pd/SnO_2 were introduced to the G-mC to form G-mC-Pd/SnO_2. Thus, metal functionalised porous graphene exhibited decrease in the surface area and pore volume, suggesting that the Pd/SnO_2 were located inside the pores of G-mC. This was confirmed by TEM images that show only a few large Pd and SnO_2 nanoparticles found outside the surface of CMK-3. It was found that the particle size of the G-mC was close to the particle size of the Pd/SnO_2 nanoparticles and was conductive compared to the CMK-3-Pd/SnO_2.

Graphene oxide was also coated on the polyacrylonitrile derived porous carbon (PAN) that is rich in nitrogen and oxygen species. By heating the coated PAN (PAN/GO) followed by activation and washing with acid produced the final product. The oxygen present in the final product inhibited the graphene layer stacking and provided strong interactions between the sheets.[205] A simplified strategy of synthesising graphene/porous carbon was reported earlier in 2015, where the CNT was coated with activated porous carbon (CNT@AC) and was used as spacers dispatched in-between the graphene sheets (RGO/CNT@AC). The coated CNTs played a vital role in inhibiting the restacking of the graphene layers displaying a better electrochemical performance compared to that of pure CNT/graphene.[206] The specific surface area was lower and the porous structure of the coated CNT was not controlled through this method. In comparison to this study, the eminent ordered porous carbon prepared from SiO_2 colloidal crystals was reported as a better spacer by Fei *et al.* and fabricated GN/PC aerogel. Their fabrication process involved the ultra-sonication of the PC and graphene oxide (GO) suspensions and after hydrothermal process at 180 ˚C, graphene/porous carbon hydrogels were obtained. Interestingly these aerogels exhibited enhanced rate performance when compared with the individual GN and PC.[66] Similar to the previous report, the pore structure of the graphene materials was simply controlled by assembling the graphene into three-dimensional structure by hydrothermal treatment. The agglomeration of the colloidal GO suspension after 150 ˚C resulted in hydrogel and dried, to assimilate the sulphur. The bounded sulphur was uniformly anchored to the graphene sheets. The porous structure thus produced was used as a model to study the influence of pores on electrochemical performances.[207] The graphene treated with PC was also doped with nitrogen and activated by adding KOH via insitu polymerisation and was used as an anode.[208] N-doping was also done through insitu carbonisation technique where glucose was mixed with GO to form RGO-HTC carbon in large scale and was activated using NH_3 to form nano-sandwich N-doped carbon materials (NNCMs)[209] as shown in Fig. 13. Among the various NNCMs synthesised at 850, 900, 950 and 1050 °C, NNCMs prepared at 1050 °C exhibited a high surface about 1959 $m^2 g^{-1}$.

5.5 Fullerene based porous carbons

Fullerenes are the purest forms of carbons connected by strong hexagonal and pentagonal rings, where their structure differs from varieties of fullerenes based on their 5 and 6 ring units. The major difference between the graphene and fullerene is that, the fullerenes have a very high thermal and mechanical stability but have a very poor surface area and electrical conductivity. Controversial to fullerenes, graphene has a very poor stability but has a high surface area and high electrical conductivity. However, the high symmetrical structure of fullerenes is unique compared to any other existing carbon materials so far, that provides opportunities to the scientific world to explore their structural properties for various applications. At the same time, the rigid structure of fullerenes could only be modified organically but due to its high thermal and mechanical stability it is not very easy to be fabricated into nanoporous fullerene structures. The rare reports on fullerene nanoporous carbons are discussed in this session.

Considering the effect of templating methods, Duncan *et al.* tried to self-assemble the fullerene by immobilising the fullerenes on the graphite surface, where the pores were generated by 1,3,5-benzenetricarboxylic acid to form fullerene monolayer.[210] Inspired by the concept of self-assembling process, the single crystal C_{60} (FNR) and single crystal C_{60}-nanotubes (FNT) were synthesised through liquid-liquid interfacial precipitation technique. These nanostructures can be transformed into nanoporous carbon (HT-FNR and HT-FNT)

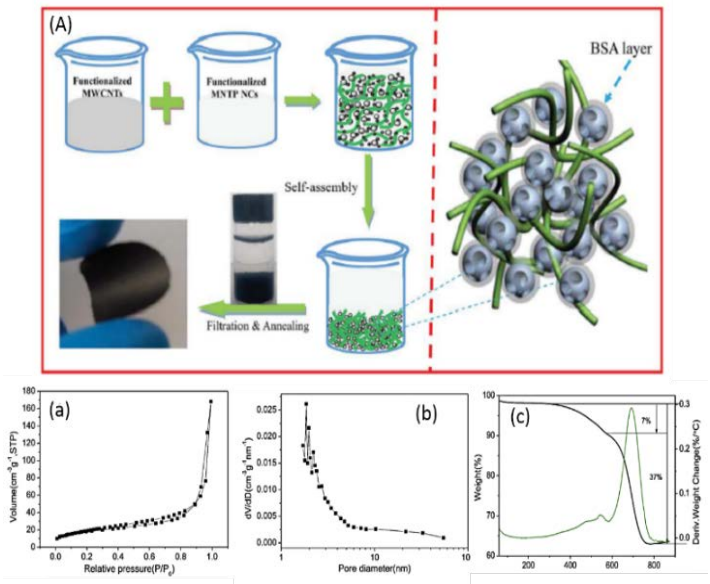

Figure 15 (A) Schematic illustration for the fabrication of MNTP NCs/MWCNTs intermediate and self-supporting MNTP C MWCNTs electrodes. (a and b) N_2 isotherm and pore size distribution of MNTP C MWCNTs electrodes and (c) their TGA/DSC curves. Reproduced with permission from ref. 241. Copyright 2017, Royal Society of Chemistry.

with random graphitic nature after the high temperature and pressure treatment. Finally, to understand the structural transformation, theoretical calculations were applied. It was proved that high temperatures and pressures favor the formation and breaking of the interfullerene bonds which is the key for the transformation of 0D fullerene nanostructures into 2D graphitic nanostructures.[211] The exfoliated graphite was used as a carbon adsorbent and the polycrystalline C_{60} powder was mixed along to be adsorbed by the exfoliated graphite. The adsorbed C_{60} on thermal treatment evaporated and the remaining particles were cold pressed.[212] The porous carbon, based on fullerene and graphite was studied for electrical, optical and various other properties. One step further in the development of fullerene based porous carbon, Tan *et al.*[213] activated the fullerene using KOH and doped the fullerene based porous carbon by nitrogen to form N-aC_{60} through thermal annealing as shown in Fig.14. Interestingly the surface area of the activated fullerene based porous carbon was 1457 $m^2\ g^{-1}$ while the N-doped fullerene based porous carbon was 1274 $m^2\ g^{-1}$. The nanoporous fullerene is a new area and the discussion on the fullerene based porous carbon signifies that a wide knowledge is necessary to understand the bonding nature between the self-assembled fullerenes and the interactions between the porous fullerenes and various other factors like polymerisation, ordered porous structures are yet unknown. Very recently, a striking report by Vinu *et al.* proved the successful fabrication of highly ordered mesoporous fullerene (Fig. 14 B), with crystalline walls for the first time. The prepared material showed excellent energy storage and conversion properties. This discovery is going to make a huge impact in the field of fullerene. We believe that this research would attract many researchers to work in this new area of research as they would be useful for a wide range of applications in the near future.[214]

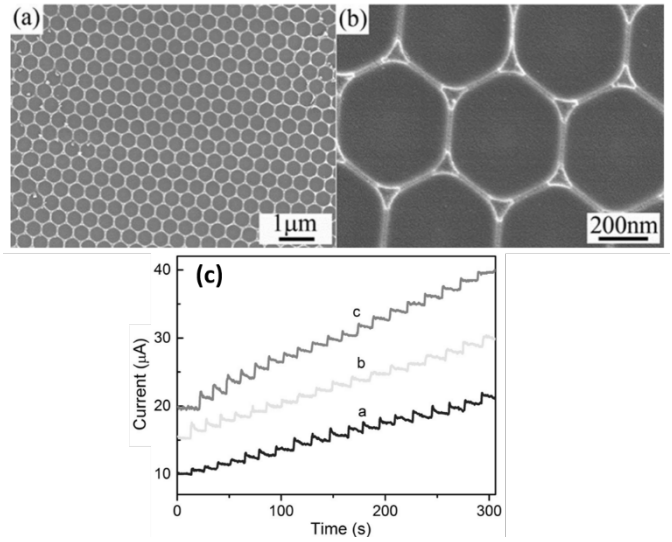

Figure 16 FESEM image of fabricated porous carbon film, (a) Low magnification, (b) high magnification and (C) The response of biosensor corresponding to different GOD concentration, curve a) 1 mg/ml, curve b) 5 mg/ml and curve c) 10 mg/ml. Reproduced with permission from ref. 251. Copyright 2014, Wiley-VCH Verlag GmbH & Co. KGaA, Weinheim.

5.6 Amine functionalised nanoporous carbon

Nanoporous carbons are unique due to its high surface area, large pore volume with highly ordered porous structure. Regardless of their excellent features, they limit themselves from surface-active sites due to their hydrophobic nature. The lack of active sites highly hinders the materials from various applications like sensing, separation, physisorption and chemisorption, catalysis, etc. The hydrophobicity of these carbons can be tuned by functionalisation, especially with organic groups rather than using metal or metal oxides for functionalisation. In the below session, the functionalization using amines are discussed, since amines have relatively a high affinity to bond with carbon. So far, two main strategies such as grafting and impregnation have been adopted for introducing amines to the porous materials.

CMK-3 was functionalised by more than one amine groups likely 1,2-diaminopropane, trans-1,2-diaminocyclohexane and *o*-phenylenediamine through C-N cross coupling reaction. The aliphatic, cyclic and aromatic amines formed amide bonds on the surface of the CMK-3 material offering the catalytic sites to produce carbonyl compounds, without any destruction to the long-range ordering of the CMK-3 material.[215] To increase the heterogenicity of the carbon, Zakova *et al.* used five different sources of amine to work on amine-amide combinations. The carbon nanoparticles (CNP) were modified with amides to manifest COOH groups and refluxed with $SOCl_2$ to yield -COCl groups to start the reaction of CNP with amines.[216] Although the XPS and Raman spectra confirmed the modification of the CNP surface with the expected bonding, the N_2 adsorption-desorption showed a tremendous decrease in the surface area after the grafting process.[217] Amine grafting was also carried out in porous polymeric networks,[218] carbonaceous nanomaterials,[219] porous carbon monoliths[220] and MCM-41.

Among these amine functionalised materials, MCM-41 invigorated with carbon nanoparticles fetched bimodal porous structure to the resultant amine functionalised MCM-41 carbon

material. The advantage of the bimodal porous structure on amine functionalisation is the increase in the adsorption phenomena.[221] The trendy way of fabricating amine functionalised porous polymer[222] and organic polymers[223] which did not require any activation process was also reported. However, the cost was comparatively higher that limits the large-scale production.

5.7 Nanoporous carbon with metal nanoparticles from metal complexes

Metal complexes, generally known as coordination compounds are complexes that form intermolecular bonds between the metal acting as an electron accepter and ligand acting as an electron donor. The ligands are also termed as mono, di, tri, or poly-dentate depending on the number of electron it donates. For instance, if the ligand donates more than one pair of electron, the bonding between the metal ion and the ligand will be more stable. The ability of the porous carbons to allow the accessibility of small ions or metals due to their open channels make them as excellent candidates to fabricate nanoporous carbons with metal complexes.[224]

Copper(II) acetate[225] and copper(II) /silver(I) carboxylates were immobilised in the nanoporous carbons and their combination was used to study the dihydrogen complexion.[226] Foley *et al.* also reported the preparation of simple complexes of copper and silver loaded nanoporous carbon which showed highly selective adsorption of 1- 3 mol of hydrogen per metal center. It was assumed that the cooperative interactions between hydrogen, the nanoporous structure, and the highly dispersed metal centers of the complexes in the mesochannels supported the enhancement of the hydrogen adsorption.[225] It was also reported that highly ordered nanoporous carbons with metal nanoparticles were prepared through a simple carbonization of magnesium polyacrylate complex[227] and benzoate metal complexes[228] and exhibited a high specific surface area of ca 1050 m^2/g. However, the surface area of the materials was significantly enhanced (1466.4 $m^2\ g^{-1}$) when the composite was activated using KOH. By using the same carbonisation method, the cobalt ion absorbed polyaniline (PANI) was converted into Co-C-N complex, which showed excellent electrocatalytic activity.[73] The metal complex derived porous carbon was also functionalised with selenium and the selenium interacted to the metal complex porous framework through Se-O and C-O bond.[94]

5.8 Protein functionalised nanoporous carbon

Biomolecules are organic molecules derived from living tissues composed mainly of carbon and hydrogen. Among the four class of biomolecules namely carbohydrates, proteins, lipids and nucleic acids, the proteins are of great interest due to their polymeric structure since they are the natural heteropolymers containing carboxyl group and amino group connected by peptide bonds. But, the common drawback of protein is its denaturation,[229] physical instability and side reactions caused by the hydrogen bonds. Therefore, the importance of trapping the proteins for useful applications has been realized since centuries and various methods have been developed to serve the purpose. However, to best describe the approaches adopted so far to immobilise the proteins can be split into three categories, they are immobilisation through covalent bonds, non-covalent bonds which includes hydrogen bonds, electrostatic and van der Waals interactions and finally through encapsulation. The immobilisation can also be described as adsorption process where a molecule can be entrapped or adsorbed on to a support through the three types of interactions said above.

The nanoporous carbon can serve as an excellent substrate for the immobilisation of proteins[230, 231] owing to its high surface area, narrow pore size distribution and tuneable pore sizes that can be suitable for the proteins to entangle into the pores. Moreover, the hydrophobicity of the nanoporous carbon protects the immobilised protein from solubility and various other factors like mechanical and thermal instability and can even cease the denaturation of proteins.[232] The commercially available microporous carbon with small mesopores (Norit DLC super 50) was investigated for adsorption of angiotensin converting enzyme (ACE) to inhibit the peptides[233] and food protein[234] and was monitored through the N_2 adsorption desorption process. Likewise, two different types of aprotinin namely bovine serum albumin and bovine pancreatic trypsin inhibitor was adsorbed in an open structured hydrophobic carbon aerogel (C1) consisting of mesopores and their adsorption capacity was compared with the commercially available hydrophilic nanoporous carbon (C2) having higher surface area than C1. Interestingly, the C1 exhibited the highest adsorption capacity for both the proteins. This clearly shows that the mesoporous carbon has a superior capacity over other porous carbons due to their pore size and allows the migration of the proteins inside the porous channels due to the hydrophobic nature of the carbon compared with the commercially available hydrophilic carbon which tends to the agglomeration of proteins.[235, 236]

Apart from immobilisation, proteins were also used as a carbon precursors to fabricate 3D porous carbon[237, 238] and activated nanoporous carbon with high surface area and functionalised with organic groups like sulphur[239] or metal oxides like MnO_2[240] to impose electrical conductivity. Since the proteins can denature easily by physical environment like pH, high temperature and acidic conditions, instead of proteins being used as carbon source, alternatively protein themselves were used as templates to fabricate mesoporous nanocrystals as shown in Fig. 15, wherein the mesoporous $NaTiO_2$ (MNTP NC) was coated with BSA and was dispersed in the oxidised multiwalled carbon nanotube solution (MWCNTs). Finally, the MWCNT and MNTP NC were assembled through electrostatic interaction and thermally annealed to form MNTP/MWCNT film.[241] This film exhibited surface area of only 88.7 $m^2\ g^{-1}$ with the typical type IV isotherm and they were analysed to be composed of 63 wt% MNTP and 30 wt% MWCNT.

In another report, the interaction of plasma or the blood proteins with graphitic carbon modified SBA-15 were also investigated and concluded that the graphitic domains influence the interactions of complex protein-nanoparticle.[242]

From the above reports on protein assisted templating methods, it could be noticed that the bare protein needs a templating substrate which otherwise would collapse the protein. Moreover, the proteins being used as a carbon precursor also have the major drawback of denaturation during carbonisation process. As an alternate way, hydrothermal method was employed to carbonise egg-protein using graphene nanosheets which play the role of template as well as catalyst. By this method, the protein can be avoided from any physical or chemical damage through the strong bonding between the GO and protein, which was further activated using KOH to yield heteroatom doped highly porous carbon material.[243]

6. Applications of functionalized nanoporous carbon materials

As nanoporous carbons with different functional groups can offer interesting chemical and physical properties, these materials were effectively utilized for various applications.[150, 244, 245] Many investigations have focused on the usage of functionalized nanoporous carbon materials for a range of potential applications including conventional Li-ion and post Li batteries, supercapacitors, electrocatalysts for oxygen reduction reaction (ORR), fuel cell supports, hydrogen storage, CO_2 capture and field emission properties. This is mainly due to the fact that these fascinating materials can offer highly ordered porous structures, high specific surface areas, large pore volumes and a uniform pore size distribution. In this section, we will address the importance of the functionalization of nanoporous carbons and how these functionalities and excellent properties can elevate the application possibilities in various fields.

6.1 Nanoporous carbon for sensing

The application of carbon based materials for sensing has been widely studied and the demand for selective sensing are changing day-by-day for various reasons including environmental monitoring and safety, medical diagnostics etc. Majority of the sensing materials exhibit a high sensitivity, but high selectivity is the key and a new component that is now added as a trend to the sensing materials. The non-porous materials like graphene, carbon nanotubes and porous materials like activated carbon etc fall under the high sensitivity materials. On the other hand, the functionalized nanoporous materials can offer both high sensitivity and selectivity towards sensing which is discussed below.

The nanoporous carbon can be used for selective sensing by various methodologies like functionalising NC with metal or metal oxide, surface modification and doping, to sense the toxic gases, heavy metals, biomolecules etc. The selective sensing of NH_3 gas was performed by heteroatom doping by Travlou *et al.* where the interaction of NH_3 with humidity (H_2O) played a major role in sensing through hydrogen bonding and transport of proton through ionic conductivity.[246] The similar sensing mechanism was followed to sense NH_3 gas using the polymer derived nanoporous carbon. It was found that the weak interaction between the surface functional groups of nanoporous carbon and the ammonia caused the protonation of NH_3 to NH_4^+ that resulted in the electrochemical performance towards gas sensing.[247] Travlou *et al.* also demonstrated a series of the toxic gas sensing and have summarised the role of oxidation to examine the -N and -O heteroatoms on the nanoporous carbon surface and the effect of pores contributing to the electrochemical responses at different ammonia concentration and further studied the selectivity of sensor by exposing the carbons at oxidized state to the H_2S.[248] The sensing of heavy metal ions[249] and toxic chemical like hydrogen peroxide[250] was also done by using nitrogen doped porous carbon and nanoporous carbon fibres. The ordered nanoporous carbon was also fabricated in film forms by Jia *et al.* who were successful in creating a high surface area with tunable the pore sizes. These porous films exhibited an enough space for the immobilisation of glucose oxidase that exhibited an excellent bio sensing performance at a detection limit of 1.5 mM,[251] as shown in Fig. 16. The nanoporous carbon films with nickel for selectively sensing glucose was also demonstrated.[252] Nanoporous carbon was also functionalized with copper to have an active surface area that showed enhanced sensitivity for the detection of biochemicals.[253] Nanoporous carbons were also employed as sensors for selectively detecting various biomolecules like DNA bases, acids like ascorbic acid, uric acid, and NADH.[254, 255]

6.2 Nanoporous carbon for drug delivery

The effective drug carrier/drug vehicle is the most demanding component in drug delivery applications. The addition of the specific targeting in the drug delivery system is also an important factor for deciding on the efficacy of the drug delivery system. There are many carriers like nanoporous silica, polymers, micelles, nanotubes, nanoporous carbon etc have been employed for this purpose. However, the biocompatibility of these materials is still under research and recently the nanoporous carbon or the functionalised nanoporous carbons are of interest in the field of drug delivery.

Clarithromycin, a drug normally used for the treatment of tonsillitis, sinusitis and pharyngitis, causes side effects like swelling of mucosal tissues. In order to reduce the side effects of clarithromycin, the nanoporous carbon functionalised with amine groups was used as a carrier molecule (Fig. 17). It was reported that the amine modified nanoporous carbon was completely biocompatible.[256] The nanoporous carbon derived from MOF was also examined through cytotoxicity assay and the narrow pore size distribution was found to be suitable for the controlled release of cisplatin.[257] The dissolution and the poor solubility of the valsartan drug in the water was also addressed by Zhang *et al.* who used the porous carbon monoliths possessing ordered macropores and uniform mesopores of about 5.2 nm as a drug career.[258] It has been reported that the material exhibited a higher release rate compared with the pure valsartan.

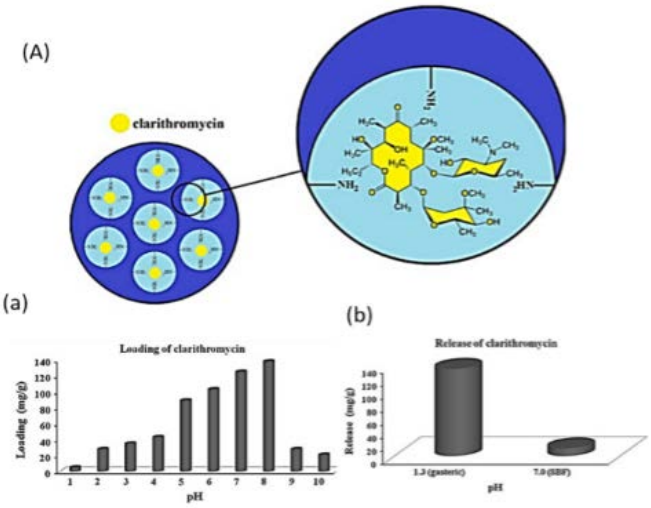

Figure 17 (A) Schematic representation of loading of clarithromycin drug in the amine-functionalised nanoporous carbon. (a) Effect of pH on loading the drug and (b) Effect of pH in the drug release. Reproduced with permission from ref. 256. Copyright 2013, Springer.

6.3 Nanoporous carbon for catalysis

The increasing demand in the consumption of fossil fuels has almost depleted the fossil fuel sources, hence the renewable energy must be found and developed to save the environmental pollution caused by the fossil fuels and to mitigate greenhouse gasses. As an alternate source, many renewable energy sources are emerging and being developed with the aim of replacing the depleting sources. Among them, the hydrogen fuel is a blooming area in catalysis due to its non-toxic nature, fast recharging ability and high stability. To produce the hydrogen, two well-known pathways have been used namely, the dehydrogenation and dehydration. However, the later pathway gives out the toxic carbon monoxide (CO), which is highly dangerous to the environment and immense control should be taken during the production of hydrogen. The main problem persisting in the field of catalysis is the separation of the product and their reusability. Hence, it is necessary to fabricate efficient heterogeneous catalysts which is highly cooperative with reaction temperature and the PH of reaction medium is desirable in recent years.

The synthesis of nanoporous carbon deposited with Pd nanoparticles to synthesise the heterogeneous catalyst with the strategy of sodium hydroxide assisted reduction was reported by Zhu *et al.* The sodium hydroxide was used here for the reason of uniform dispersion of metal on the surface of the nanoporous carbon and the reduction assisted by the sodium hydroxide resulted in the generation of hydrogen from the formic acid decomposition without the CO side reaction. Interestingly, the turn over frequency (TOF) was also 2623 h^{-1} with a 100% hydrogen selectivity,[259] shown in Fig. 18. The N-doped nanoporous carbon was also surface functionalised with AgPd zeolite framework for the decomposition of formic acid and the TOF reported was 936 h^{-1} at 353 K.[260] These two reports clearly showed the advantage of nanoporous carbon over the zeolite framework decorated with nanoporous carbon. Oxidation had a key role in the surface modification of the nanoporous carbons and Leticia et al, reported on the conversion of oxidized surface to exhibit chemical reaction in the porous matrix and studied the photochemical response.[261]

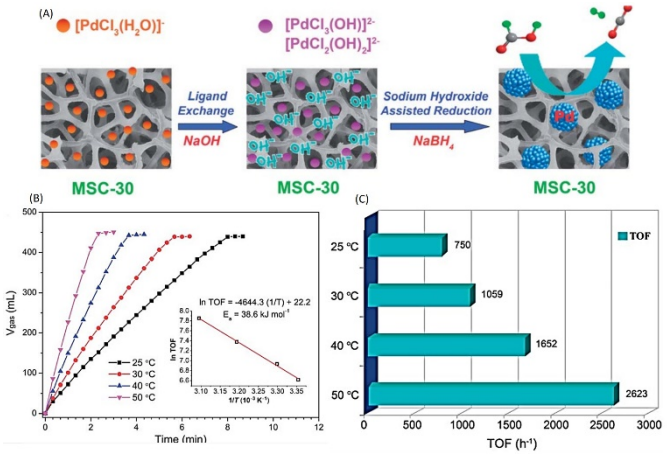

Figure 18 (A) Schematic representation for NaOH assisted reduction method of Pd/MSC-30 catalyst and gas evolution from the dehydrogenation of FA–SF. (B) Volume of the generate CO_2 +H_2 versus time and (b) corresponding TOF values of H_2 generation Inset of (C) Arrhenius plot (ln(TOF) vs. 1/T. Reproduced with permission from ref. 259. Copyright 2013, Royal Society of Chemistry.

6.4 Nanoporous carbon in adsorption and separation

Adsorption is the most conventional application of nanoporous carbon compared to various other applications of nanoporous carbon owing to their high surface area and tunable and uniform pore size distribution. Despite of the advantage of the nanoporosity, apparently, purification process which is otherwise said separation remains to be a difficult task so far. Hence, there is a clear need of developing advanced nanostructures for the efficient adsorption and separation applications.

The neonicotinoid insecticides was extracted from water and fatmelon samples by the magnetic MOF derived nanoporous carbon reported by Hao *et al.*[262] In their typical synthesis, the magnetic nanoporous carbon was prepared by one step direct carbonisation of ZIF-67 and the embedded Co nanoparticles offered the magnetic property to the material which could demonstrate the adsorption and removal of insecticide through liquid chromatography. Mesoporous carbon derived from MOF was also reported later for the separation of CO_2 and CH_4 from the mixture.[263] On the other hand, the magnetic mesoporous carbon (Ni-CMK-3) was also reported for the adsorption and removal of sulfur from oil[264] and the pure CMK-3 with a high surface area of 1268 m^2 g^{-1} was employed for the adsorption and recovery of 2-phenylethanol which is a rose oil component.[265] Following the use of mesoporous carbon in adsorption and separation, Ma *et al.* functionalised nanoporous carbon with highly uniform MgO nanoparticles through EISA process for the separation of methanol. The largest adsorption capacity of 11.90 mmol/g was observed.[266] Perreault *et al.* functionalised and grafted mesoporous carbon with diglycolyl chloride (DGCI) and N, N^1-bis-chloropropyl diglycolamide (CI-PDGA) to form CMK-8-DGO and CMK-8-PDGA. These two grafted CMK-3 materials were used as adsorbents to study the adsorption of lanthanides. Although both the

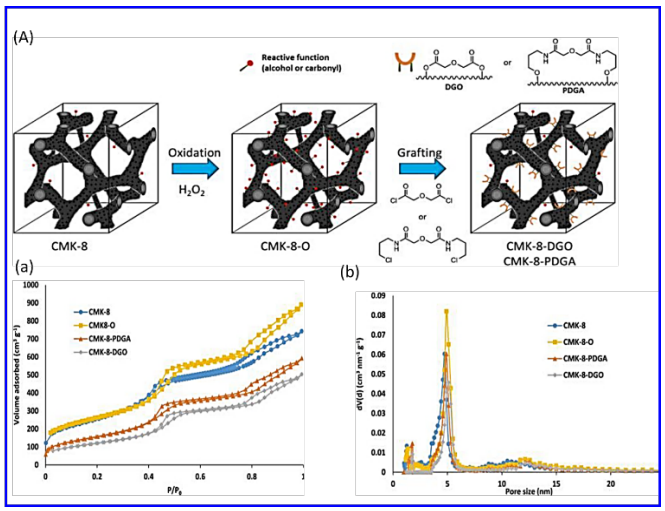

Figure 19 (A) Schematic illustration for the synthesis of the functional mesoporous carbons. (a) N_2 adsorption-desorption isotherms for pristine and modified mesoporous carbons and (b) Pore size distributions of the CMK-8. Reproduced with permission from ref. 267. Copyright 2017, American Chemical Society.

components showed type IV isotherm, at lower pH the CMK-8-DGO exhibited excellent reusability of Ln(Fig. 19).[267]

An interesting report on the effect of different pore structures in the adsorption and separation of CO_2 from the mixture of CO_2 and hydrogen was presented by Kumar *et al.* The molecular stimulation studies clearly showed that the adsorption is and separation was quite sensitive to pore structure and the composition of nanoporous carbon nanostructures. It was found that the porous carbons with tube like structure was the best for the high selectivity of adsorption of CO_2 molecules from the CO_2 and hydrogen mixture. Although nanoporous carbons with slit, foam like and random porous structure showed the adsorption but the selectivity was much inferior to that of porous carbon with tube like structures.[268]

6.5 Nanoporous carbon for batteries

Modified nanoporous carbon materials have been extensively utilized as electrode materials in the Lithium ion and post Li-ion batteries such as Li-S, Na-ion and Na-S batteries owing to their superior textural properties together with high conductivity and stability. Duan *et al.* reported on the usage of Sn nanoparticles incorporated mesoporous carbon as an anode material for Li-ion battery.[178] The charge/discharge voltage curves observed for nano-Sn/mesoporous carbon showed a typical sloping voltage profile associated with lithium alloying-dealloying with nano-sized Sn in the sample. The initial columbic efficiency was 60%, which was calculated according to the discharge capacity of 1246 mAh g^{-1} and charge capacity of 747 mAh g^{-1}. The columbic efficiency increases to 85% during the 2nd cycle, 90% to the 3rd cycle, and 97% above after 7 cycles. Urchin-like Fe_3O_4@C-N composites displayed an excellent electrochemical performance with a reversible specific capacity of 800 mAh g^{-1} after 100 cycles at 500 mAh g^{-1} in the 0.01–3 V voltage range at room temperature.[194] This significant electrochemical performance of urchin-like Fe_3O_4@C-N composites was attributed to the unique urchin-like structure and the N-doped mesoporous carbon shell.

Shen *et al.* have used mesoporous $Li_4Ti_5O_{12}$/C nanocomposites as an anode material in Li ion battery. Cyclic voltammetry curve of the mesoporous $Li_4Ti_5O_{12}$/C electrode at a scan rate of 0.2 mV s^{-1}, at a potential window of 1.0–2.5 V (vs. Li/Li^+) showed a pair of well-defined redox peaks at 1.65/1.50 V, which was attributed to the redox reaction of Ti^{4+}/Ti^{3+}, respectively.[192] These features revealed that the nanocomposite electrode had fast lithium ion insertion and extraction kinetics that was attributed to the highly ordered mesoporous structure with an enhanced electrical conductivity. $Li_4Ti_5O_{12}$/C nanocomposite possessed superior cyclic stability performance of more than 1000 cycles at the discharge capacity of 103.1 mAh g^{-1} at a high rate of 20 C with only 5.6% capacity loss (Fig. 20 e-f). Tan *et al.* reported that the N-doped mesoporous carbon-capped MoO_2 nanobelts (MoO_2@NC) electrode delivered a high first-cycle discharge and charge capacities of 942.3 and 690.7 mAh g^{-1}, respectively, with a Coulombic efficiency (CE) of 73.3 %. In the second cycle, the CE of the anode sample increased to 94.6 %, indicating a good lithium ion insertion/extraction performance during the cycling process. The discharge capacity MoO_2@NC electrode remained at 692.4 mAh g^{-1} after 100 cycles at a current of 0.5 A g^{-1}.[197]

Sun *et al.* also demonstrated that the Se_2S_6/NMC electrode exhibited the initial discharge capacity of 1195 mAh g^{-1}, which was almost close value to the theoretical capacity of 1226 mAh g^{-1} for Se_2S_6. They also registered excellent cycle stability and a high initial Coulombic efficiency of 96.5% as well as a high reversible capacity of 883 mAh g^{-1} after 100 cycles and 780 mAh g^{-1} after 200 cycles at 250 mA g^{-1}, respectively (Fig. 20 c-d).[198] HNMC material prepared from honey showed a superior performance towards Li ion battery with a reversible capacity of 1359 mAh g^{-1} after 10 cycles at 100 mA g^{-1} and excellent rate capability and cycling stability of 722 mAh g^{-1} after 200 cycles at 1 A g^{-1} (Fig. 20 a-b). The same material demonstrated the initial discharge and charge capacities of 977 and 427 mAh g^{-1}, respectively for Na ion battery.[58]

Liang *et al.* have investigated the performance of mesoporous nanocomposite by using N-OMC/SiO_2 as an anode material for lithium-ion batteries. The initial discharge and charge capacities of the N-OMC/SiO_2 nanocomposite electrode were measured to be as high as 3900 and 1996 mAh g^{-1}, respectively, with a Coulombic efficiency of 51%. The discharge capacity retained a large value of 740 mAh g^{-1} after 50 cycles, which was about two times higher than the theoretical value of graphite.[93] TiO_2 supported on nitrogen-doped carbon foams (NCFs) were also used as a free-standing and flexible electrode for lithium-ion batteries (LIBs). When TiO_2-NCF was directly used as a flexible electrode in a LIB, a capacity of 188 mAh g^{-1} was achieved at a current density of 200 mA g^{-1} under a potential window of 1.0–3.0 V, and a specific capacity of 149 mA h g^{-1} after 100 cycles at a current density of 1000 mA g^{-1} is maintained.[269] The addition of sulphur into the NOMCs can help these nanostructures to be used in Li-S battery applications. Qu *et al.* reported on the preparation of sulfur–HNMC composite with 53.3 wt% sulphur by a melt-diffusion method for high rate capability and long cycling stability cathode materials in Li-S battery.[270] The S–HNMC composite cathode exhibited a high

initial discharge capacity of 1209 mAh g^{-1} and retained as high as 600 mAh g^{-1} after 200 cycles at 1 C. Chen *et al.* reported on the usage of NM-CMK-3/S composite with 50 t% of Sulfur in the Li-S battery, which shows the high initial capacity of ca. 950 mAh g^{-1}, 100% Coulombic efficiency, and excellent cyclic stability of about capacity retention ratio of 80% (750 mAh g^{-1}) after 100 cycles with a decay of only 0.2% per cycle.[139] The high performance was attributed to the presence of microporsity and nitrogen contents which provided synergetic effects. These results explained the importance of having nitrogen on the surface of the carbon walls for energy storage applications.

Balach *et al.* described the high initial discharge capacity of 1364 mAh g^{-1} at 0.2C for NOMC/S composite with 50wt% of sulfur. The composite material also showed extremely high cycling stability with a high reversible capacity of 566 mAh g^{-1} and a negligible degradation rate of 0.037% after 1200 cycles at 0.5 C.[145] Liu *et al.* demonstrated that the S/CPAN-800 composite was an excellent material for Li-S cells, which has delivered a high initial discharge capacity of 1585 mAh g^{-1} and enhanced capacity retention of 862 mAh g^{-1} at 0.1 C after 100 cycles and high Coulombic efficiency of around 100%. These results greatly outperformed the S/CMK-3 composite cell without nitrogen

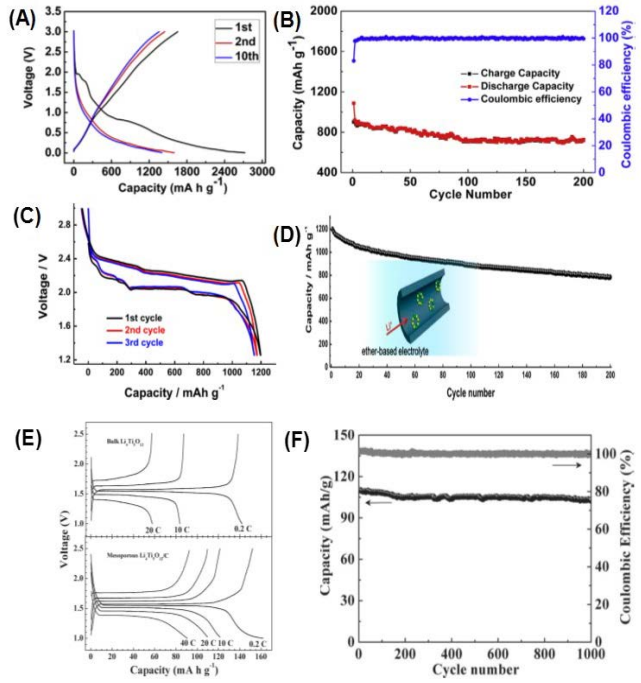

Figure 20 (A) Charge-discharge curves of HMNC-700 at 0.1 Ag^{-1}. (B) Cycling performance and corresponding Coulombic efficiency at a current density of 1 Ag^{-1}. Reproduced with permission from ref. 58. Copyright 2016, Elsevier. (C) The charge-discharge profiles of Se S/NMC. (D) Cycling performance of Se S/NMC at 250 mA g^{-1}. Reproduced with permission from ref. 198. Copyright 2016, American Chemical Society. (E) The galvanoststic charge-discharge curves of bulk $Li_4Ti_5O_{12}$/C. (F) Specific capacity and Coulombic efficiency of mesoporous $Li_4Ti_5O_{12}$/C. Reproduced with permission from ref. 192. Copyright 2012, Wiley-VCH Verlag GmbH & Co. KGaA, Weinheim.

doping, which maintained only 400 mAh g^{-1} capacity at 0.1 C after 100 cycles.[271] The enhanced performance was attributed to the nitrogen doping combined with sulphur, which significantly improved the wettability of electrolyte and the conductivity of the electrode. These results reveal the importance of doping of dual heteroatoms in the carbon framework structure of NOMCs.

6.6 Nanoporous carbon for carbon capture and storage

Global warming leading to drastic climatic changes happening due to the increasing concentration of carbon dioxide in the atmosphere added through various anthropogenic sources is inevitably one of the major environment crises of our times.[272, 273] There is an urgent need of developing materials and technologies to combat the dangerous emissions of CO_2 from industrial sectors such as power generation plants, cement production, petrochemical production, aluminium, steel and plastic manufacturing industries etc. Carbon based materials especially, ordered mesoporous carbon-based adsorbent with highly developed textural parameters are regarded as a potential solution to tackle the problem of industrial CO_2 emission. Two key parameters required for efficient CO_2 capture by an adsorbent include high specific surface area and the presence of nitrogen containing functional groups on the surface of carbon.[274] Several reports can be found in the literature for increasing surface area of different kinds of carbons using chemical activation.[275, 276] However, this procedure might not be suitable for ordered carbons as it may result in deformation of the order and affect the properties of the carbon. A few ordered mesoporous carbons are discussed below to ascertain the role they can play in capturing CO_2.

Wang *et al.* synthesized ordered mesoporous carbon CMK-3 through hard templating procedure using SBA-15 as a template for CO_2 capture.[277] They reported a surface are of 1115 $m^2 g^{-1}$ and pore volume of 1.11 $cm^3 g^{-1}$ and the material adsorbed 42 $mmolg^{-1}$ of CO_2 under high-pressure conditions (36 bar). It is to be noted this much high CO_2 uptake was observed using CMK-3 preabsorbed with water that decreased to 18.5 $mmolg^{-1}$ with dry CMK-3. The heat of adsorption was observed to 55 $kJmol^{-1}$, which indicates strong physisorption between CMK-3 and CO_2.

As previously discussed, the textural properties of the OMCs were significantly improved after the activation with KOH. Especially, the quantity of the micropores can be significantly enhanced after the activation. Bao *et al.* reported that the presence of ultra micropores of size <0.5 nm is a critical factor for enhancing the CO_2 adsorption and CO_2/N_2 selectivity of the nitrogen doped hierarchical carbon derived from polypyrrole.[278] They compared the CO_2 adsorption statistics for N-doped carbons made at 500°C and 800°C and even though the latter had a significantly high surface area, it still showed a relatively lesser amount of CO_2 adsorption, which defies the common theory that high surface area, leads to high CO_2 adsorption. Eventually, a low temperature carbonization to protect the ultra micropores widening and retaining of nitrogen containing functional groups was concluded as to be the most critical parameters for high CO_2 adsorption.

6.7 Electrocatalysis

Hetero-atom and non-precious foreign element doped carbon nanomaterials are considered as the low cost and highly efficient electrocatalysts alternative to the commercial platinum (Pt) based electrocatalysts. Among the doped carbon nanomaterials, nanoporous carbon materials modified with B,

N, S, P and non-precious elements are more attractive electrocatalysts for the oxygen reduction reaction (ORR), hydrogen evolution reaction (HER) and oxygen evolution reaction (OER). In this section, we will summarize the role of structure, morphology and the single or dual heteroatom doping in the OMCs affecting the final electrocatalytic performance of these materials.

6.7.1 Oxygen reduction reaction (ORR)

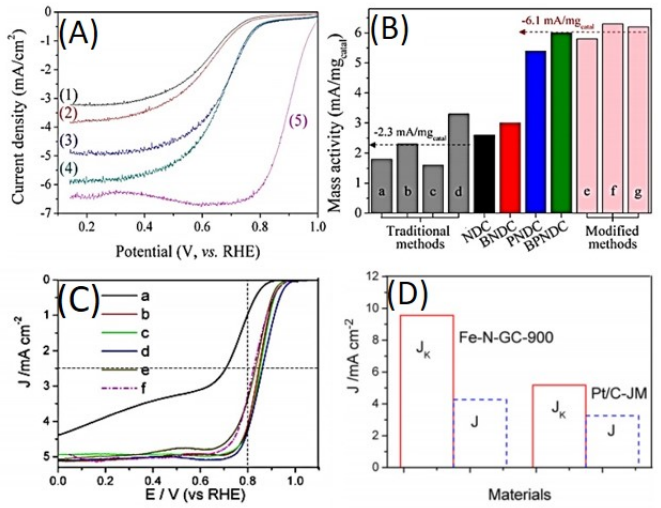

Figure 21 (A) ORR results in 1M HClO4 for the prepared catalysts, (1) NDC, (2) BNDC, (3) PNDC, (4) BPNDC, and (5) Pt/C (40 wt %). (B) Calculated mass activities at 0.6 V (vs RHE) for the prepared catalysts and other N-doped carbon catalysts. (C) RDE polarization curves of Fe–N–GC materials prepared at different carbonization temperatures and Pt/C. (D) RDE voltammograms of FeNCSs and Pt/C at 1600 rpm. Reproduced with permission from ref. 279 and 182. Copyright 2012 and 2014, American Chemical Society.

ORR is a key process in the fuel cells (FCs) for generating electricity by electrochemical reduction of oxygen and oxidation of hydrogen by production of water as the by-product. The most suitable electrocatalyst for ORR is the platinum (Pt) based electrodes. However, the scarcity and the high cost of Pt are the primary barriers to commercialize the Pt based electrocatalyst for fuel cells. Apart from the high cost, the Pt-based electrode also suffered from the susceptibility to fuel crossover and CO poisoning under electrochemical conditions. Therefore, numerous efforts have been devoted in seeking alternative non-platinum ORR electrocatalysts for FCs with a low cost and a high ORR activity. In this part, we review the latest advances on the fabrication of electrocatalysts based on the doped and functionalized nanoporous carbon materials. Choi *et al.* demonstrated that the additional doping of B and/or P in the nitrogen doped nanoporous carbon can enhance the asymmetry of atomic spin density and improved the ORR catalytic activity.[279] The ORR activity of the B, N-doped and P, N-doped nanoporous carbon showed 1.2 and 2.1 times higher than N-doped nanoporous carbons at 0.6 V (vs RHE) in acidic media. The nanoporous nitrogen doped carbon catalyst incorporated with both of the B and P (BPNDC) depicted the best ORR activity of 2.3 times higher than NDC at 0.6 V (vs RHE), which records –6.0 mA/mg of mass activity (Fig. 21 a-b).[279, 280] NOMC prepared from honey and glucose/ammonia precursors exhibited a significantly lower potential at −0.23 V as well as a sharply increased peak current towards the ORR. The apparent number of electrons involved in ORR for NOMC-800 prepared at 800 C is close to 4-electron, according to Koutecky–Levich equation. This indicates that the oxygen reduction follows mainly the four-electron pathway either by reducing oxygen directly to OH^- ions or by reducing it to hydrogen peroxide which is subsequently further reduced to OH^- ions.[57, 98, 161]

NOMCs synthesized via a facile dual soft-templating procedure showed the most positive onset potential (–0.11 V) and the highest reaction current density at a certain overpotential, suggesting the fastest reaction kinetics via close to four electron reaction pathway with higher limiting current density.[90, 99, 101] NOMC materials prepared from pyrrole or aminopyridine and Fe catalyst outperformed the Pt counterpart and the performance was significantly improved by increasing the pyrolysis temperature from 800 to 1000 °C.[67, 281] Nitrogen-doped mesoporous carbon nanosheets (NMCNs) fabricated from the thermal treatment of polyaniline enwrapped cobalt hydroxide ($Co(OH)_2$) nanosheets followed by the subsequent acid etching manifested an excellent ORR performance with the onset potential of –0.119 V, the half-wave potential of –0.182 V and the limiting current density of 5.06 mA cm^{-2}. These values were comparable to the commercial Pt/C (–0.164 V and 5 mA cm^{-2}).[282]

A nitrogen-doped mesoporous carbon containing a network of carbon nanotubes (CNTs) also showed an excellent ORR activity, with 59 mV more positive onset potential and 30 mV more positive half-wave potential than a Pt/C catalyst, and also much longer durability and stronger tolerance to methanol crossover than a Pt/C catalyst.[283] Highly ordered N-doped mesoporous carbon/graphene frameworks (N-MCF/N-MGF) prepared by using super lattice of self-assembled Fe_3O_4 nanoparticles as template showed a 47 mV positive shift in the half-wave potential and higher current densities compared with the Pt/C (2.24 and 0.74 mA cm^{-2}), demonstrating its superior ORR activity compared with the commercial Pt/C catalyst.[284]

Park *et al.* showed the ORR catalytic activity of NOMC materials, which demonstrated the high selectivity toward H_2O_2 over 90%. At 0.1 V, NOMC exhibited a ring current of 0.148 mA, which corresponds to H_2O_2 formation at a rate of 3.06 pmol s^{-1}.[62] Chen *et al.* also observed a well-defined oxygen reduction peak at 0.68 V (vs RHE) in CV curve under O_2 saturated 0.1 M KOH solution for NHPCM prepared by using N-doped hierarchical porous silica monolith template and furfuryl alcohol as the carbon source. The number of electrons involved in ORR for NHPCM is in the range of 3.7 to 3.9 indicating that an intrinsic four-electron pathway is the dominant mechanism. No significant change was observed in the ORR current density of NHPCM electrode after MeOH was added into the electrochemical cell, suggesting that it has remarkable improved ability to avoid the crossover effects.[65]

Sulfur doped OMCs such as OMC-S-1, OMC-S-2 and OMC-S-3 having sulphur contents in the range of 1.4 to 1.5 Wt.% exhibited higher currents of 238.0, 282.3 and 376.4 µA, during the ORR, which are higher than that of unmodified OMC electrode. The number of electrons calculated to be for ORR on OMC-S-3 were 3.3, 3.4, 3.5, 3.6 and 3.8 at different potentials,

which indicates that OMC-S-3 typically provides a four-electron transfer pathway for ORR.[113] Yang *et al.* observed ORR peak at −0.19 V for P doped well-ordered mesoporous carbon (POMC), which confirmed the excellent electrocatalytic activity of POMC for oxygen reduction.

POMC also exhibited high catalytic activity for ORR with an extraordinary selectivity for oxygen to evade crossover effects of the methanol and thereby outperformed the commercial Pt/VC electrode. For the Pt/VC catalyst, a very strong peak at −0.18 and −0.21 V was observed for methanol oxidation in the CV curve, whereas the cathodic ORR peak vanished. In contrast, no noticeable change was observed in the oxygen-reduction current on POMC electrode.[107, 285] Boron doped ordered mesoporous carbons (BOMCs) were also employed for ORR. These catalysts exhibited a substantial ORR cathodic peak at around −0.27 V. The maximum peak current density on BOMCs is −1.46 mA cm^{-2}, whereas unmodified OMCs and Pt/C registered maximum peak current densities of −0.84 and −0.97 mA cm^{-2}, respectively.[103] BOMCs electrode showed the significant onset potential shift towards positive side to −0.16 V with the limiting diffusion current density at −0.80 V, which is about 1.7 times stronger than that of undoped OMCs catalysts. The number of electrons participated in the ORR for BOMCs electrode at −0.50 V was found to be 3.86 and increased to 4 at more negative potentials, indicating that oxygen reduction follows mainly the four-electron pathway either by reducing oxygen directly to OH^- ions or by reducing it to peroxide which is subsequently further reduced to OH^- ions. S and N dual doped ordered mesoporous carbon (SN-OMC) materials were also successfully employed for ORR applications. It was found that the dual doping helped to enhance the ORR electrocatalytic activity (−0.186 V) in alkaline media with desirable current density, methanol tolerance and long-term stability. The number of electrons involved for SN-OMC during the ORR ranges from 3.93 to 3.95, very close to 4.0, indicating that it favoured a four-electron ORR process.[111, 112]

The ORR onset-potential (1.01 V), $E_{1/2}$ value (0.86 V), and current density (9.6 mA cm^{-2}) of the Fe–N–GC electrode prepared by heating 2,2-bipyridine and Fe chelates at 900 °C with 0.2 mg cm^{-2} loading were higher and larger than those of the values obtained on commercial Pt/C-JM electrode with 20 μg_{Pt} cm^2 loading and the previously reported NPMCs with 0.3–0.4 mg cm^{-2} loading in 0.1 M KOH solution. These results indicated its superior catalytic activity in alkaline medium (Fig. 21 c-d).[181, 182] Ultra fine Fe_2N nanocrystals incorporated in mesoporous nitrogen doped graphitic carbon spheres (Fe_2N/MNGCS) were also utilized for ORR applications. The catalysts demonstrated the half-wave potential of 0.881 V vs RHE, high selectivity towards $4e^-$ oxygen reduction process, excellent long-term stability with 95.2% of the initial current retention after 60,000 s of continuous operation and good tolerance against methanol crossover effect (94.9% of the current remained prior to 4.0 M methanol injection in alkaline media. This performance was much superior to that of the commercial Pt/C catalyst.[286] Pt nanoparticles supported on nitrogen-doped porous carbon microspheres (Pt/C_N) demonstrated ultrahigh ORR activity at a pH of 8.4 with a mass activity and specific activity of 564 mA mg^{-1} Pt and 834 mA cm^{-2} Pt, respectively, which may have been due to the presence of an appropriate amount of N atoms doped into the nanoporous carbon matrix.[177] Pt nanoparticles on N-doped ordered mesoporous carbon−Co composites (Pt/Co-N-OMC) displayed

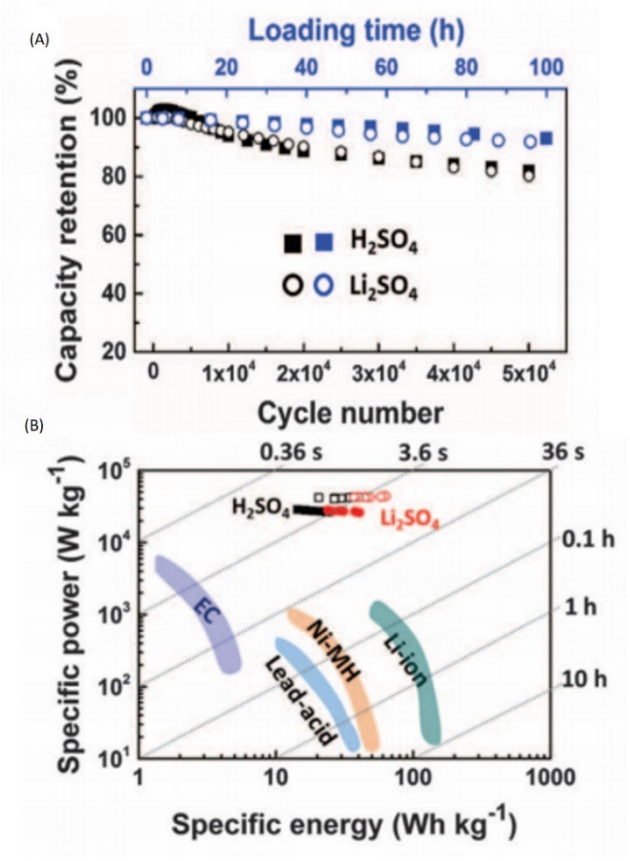

Figure 22 (A) OMFLC-N devices retain >92% after 100 hours of sustained loading and retain >80% of their initial response after 50,000 cycles. (B) Ragone plot of specific energy versus specific power for OMFLC-N SM symmetric devices using 0.5M H_2SO_4 and 2M Li_2SO_4 electrolytes, along with other standard devices. Reproduced with permission from ref. 56. Copyright 2015, American Association for the Advancement of Science.

the mixed kinetic diffusion current between 0.48 to 0.75 V with the highest onset potential at ~0.72 V in oxygen saturated 0.5 mol L^{-1} H_2SO_4 electrolyte at a rotation rate of 1600 rpm and scan rate of 5 mV s^{-1} and it also exhibited the highest limiting current and onset potential.[287]

Hollow graphitic carbon spheres with Fe–N-doped mesoporous shells (FeNCSs) prepared via in situ polymerization exhibited very superior ORR activity with a half-wave potential ($E_{1/2}$) of 0.886 V in 0.1 M KOH, 15 mV more positive than that of commercial Pt/C catalysts.[288] Liang *et al.* elucidated the four-electron reduction performance of oxygen in 0.5 M H_2SO_4 at room temperature by using cobalt−nitrogen-doped (C−N−Co) and iron−nitrogen-doped nanoporous carbon (C−N−Fe), prepared from vitamin B12 (VB12) and the polyaniline-Fe (PANI-Fe) complex. Among all of the catalysts, C−N−Co fabricated from VB12 and silica nanoparticles exhibited a remarkable ORR activity with a half-wave potential of 0.79 V, which is only ~58 mV deviation from Pt/C and further demonstrated a high selectivity of four electron, and excellent electrochemical stability up to 10000 cycles.[180]

Mesoporous Fe[10]@NOMC catalyst prepared from ferrocene-based ionic liquid was also utilized for ORR. The results showed that the catalyst exhibited a comparable onset potential and the half-wave potential (0 V vs. MMO) for the Pt/C and close values to the Fe/Fe_3C-melamine/N-KB composite but superior long-term stability to 20 wt% Pt/C in identical test conditions for ORR with four-electron transfer pathway under alkaline conditions. Fe[10]@NOMC catalyst showed perfect ORR selectivity in methanol containing electrolyte, whereas a significantly high methanol oxidation current is detected for the Pt/C catalyst under the same conditions.[183] Fe_3O_4 embedded into nitrogen-doped mesoporous carbon spheres (Fe_3O_4/NMCS) with the iron content of 3.35 wt% was used as a robust catalyst for the ORR in alkaline media. It showed the excellent electrochemical performance in terms of more positive onset potential of 1.036 V vs RHE, half-wave potential of 0.861 V and much better methanol tolerance and long-term durability, in comparison with that of 20% Pt/C.[289]

Three-dimensionally (3D) ordered mesoporous Fe-N/C fabricated from the soft templating approach manifested the high onset potential (1.018 V), half-wave potential (0.812 V) and limited-diffusion current density (5.98 mA cm^{-2}) in both acidic and alkaline electrolytes. The number of transferred electrons (n) was calculated to be 4.08-4.20 between 0.40 and 0.60 V for mesoporous Fe-N/C, confirming the dominant 4 e^- oxygen reduction mechanism.[290] Cobalt-nitrogen-doped three-dimensionally (3D) ordered macro-/mesoporous carbons (Co-N-OMMCs) prepared from dual-templating synthesis approach exhibited a highly positive ORR half-wave potential of ~0.83 V vs. RHE, which is only ~0.01 V deviation from the Pt/C catalyst (~0.84 V vs. RHE). The catalysts also provided a higher diffusion-limited current density than commercial Pt/C, indicating a large quantity of exposed active sites on the Co-N-OMMC. The number electrons involved in the ORR for Co-N-OMMC was calculated to be 3.9 at 0.5 V vs. RHE, revealing that the Co-N-OMMC favoured a 4e^- oxygen reduction process and O_2 was reduced to OH^-, which is same with Pt/C catalyst. The chronoamperogram of the Co-N-OMMC showed negligible performance attenuation even after 25 h of continuous operation at 0.5 V vs. RHE, in contrast to a sharp activity loss of commercial Pt/C, demonstrating the high stability of Co-N-OMMC for ORR.[187]

6.8 Nanoporous carbon for supercapacitance

Supercapacitors, which are also known as electrochemical capacitors, provide a high power density (>10 kW kg^{-1}), fast charge/discharge process (within seconds) and long cycling life (>10^5 cycles).[291, 292] Nanoporous carbon based materials are considered as the attractive electrode materials for supercapacitors owing to their extremely high specific surface areas, large pore volumes and pore diameters, in combination with the simple synthesis processing, non-toxicity and high chemical stability. There have been a quite number of review articles reported on this topic.[291-293] Therefore, in this review, recent developments on the utilization of these nanostructures for supercapacitor applications for the past five years are reviewed. In 2015, Lin *et al.* successfully used N-doped mesoporous few-layer carbon with a large surface area of 1900 m^2 $g^{-1}$for the supercapacitor applications. It was reported that the materials showed the highest ever specific capacitance of 810 F g^{-1} and 710 F g^{-1} and volumetric capacity of 560 F cm^{-3} and at 1 A g^{-1} in 0.5 M H_2SO_4 and 2 M Li_2SO_4 electrolyte using an Ag/AgCl reference electrode and a Pt counter electrode.[56] The electrochemical cell withstood the capacity for 50,000 cycles between 0 and 1.2 V. The device also demonstrated the highest specific energy of 23.0 Wh kg^{-1} and a specific power density of 18.5 kW kg^{-1} based on the device weight in 2 M Li_2SO_4 electrolyte. Electrochemical impedance spectroscopy showed that OMFLC-N has the lowest equivalent series resistance of ~0.8 ohms, better than that of OMFLC without N doping and CMK-3 (Fig. 22). Wei *et al.* reported on the supercapacitor device fabrication by using rich nitrogen-doped ordered mesoporous carbon, which showed the specific capacitances of 262 F g^{-1} (in H_2SO_4) and 227 F g^{-1} (in KOH) at a current density of 0.2 A g^{-1} and 244 F g^{-1} (in H_2SO_4) and 213 F g^{-1} (in KOH) at a current density of 0.5 A g^{-1}, which are much better than that for the mesoporous carbon FDU-15 without any nitrogen content (110–130 F g^{-1}).[87] These results revealed that the coating of nitrogen doped carbon on the surface of the support was much more effective than the bulk NOMSs in the supercapacitor applications.

The nitrogen doped hierarchical porous carbon nets exhibited high specific capacitance of 537.3 F g^{-1} and 306.3 F cm^{-3} at 0.5 A g^{-1} current density in a 0.5 M H_2SO_4 electrolyte. The material also presented an outstanding cycling stability with 98.8% retention of their initial capacitance after 10000 cycles at 5 A g^{-1}.[164] NOMC prepared from phenol–urea–formaldehyde exhibits specific capacitance of 225 F g^{-1} at a current density of 0.5 A g^{-1} and it is showed good electrochemical stability even after 1000 cycles at current density of 5.0 A g^{-1}.[92]

Microporosity has been introduced in the NOMCs via activation and other techniques to enhance the specific capacitance of the materials. Liu *et al.* reported on the enhanced supercapacitor performance of activated NOMC electrode material with the mass loading of ~3 mg cm^{-2} yielded a high specific capacitance of 186 F g^{-1} at a current density of 0.25 A g^{-1} and a good capacitance retention of 75% at a high discharge current density of 20 A g^{-1} in ionic liquid electrolyte. Increasing the mass loading to ~12mg cm^{-2} gave rise to only a 10% capacitance decay at 20 A g^{-1}.[159] Almeida *et al.* demonstrated that the NMC-T material showed a specific capacitance of 190.2 F g^{-1} and retained 73% of its capacitance when the current density was increased from 0.5 to 8.0 A g^{-1}. In addition, the specific capacitance of NMC-T retained up to 98% of their stored charges or initial capacitance after 1,000 charge–discharge cycles at a current density of 2.0 A g^{-1}.[66] NOMCs prepared via aqueous cooperative assembly route demonstrated a high specific capacitance of 186 F g^{-1} at a current density of 0.25 A g^{-1} and a good capacitance retention of 75% at a high discharge current density of 20 A g^{-1} in ionic liquid electrolyte.[159]

Nitrogen-doped micro-mesoporous carbon material exhibited a reversible specific capacitance of 226.3 F g^{-1} at the current density of 1.0 A g^{-1} in 6 M KOH electrolyte and 75.5% of its initial capacity can be retained after 2000 cyclic tests.[137] A maximum capacitance of 237 F g^{-1} is reached for the NOMC prepared by using ionic liquid precursor at a current density of 0.1 A g^{-1}. The specific energy of a cell made from two identical NOMC electrodes is more than 83 Wh kg^{-1} (unpackaged) for 1100 cycles at a current density of 1 A g^{-1}, which is correspond to a specific energy of 25 Wh kg^{-1} in a commercial-style, packaged device, which typically contains 30 wt% active material.[81]

Hierarchical mesoporous carbons with different boron contents (from 0.42 to 2.37 wt.%) showed a specific capacitance of 180 F g^{-1} in H_2SO_4 aqueous solution at a current density of 1 A g^{-1}.[106] Sun *et al.* described an advanced supercapacitor material based on nitrogen doped porous graphitic carbon (NPGC), which showed an excellent capacitive behaviour with specific capacitance of 293 F g^{-1} at a current density of 1 A g^{-1}, long-term cycling stability at about 5000 cycles, and high coulombic efficiency in KOH electrolyte.[96] Tang *et al.* implemented supercapacitor device by using NHPC-3D having 8.2 wt.% of nitrogen functionalities as the active electrode material, that exhibits a specific capacitance as high as 252 F g^{-1} at a current density of 2 A g^{-1}. The device also shows high capacitance retention of 75.7% with specific capacitance of 190 F g^{-1} at a higher current density of 20 A g^{-1}.[73] A NOMC material demonstrated a reversible specific capacitance of 308 F g^{-1} at a current density of 0.2 A g^{-1} in aqueous H_2SO_4 electrolyte with 58% capacity retention of 131 F g^{-1} at a current density of 20 A g^{-1}.[97] Song *et al.* depicted that the NMMC electrode has the high specific capacitance of 325 F g^{-1} at current density of 0.2 A g^{-1} in aqueous H_2SO_4 electrolyte.[76] Xu *et al.* demonstrated that a microsphere-like nitrogen-doped mesoporous carbon/nickel-cobalt layered double hydroxide (NMC/NiCo-LDHs-M) composite displayed a high specific capacitance of 272.6 F g^{-1} at 1 A g^{-1} and outstanding electrochemical capacitance retention of 87.2% of initial capacitance even after 10,000 cycles.[101]

OMCs derived from zeolite based templates have been employed as electrodes for supercapacitor applications owing to their better specific surface area and small pores. Kyotani *et al.* studied supercapacitance performance of zeolite templated B and N doped ordered microporous carbon (N-ZTC) materials by using zeolite Y as a template. Among the materials prepared, N-ZTC demonstrated with a high capacitance of 180 F g^{-1} in 1 M $TEABF_4$/PC electrolyte.[294] Amoros *et al.* reported on the fabrication of thin films of zeolite-templated carbon (ZTC) on a carbon current collector by the combination of chemical and electrochemical synthesis protocols.[295] FAU nanozeolites were deposited by an electrophoretic deposition (EPD) technique from colloidal suspensions on porous carbon discs. Binderless continuous thin films of ZTC were materialized by subjecting the resulting composites to chemical vapour deposition (CVD) of acetylene gas followed by HF washing. The prepared thin ZTC layers show area capacitance values over 12 mF cm^{-2}, which is one of the best value for electrodes in microcapacitors. The functional groups on these microporous carbons play a huge role in enhancing the electrochemical performance of the ZTCs. For example, Kyotani *et al.* also reported on the large pseudocapacitance (330 F g^{-1}) of electrochemically oxygen functionalized zeolite template carbon (ZTC) in organic electrolyte.[296] The formation of anion and cation radicals of oxygen functionalities offers pseudocapacitance which is responsible for the enhancement of the total specific capacitance of the functionalized ZTC. These results provide a clear evidence that the functionalization of the ZTC is one of the key elements and can be used for tuning the electrochemical performance of ZTC.

Linnemann *et al.* demonstrated on the simplifying of the supercapacitor electrode fabrication process through the electrodeposition of the carbonized metal organic framework (MOF) based films on the current collector.[297] The MOF films are well attached to the metal substrate during the carbonization process under argon atmosphere forming highly electrochemically active Co_3O_4/C and Mn_3O_4/C hybrid materials. At the 50th cycle, the integral capacitance of the Mn_3O_4/C bilayered system was 160 F g^{-1} referring to Mn, 116 F g^{-1} referring to Mn_3O_4 and 102 F g^{-1} referring to MnO_2 at the scan rate of 20 mV s^{-1}. This value is superior to the Mn_3O_4/graphene material reported by Lee *et al.*[298]

Fransaer *et al.* reported on the preparation of mesoporous layered Ni-Co mixed metal oxides-carbon composite electrodes on the Ni foam by using Ni-Co mixed metal-organic frameworks (MOFs) with the above mentioned method.[299] This electrode exhibited a high capacitance of 2098 mF cm^{-2} and superior rate performance of 93% from 1 to 20 mA cm^{-2} at a current density of 1 mA cm^{-2}. These are the best methods for the fabrication of efficient supercapapacitor electrodes using MOF derived carbons which does not require any additional processing steps or templates.

N- and O functional groups containing nanoporous carbons derived from zeolite template showed a large pseudo-capacitance of 312.4 F g^{-1} in H_2SO_4 electrolyte and it can operate at 1.2 V in H_2SO_4 with a good durability beyond 4000 cycles.[300] Wang *et al.* demonstrated that the NOMC materials can have the specific capacitances of 76 F g^{-1} and 21 F g^{-1}, respectively, at a current density of 0.1 A g^{-1}, which was measured by galvanic charge and discharge process.[86] The diffusive resistances (R_D) of NOMC electrodes are of 0.7 and 1.3 ohm, respectively. The specific capacitance of nitrogen and sulphur doped ordered mesoporous carbon (NSOMC) reached 180 F g^{-1} in KOH aqueous solution at a current density of 1 A g^{-1}, with approximately 39.5% enhancement over CMK-3, despite the specific surface areas of NSOMC is only about 70% of the CMK-3.[110] NOMC material with a nitrogen content of 6.7 wt% showed a high capacitance of 264 F g^{-1} in 1.0 M H_2SO_4 electrolyte at a current density of 0.5 A g^{-1} and a good rate capability with a capacitance retention of 226 F g^{-1} at 10 A g^{-1}. The NOMC electrode also delivered an excellent cycling stability without capacitance fading over 10000 cycles.[59] Ling *et al.* demonstrated that NOMC prepared by using PDA precursor exhibited a high specific capacitance of 538 F g^{-1} at a sweep rate of 5 mV s^{-1}. NOMC material delivered a large capacitance of 186 F g^{-1} at a high current density of 3 A g^{-1}. The NONC

supercapacitor electrode remained more than 93% of the initial capacitance even after 5000 cycles, exhibiting excellent cycling stability.[60] A graphitic ordered mesoporous carbon (G-OMC) prepared from DA and NiO template showed the specific capacitance of 183 F g^{-1} and 68 μF cm^{-2} at current density of 0.1 A g^{-1}.[61] Although the N and NiO functionalities were there in the samples, they registered poor specific capacitance which might be attributed to the low specific surface area of the prepared samples.

Nitrogen- and sulfur-codoped 3D cubic ordered mesoporous carbon (KNOMC) with controlled dopant content (10.0−4.6% for nitrogen and 0.94−0.75% for sulfur) demonstrated the specific capacitance of 320 F g^{-1} at a current density of 1 A g^{-1} in 2M aqueous KOH electrolyte. However, the specific capacitance decreased quickly during the first 10 cycles, but the specific capacitance retained almost 100.0% during the 20−1000th cycles. After 1000 cycles, the specific capacitance reached to 247 F g^{-1}.[301] NOMCs with a high surface area of 1741 m^2 g^{-1} and nitrogen content up to 15 wt.% exhibited a specific capacitance of 230 F g^{-1} at a current density of 0.5 A g^{-1} and good rate capability of 175 F g^{-1} at 20 A g^{-1} with capacitance retention of 77.4% in 6 M KOH aqueous electrolyte.[78] These results revealed that the optimum amount of N and S together with the excellent surface area and structural order is the key to obtain high specific capacitance for the samples.

Nitrogen and phosphorus dual doped ordered mesoporous carbon (NPOMC) demonstrated a high specific capacitance of 220 F g^{-1} at a current density of 1 A g^{-1}, a good rate capability of 178 F g^{-1} at 16 A g^{-1} with capacitance retention of 81% and an excellent cycling stability of 91% in 6 M KOH aqueous electrolyte.[171] This value was lower than the N and S doped or N and O doped NOMCs. Hierarchically nitrogen doped ordered mesoporous carbons (HNMC) synthesized from polyhedral oligosilsesquioxanes (POSS) demonstrated a nearly ideal rectangular shape CV in a wide voltage window from −2 to 2 V. These HNMC materials showed a gravimetric and volumetric specific capacitance of 163 F g^{-1} and 106 F cm^{-3} at a current density of 0.25 A g^{-1} in ionic liquid electrolyte and also showed the slow capacitance decay with increase of discharge rates, in particular, at 20 A g^{-1}. It also showed a high capacity of 141 F g^{-1} with 89% capacitance retention.[162] Binder free supercapacitor electrodes based on nitrogen-doped mesoporous carbon microfibers (NMCMFs) exhibited specific capacity of 189 F g^{-1} at a scan rate of 5 mV s^{-1}, excellent rate capability of 107 F g^{-1} at 100 mV s^{-1} and durability (maintained over 96% of the initial capacitance after 10000 cycles) in 6 M KOH aqueous electrolyte.[163] All these results revealed that optimized doping and the structural control of OMCs are the key to fabricate the best electrode system for the energy storage application. Ultimately, this information could be used for the design of the best energy storage system with a considerable cost reduction by adopting necessary low-cost modification of OMCs.

6.9 Carbon nanomaterials based pathogen sensors

Carboxyl modified carbon dots prepared by hydrothermal carbonization of citric acid combined with amine based aptamer formed a very effective CD-aptamer complex which provided a very fast and sensitive fluorescent detection of *Salmonella typhimurium*. The limit of bacterial detection was 50CFUml^{-1} while a linear relation was found between concentration of bacterium and fluorescence intensity in the range of 10^3 to 10^5CFUml^{-1}. This conjugated probe was also tested for real samples of eggshell and tap water and the results were very similar to conventional plate count method which suggests the potential application of these systems for detection of salmonella typhimurium in real situations.[302]

Simultaneous detection of Vibrio parahaemolyticus and Salmonella typhimurium was also possible using a combination of green (gQD) and red quantum (rQD) dots with carbon nanoparticles. With the attachment of a specific aptamer, the respective QD's-CNP assembly was able to measure the FRET fluorescent changes from interaction of target bacteria within a linear range of 50 to 10^6CFUml^{-1} and detection of limit as 25 and 35CFUml^{-1} for each bacterium respectively. The detection capability of the sensor platform using plate count method showed consistency when compared to shrimp and chicken as real solid samples for analysis.[303]

An GQDs–AuNPs FRET biosensor was developed for S. aureus specific gene sequence detection by immobilising capture probe on GQD and conjugation of reporter probes on AuNPs. Then, the hybridization of target S. aureus oligos within a conc. range of 100nM to 400nM packed between the GQD and AuNP layers formed a sandwich structure which triggered fluorescence resonance energy transfer (FRET) effect. One of the interesting features of this work was that the detection limit of this biosensor was 1nM for S. Aureus specific gene detection, which clearly demonstrated the good selectivity. In a single and double mismatched oligos system at 200nM, the sensor recorded a quencher efficiency of 93% for target oligos and 22-37% for mismatched oligos which indicated the specificity of the sensor. This simple technology could be used for the whole genome of S.Aureus detection which would open the platform for the detection of foodborne pathogens. This would significantly support the food safety and environmental screening.[304]

7. Conclusion and future prospects

Despite the fact that tremendous amount of progress has been made in the fabrication of nanoporous carbons with contemporary structures and unique morphologies, exciting opportunities have still persisted for their functionalization in developing multifunctional properties for divergent specific applications. The integration of different heteroatoms into the nanoporous carbon framework together provided us a new class of materials exhibiting many unmatched properties. By controlling both chemistry and geometry of these functionalized hybrid nanoporous carbon based materials using different templates or micelles, these functional materials have already had applications in wide variety of different technological and scientific fields. Various strategies have been applied for the fabrication of nanoporous carbon materials with exemplary textural parameters starting from the basic synthesis

methods, such as templating techniques to the advanced surfactant mediating approaches.

In this review, we have reviewed and discussed the recent significant breakthroughs on the synthesis, and structure, morphology and functionalities control of ordered nanoporous carbon materials. We have also shown that how the structures and morphological control affect the final textural properties of the materials and their roles on the final performance of the materials in various applications including adsorption, carbon capture, energy storage batteries and supercapacitors, electrocatalysis and heterogeneous catalysis were discussed in detail. We have also imparted the exhaustive analysis in the structure-function correlation of functionalized nanoporous carbon materials and considered their diverse preparation methods including mono or binary and even ternary doping methods by using different heteroatoms (B, N, O, S, and P) and foreign elements (Fe, Co, Ni and Cu) containing natural and synthetic carbonaceous precursors, surface modifications and functionalization with organic and inorganic molecules and nanostructures.

With these developed robust and reliable doping, functionalization and templating strategies, a broad range of nanoporous functionalized carbon materials with pore cavity sizes in the range of 2-50 nm and various dimensions (1D, 2D and 3D) can be readily and selectively fabricated for promising advanced technological applications. The prepared functionalized nanoporous carbon materials have been effectively used mainly in electrochemical energy conversion and storage devices fabrication technologies. Their involvement in electrochemical energy storage applications, including Li-ion batteries, post Li-ion batteries including Li-S, Li-air and Na-ion batteries, and supercapacitors were presented in detail. Recent discoveries on energy conversion applications such as electrochemical oxygen reduction reaction (ORR), hydrogen evolution reaction (HER) and oxygen evolution reaction (OER) on functionalized nanoporous carbon materials were also introduced in detail. By finely tuning the textural parameters, morphology and doping concentrations of the nanoporous carbon materials at different length scales, their performance in adsorption, carbon capture, sensing, electrochemical energy storage and conversion performances can be significantly enhanced.

Before inception of the block copolymer assisted soft template synthesis method for the preparation of highly ordered mesoporous carbon materials, pre-prepared inorganic porous materials mediated hard template nanocasting approach was considered as the only method that can be used for the successful fabrication of mesoporous carbon with well-defined pores. The soft-template method relies on supramolecular micelle assemblies, which enhances the polymerization processes of carbon molecular precursors. The soft templating method is thermodynamically driven, and therefore depends on the chemical interactions between supramolecular templates and carbon molecular precursors. Because of their facile synthesis and processing characteristics, soft templating synthesis processes governed by the block copolymer templates have dominated and create new possibilities for the synthesis of mesoporous carbons overcoming the intrinsic limitations imposed by the hard template method.

In this review, we have thoroughly conferred the recent research developments and trends in both hard templating and soft templating techniques for the synthesis of highly ordered nanoporous carbons without any dopants and also functionalized nanoporous carbons with mono, binary and ternary hetero atoms doping and foreign elements. Hetero atom doping, functionalization and morphological control of nanoporous carbon materials are highly depend on the processing conditions, which make the precise tailoring for extremely high textural parameters such as specific surface area, pore volume and pore diameter in nanoporous carbon materials, which dictate their efficiency in many applications.

From the last few decades, there have been tremendous amount of research and development activities devoted to the discovery of new materials and technology for energy generation, storage and conversion, owing to the development of alternative, economical and sustainable energy resources to meet the ever growing global energy demand and environmental impact on the heavy dependence of traditional fossil fuel based energy resources, which poses serious challenges to human health, energy security, and environmental protection. As presented in this review, the fuel cell technology offers a viable approach to generate electricity from the electrochemical reaction of hydrogen and oxygen by production of water as the by-product, and virtually no pollution. The slow ORR kinetics on the cathode side is a key step to limit the energy conversion efficiency of a fuel cell and requires a substantial amount of the catalyst. Traditionally, platinum (Pt) has been regarded as the best ORR catalyst. However, Pt-based electrode suffers from multiple drawbacks such as high cost, scarcity, and susceptibility to fuel crossover, time-dependent drift and CO poisoning under electrochemical conditions. Along with the intensive research efforts in reducing or replacing Pt-based electrode in fuel cells, heteroatom and non-precious metal doped nanoporous carbon materials have been discovered as a new class of electrocatalysts for ORR, which could dramatically reduce the cost and increase the efficiency of fuel cells. The functionalized nanoporous carbon materials successfully catalyze the O_2 molecule via 4 electron reduction pathways at same or lower potentials than golden standard Pt based catalysts under both acidic and basic conditions. The nanoporous carbon materials also possessed excellent long-term stability with almost retention of the initial current even after several hours of continuous operation. They also showed a good tolerance against methanol crossover effect. The enhanced catalytic performance of the functionalized nanoporous carbon materials has been attributed to the electron-accepting/donating abilities of the heteroatoms or functional elements present in the nanoporous carbon framework, which create net charge on adjacent carbon atoms to facilitate the O_2 adsorption and net charge transfer for ORR.

Another great opportunity for functionalized nanoporous carbon materials lies in the efficient storage of energy

generated by fuel cell technology, which is a win-win situation for these fascinating materials. The use of functionalized nanoporous carbon materials has generated much excitement in the field of energy storage systems, including supercapacitors, Li-ion batteries and post Li-ion batteries. As it was clearly explained in this review, the functionalized nanoporous carbon architectures can be introduced with heteroatoms, redox functional groups, functional elements, metals, metal oxides, conducting polymers and alloys based materials to enhance both electron and ion transport in the active materials for improvement of energy storage capability and stability of the batteries and supercapacitor devices. Apart from the energy conversion and storage devices including, fuel cells, batteries and supercapacitors, the future challenge is to design and development of functionalized nanoporous carbon materials having suitable band structure, with inbuilt functional moieties including organic or inorganic nanostructures in the mesochannels electrodes. These electrodes should be able to split the water molecules under electrochemical conditions for the facile production of hydrogen and oxygen which can be connected to fuel cell technology that offers a viable approach to electricity generation directly from water without any pollution.

Although the functionalised nanoporous carbons offer excellent performances in the energy oriented applications, it is still needed to achieve the cost-effective way for their large-scale production of cheap electrode materials and the electrocatalysts which are both highly stable and reliable. These are the major limitations for these exciting materials. Therefore, the future challenge is to synthesize the highly pure functionalized nanoporous carbon materials without any contamination in more economical way without using harsh conditions and expensive reagents but with a low-cost biodegradable carbon or nitrogen precursors. As discussed above in this review, the functionalized nanoporous carbon materials having high specific areas were found to be the best materials for CO_2 adsorption. The future mega challenge for materials scientists is to utilize both the in-built electronic and absorption properties of the functionalized nanoporous carbons to convert the adsorbed CO_2 into fuels and chemicals by using water as the hydrogen source through the electrocatalysis. The proof-of-concept studies will certainly stimulate more research in the electrochemical reduction of CO_2.

Nowadays, functionalized nanoporous carbon materials are fascinating even in the biomedical fields. Their biocompatibility for tissue engineering and theragnostic applications such as bio sensing, drug delivery, gene therapy, bio imaging, phototherapy and hybrid theragnostic is highly challenging by which one can understand that, numerous research efforts needed in these areas to develop and invent novel functionalised nanoporous materials in the future.

Irreversible agglomeration of nanoporous carbon layers and uncontrollable doping of heteroatoms atoms at the molecular level during their preparation through the high temperature pyrolysis methods are important challenges and yet to be addressed. Although the heteroatom doping has made remarkable progress, their facile synthetic routes are still on its way of developments and the multiple heteroatom doping at controllable places in nanoporous carbon frameworks. Further, process simplification is needed to lower the consumption of consumables and energy as well as decrease waste generation. Moreover, the low yield of ordered nanoporous carbon materials provided by current synthesis methods also remains an issue from the perspective of their potential use in industrial processes. Irreversible acidic and basic moiety functionalization of nanoporous carbons with known and desired functional groups, it is possible to control anchoring of hetero atoms on their surface in a desirable way. Surface functionalization of nanoporous carbons also improve their solubility, stability and reduce the agglomeration, which can help them with improved performance towards selective sensing of hazardous heavy metals, pathogens and toxins. It is quite surprising that recent days the interest towards the application of functionalised nanoporous carbon for the drug delivery has been increasing, mainly due to the functionalisation methods that has the ability to enhance the compatibility of the nanoporous carbon materials. These methodologies allow the immobilisation of the DNA, protein, enzymes and drugs that can be finally involved in the in-vivo drug delivery. However, the practical applications of these materials are still under investigation and very few studies have offered as the proof of concepts. Therefore, a wide spectrum of research is deliberately needed for the biomedical applications.

The research articles reviewed in this review article, illustrate the fabrication of nanoporous carbons and their great interest towards their properties and applications. Carbons have already made a revolution in the world and the nanoporous carbon materials are their fascinating parts and the present trends in the ocean of carbon is the functionalisation of nanoporous carbon which is now making a history through small modifications and an outstanding improvement in the world. There is no doubt that a lot of opportunities are hidden and the researchers should explore more on utilizing the amazing potential of these functionalized ordered nanoporous carbons in the above suggested applications covering, energy, environment and health sectors. We are confident that the information presented in this review would definitely support the advances in the research and development of ordered nanoporous carbon materials.

References

1. R. Ryoo, S. H. Joo and S. Jun, *The Journal of Physical Chemistry B*, 1999, **103**, 7743-7746.
2. M. E. Davis, *Nature*, 2002, **417**, 813.
3. C. Vix-Guterl, E. Frackowiak, K. Jurewicz, M. Friebe, J. Parmentier and F. Béguin, *Carbon*, 2005, **43**, 1293-1302.
4. C. Liang, Z. Li and S. Dai, *Angewandte Chemie International Edition*, 2008, **47**, 3696-3717.
5. M. Notarianni, J. Liu, K. Vernon and N. Motta, *Beilstein Journal of Nanotechnology*, 2016, **7**, 149-196.

6. L. Wen, F. Li and H.-M. Cheng, *Advanced Materials*, 2016, **28**, 4306-4337.
7. R. Ryoo, S. H. Joo, M. Kruk and M. Jaroniec, *Advanced Materials*, 2001, **13**, 677-681.
8. S. Jun, S. H. Joo, R. Ryoo, M. Kruk, M. Jaroniec, Z. Liu, T. Ohsuna and O. Terasaki, *Journal of the American Chemical Society*, 2000, **122**, 10712-10713.
9. S. H. Joo, S. J. Choi, I. Oh, J. Kwak, Z. Liu, O. Terasaki and R. Ryoo, *Nature*, 2001, **412**, 169-172.
10. S. Che, K. Lund, T. Tatsumi, S. Iijima, S. H. Joo, R. Ryoo and O. Terasaki, *Angewandte Chemie International Edition*, 2003, **42**, 2182-2185.
11. A.-H. Lu, W.-C. Li, W. Schmidt, W. Kiefer and F. Schüth, *Carbon*, 2004, **42**, 2939-2948.
12. A. Sayari and Y. Yang, *Chemistry of Materials*, 2005, **17**, 6108-6113.
13. J. Lee, S. Yoon, S. M. Oh, C. H. Shin and T. Hyeon, *Advanced Materials*, 2000, **12**, 359-362.
14. J. Lee, S. Yoon, T. Hyeon, S. M. Oh and K. Bum Kim, *Chemical Communications*, 1999, DOI: 10.1039/a906872d, 2177-2178.
15. T.-Y. Ma, L. Liu and Z.-Y. Yuan, *Chemical Society Reviews*, 2013, **42**, 3977-4003.
16. J. C. Ndamanisha and L.-p. Guo, *Analytica Chimica Acta*, 2012, **747**, 19-28.
17. W. Li, J. Liu and D. Zhao, *Nature Review Materials,* 2016, **1**, 16023.
18. T. Kyotani, *Bulletin of the Chemical Society of Japan*, 2006, **79**, 1322-1337.
19. M. Inagaki, M. Toyoda and T. Tsumura, *RSC Advances*, 2014, **4**, 41411-41424.
20. M. Inagaki, Y. A. Kim and M. Endo, *Journal of Materials Chemistry*, 2011, **21**, 3280-3294.
21. V. Malgras, Q. Ji, Y. Kamachi, T. Mori, F.-K. Shieh, K. C. W. Wu, K. Ariga and Y. Yamauchi, *Bulletin of the Chemical Society of Japan*, 2015, **88**, 1171-1200.
22. W. Xia, A. Mahmood, R. Zou and Q. Xu, *Energy & Environmental Science*, 2015, **8**, 1837-1866.
23. H. B. Wu and X. W. Lou, *Science Advances*, 2017, **3,** eaap9252.
24. J. Schuster, G. He, B. Mandlmeier, T. Yim, K. T. Lee, T. Bein and L. F. Nazar, *Angewandte Chemie International Edition*, 2012, **51**, 3591-3595.
25. Y. Seo, K. Kim, Y. Jung and R. Ryoo, *Microporous and Mesoporous Materials*, 2015, **207**, 156-162.
26. G. Tao, L. Zhang, Z. Hua, Y. Chen, L. Guo, J. Zhang, Z. Shu, J. Gao, H. Chen, W. Wu, Z. Liu and J. Shi, *Carbon*, 2014, **66**, 547-559.
27. L. Wang and R. T. Yang, *The Journal of Physical Chemistry C*, 2012, **116**, 1099-1106.
28. A. Castro-Muñiz, Y. Hoshikawa, T. Kasukabe, H. Komiyama and T. Kyotani, *Langmuir*, 2016, **32**, 2127-2135.
29. K. Kim, M. Choi and R. Ryoo, *Carbon*, 2013, **60**, 175-185.
30. K. Nueangnoraj, H. Nishihara, K. Imai, H. Itoi, T. Ishii, M. Kiguchi, Y. Sato, M. Terauchi and T. Kyotani, *Carbon*, 2013, **62**, 455-464.
31. E. Masika and R. Mokaya, *Progress in Natural Science: Materials International*, 2013, **23**, 308-316.
32. A. Almasoudi and R. Mokaya, *Microporous and Mesoporous Materials*, 2014, **195**, 258-265.
33. A. Almasoudi and R. Mokaya, *Journal of Materials Chemistry A*, 2014, **2**, 10960-10968.
34. E. Masika and R. Mokaya, *Energy & Environmental Science*, 2014, **7**, 427-434.
35. K. Kim, T. Lee, Y. Kwon, Y. Seo, J. Song, J. K. Park, H. Lee, J. Y. Park, H. Ihee, S. J. Cho and R. Ryoo, *Nature*, 2016, **535**, 131.
36. H. Lee, K. Kim, S.-H. Kang, Y. Kwon, J. H. Kim, Y.-K. Kwon, R. Ryoo and J. Y. Park, *Scientific Reports*, 2017, **7**, 11460.
37. K. Kim, Y. Kwon, T. Lee, S. J. Cho and R. Ryoo, *Carbon*, 2017, **118**, 517-523.
38. X. Meng and F.-S. Xiao, *Chemical Reviews*, 2014, **114**, 1521-1543.
39. Y. Ren, Z. Ma and P. G. Bruce, *Chemical Society Reviews*, 2012, **41**, 4909-4927.
40. W. Li and D. Zhao, *Chemical Communications*, 2013, **49**, 943-946.
41. M. Enterría and J. L. Figueiredo, *Carbon*, 2016, **108**, 79-102.
42. K. Na, C. Jo, J. Kim, K. Cho, J. Jung, Y. Seo, R. J. Messinger, B. F. Chmelka and R. Ryoo, *Science*, 2011, **333**, 328-332.
43. J. Grand, S. N. Talapaneni, A. Vicente, C. Fernandez, E. Dib, H. A. Aleksandrov, G. N. Vayssilov, R. Retoux, P. Boullay, J.-P. Gilson, V. Valtchev and S. Mintova, *Nature Materials*, 2017, **16**, 1010.
44. Y. Wan and Zhao, *Chemical Reviews*, 2007, **107**, 2821-2860.
45. Y. Shi, Y. Wan and D. Zhao, *Chemical Society Reviews*, 2011, **40**, 3854-3878.
46. F. Schüth, *Chemistry of Materials*, 2001, **13**, 3184-3195.
47. L. Chuenchom, R. Kraehnert and B. M. Smarsly, *Soft Matter*, 2012, **8**, 10801-10812.
48. J. Parmentier, F. O. M. Gaslain, O. Ersen, T. A. Centeno and L. A. Solovyov, *Langmuir*, 2014, **30**, 297-307.
49. F. O. M. Gaslain, J. Parmentier, V. P. Valtchev and J. Patarin, *Chemical Communications*, 2006, DOI: 10.1039/B512002K, 991-993.
50. J. Li, E. Fiset, J. Yang, P. Yuan, X. Ling, D. Hulicova-Jurcakova, C. Yu and L. Wang, *Journal of Materials Chemistry*, 2012, **22**, 21472-21480.
51. L. Sterk, J. Górka, A. Vinu and M. Jaroniec, *Microporous and Mesoporous Materials*, 2012, **156**, 121-126.
52. L. Liu, Q.-F. Deng, B. Agula, T.-Z. Ren, Y.-P. Liu, B. Zhaorigetu and Z.-Y. Yuan, *Catalysis Today*, 2012, **186**, 35-41.
53. T. Kimura, A. M. Emre, K. Kato and Y. Hayashi, *Journal of Materials Chemistry A*, 2013, **1**, 15135-15141.
54. G. P. Mane, S. N. Talapaneni, C. Anand, S. Varghese, H. Iwai, Q. Ji, K. Ariga, T. Mori and A. Vinu, *Advanced Functional Materials*, 2012, **22**, 3596-3604.
55. S. N. Talapaneni, K. Fugane, A. Vinu and T. Mori, *Advanced Porous Materials*, 2017, **5**, 26-35.
56. T. Lin, I.-W. Chen, F. Liu, C. Yang, H. Bi, F. Xu and F. Huang, *Science*, 2015, **350**, 1508-1513.
57. J. Lu, X. Bo, H. Wang and L. Guo, *Electrochimica Acta*, 2013, **108**, 10-16.
58. Y. Zhang, L. Chen, Y. Meng, J. Xie, Y. Guo and D. Xiao, *Journal of Power Sources*, 2016, **335**, 20-30.
59. D.-D. Zhou, W.-Y. Li, X.-L. Dong, Y.-G. Wang, C.-X. Wang and Y.-Y. Xia, *Journal of Materials Chemistry A*, 2013, **1**, 8488-8496.
60. Y. Liang, H. Liu, Z. Li, R. Fu and D. Wu, *Journal of Materials Chemistry A*, 2013, **1**, 15207-15211.
61. D. Yuan, F. Zeng, J. Yan, X. Yuan, X. Huang and W. Zou, *RSC Advances*, 2013, **3**, 5570-5576.
62. J. Park, Y. Nabae, T. Hayakawa and M.-a. Kakimoto, *ACS Catalysis*, 2014, **4**, 3749-3754.

63. A. Chen, K. Xia, Y. Yu, H. Sun, L. Liu, S. Ren and Y. Li, *Journal of The Electrochemical Society*, 2016, **163**, A3063-A3068.
64. A. Chen, K. Xia, L. Zhang, Y. Yu, Y. Li, H. Sun, Y. Wang, Y. Li and S. Li, *Langmuir*, 2016, **32**, 8934-8941.
65. Y. Chen, R. Ma, Z. Zhou, G. Liu, Y. Zhou, Q. Liu, S. Kaskel and J. Wang, *Advanced Materials Interfaces*, 2015, **2**, 1500199.
66. V. C. Almeida, R. Silva, M. Acerce, O. P. Junior, A. L. Cazetta, A. C. Martins, X. Huang, M. Chhowalla and T. Asefa, *Journal of Materials Chemistry A*, 2014, **2**, 15181-15190.
67. K. Wan, G.-F. Long, M.-Y. Liu, L. Du, Z.-X. Liang and P. Tsiakaras, *Applied Catalysis B: Environmental*, 2015, **165**, 566-571.
68. S. Shrestha, N. Morse and W. E. Mustain, *RSC Advances*, 2014, **4**, 47039-47046.
69. K. Wan, M.-y. Liu, Z.-p. Yu, Z.-x. Liang, Q.-b. Liu, J.-h. Piao and Y.-y. Zheng, *International Journal of Hydrogen Energy*, 2016, **41**, 18027-18032.
70. K. Wu and Q. Liu, *Applied Surface Science*, 2016, **379**, 132-139.
71. Á. Sánchez-Sánchez, F. Suárez-García, A. Martínez-Alonso and J. M. D. Tascón, *Carbon*, 2015, **94**, 152-159.
72. G. Tao, L. Zhang, L. Chen, X. Cui, Z. Hua, M. Wang, J. Wang, Y. Chen and J. Shi, *Carbon*, 2015, **86**, 108-117.
73. J. Tang, T. Wang, R. R. Salunkhe, S. M. Alshehri, V. Malgras and Y. Yamauchi, *Chemistry – A European Journal*, 2015, **21**, 17293-17298.
74. D.-S. Yang, D. Bhattacharjya, M. Y. Song, F. Razmjooei, J. Ko, Q.-H. Yang and J.-S. Yu, *ChemCatChem*, 2015, **7**, 2882-2890.
75. K. Huo, W. An, J. Fu, B. Gao, L. Wang, X. Peng, G. J. Cheng and P. K. Chu, *Journal of Power Sources*, 2016, **324**, 233-238.
76. Y. Song, S. Hu, X. Dong, Y. Wang, C. Wang and Y. Xia, *Electrochimica Acta*, 2014, **146**, 485-494.
77. X. Gao, Z. Chen, Y. Yao, M. Zhou, Y. Liu, J. Wang, W. D. Wu, X. D. Chen, Z. Wu and D. Zhao, *Advanced Functional Materials*, 2016, **26**, 6649-6661.
78. Q. Shi, R. Zhang, Y. Lv, Y. Deng, A. A. Elzatahrya and D. Zhao, *Carbon*, 2015, **84**, 335-346.
79. X. Yang, H. Ma and G. Zhang, *Langmuir*, 2017, **33**, 3975-3981.
80. F. Hasché, M. Oezaslan, P. Strasser and T.-P. Fellinger, *Journal of Energy Chemistry*, 2016, **25**, 251-257.
81. B. E. Wilson, S. He, K. Buffington, S. Rudisill, W. H. Smyrl and A. Stein, *Journal of Power Sources*, 2015, **298**, 193-202.
82. A. Chen, Y. Yu, Y. Zhang, T. Xing, Y. Wang, Y. Zhang and J. Zhang, *Journal of Hazardous Materials*, 2014, **279**, 280-288.
83. D. Liu, J.-H. Lei, L.-P. Guo, D. Qu, Y. Li and B.-L. Su, *Carbon*, 2012, **50**, 476-487.
84. L. Liu, Q.-F. Deng, X.-X. Hou and Z.-Y. Yuan, *Journal of Materials Chemistry*, 2012, **22**, 15540-15548.
85. J. Yu, M. Guo, F. Muhammad, A. Wang, G. Yu, H. Ma and G. Zhu, *Microporous and Mesoporous Materials*, 2014, **190**, 117-127.
86. X. Wang, C.-G. Liu, D. Neff, P. F. Fulvio, R. T. Mayes, A. Zhamu, Q. Fang, G. Chen, H. M. Meyer, B. Z. Jang and S. Dai, *Journal of Materials Chemistry A*, 2013, **1**, 7920-7926.
87. J. Wei, D. Zhou, Z. Sun, Y. Deng, Y. Xia and D. Zhao, *Advanced Functional Materials*, 2013, **23**, 2322-2328.
88. J. Xu, X. Zhao, A. Wang and T. Zhang, *Carbon*, 2014, **80**, 610-616.
89. D. Saha, A. Spurri, J. Chen and D. K. Hensley, *Microporous and Mesoporous Materials*, 2016, **229**, 8-13.
90. J. Li, Z. Li, J. Tong, C. Xia and F. Li, *RSC Advances*, 2015, **5**, 70010-70016.
91. A. Chen, Y. Yu, Y. Zhang, W. Zang, Y. Yu, Y. Zhang, S. Shen and J. Zhang, *Carbon*, 2014, **80**, 19-27.
92. M. Xie, Y. Xia, J. Liang, L. Chen and X. Guo, *Microporous and Mesoporous Materials*, 2014, **197**, 237-243.
93. Y. Liang, L. Cai, L. Chen, X. Lin, R. Fu, M. Zhang and D. Wu, *Nanoscale*, 2015, **7**, 3971-3975.
94. J. H. Lee, H. J. Lee, S. Y. Lim, B. G. Kim and J. W. Choi, *Journal of the American Chemical Society*, 2015, **137**, 7210-7216.
95. M. Li and J. Xue, *The Journal of Physical Chemistry C*, 2014, **118**, 2507-2517.
96. L. Sun, C. Tian, Y. Fu, Y. Yang, J. Yin, L. Wang and H. Fu, *Chemistry – A European Journal*, 2014, **20**, 564-574.
97. Y. Song, L. Li, Y. Wang, C. Wang, Z. Guo and Y. Xia, *ChemPhysChem*, 2014, **15**, 2084-2093.
98. C. Guo, X. Tong and X.-Y. Guo, *International Journal of Hydrogen Energy*, 2016, **41**, 22941-22951.
99. B. Bayatsarmadi, Y. Zheng, M. Jaroniec and S. Z. Qiao, *Chemistry – An Asian Journal*, 2015, **10**, 1546-1553.
100. G. Shen, X. Sun, H. Zhang, Y. Liu, J. Zhang, A. Meka, L. Zhou and C. Yu, *Journal of Materials Chemistry A*, 2015, **3**, 24041-24048.
101. C.-T. Hung, N. Yu, C.-T. Chen, P.-H. Wu, X. Han, Y.-S. Kao, T.-C. Liu, Y. Chu, F. Deng, A. Zheng and S.-B. Liu, *Journal of Materials Chemistry A*, 2014, **2**, 20030-20037.
102. T. Zhou, Y. Zhou, R. Ma, Z. Zhou, G. Liu, Q. Liu, Y. Zhu and J. Wang, *Carbon*, 2017, **114**, 177-186.
103. X. Bo and L. Guo, *Physical Chemistry Chemical Physics*, 2013, **15**, 2459-2465.
104. A. Nsabimana, X. Bo, Y. Zhang, M. Li, C. Han and L. Guo, *Journal of Colloid and Interface Science*, 2014, **428**, 133-140.
105. T. Wang, C. Zhang, X. Sun, Y. Guo, H. Guo, J. Tang, H. Xue, M. Liu, X. Zhang, L. Zhu, Q. Xie and J. He, *Journal of Power Sources*, 2012, **212**, 1-12.
106. M. Enterría, M. F. R. Pereira, J. I. Martins and J. L. Figueiredo, *Carbon*, 2015, **95**, 72-83.
107. D.-S. Yang, D. Bhattacharjya, S. Inamdar, J. Park and J.-S. Yu, *Journal of the American Chemical Society*, 2012, **134**, 16127-16130.
108. P. Song, L. Zhu, X. Bo, A. Wang, G. Wang and L. Guo, *Electrochimica Acta*, 2014, **127**, 307-314.
109. J. Xu, Y. Zhao, C. Shen and L. Guan, *ACS Applied Materials & Interfaces*, 2013, **5**, 12594-12601.
110. D. Zhang, Y. Hao, L. Zheng, Y. Ma, H. Feng and H. Luo, *Journal of Materials Chemistry A*, 2013, **1**, 7584-7591.
111. T. Jiang, Y. Wang, K. Wang, Y. Liang, D. Wu, P. Tsiakaras and S. Song, *Applied Catalysis B: Environmental*, 2016, **189**, 1-11.
112. X. Song, H. Ren, J. Ding, C. Wang, X. Yin and H. Wang, *Materials Letters*, 2015, **159**, 280-283.
113. H. Wang, X. Bo, Y. Zhang and L. Guo, *Electrochimica Acta*, 2013, **108**, 404-411.
114. X. Zhao, Q. Zhang, B. Zhang, C.-M. Chen, A. Wang, T. Zhang and D. S. Su, *Journal of Materials Chemistry*, 2012, **22**, 4963-4969.
115. S. R. Stoyanov, A. V. Titov and P. Král, *Coordination Chemistry Reviews*, 2009, **253**, 2852-2871.

116. Y. Deng, Y. Xie, K. Zou and X. Ji, *Journal of Materials Chemistry A*, 2016, **4**, 1144-1173.
117. K. N. Wood, R. O'Hayre and S. Pylypenko, *Energy & Environmental Science*, 2014, **7**, 1212-1249.
118. L. Dai, Y. Xue, L. Qu, H.-J. Choi and J.-B. Baek, *Chemical Reviews*, 2015, **115**, 4823-4892.
119. S. Joseph, Devaraju M. Kempaiah, M. Benzigar, A. V. Baskar, S. N. Talapaneni, S. H. Jhung, D.-H. Park and A. Vinu, *J. Mater. Chem. A*, 2017, **5**, 21542-21549.
120. S. N. Talapaneni, S. Anandan, G. P. Mane, C. Anand, D. S. Dhawale, S. Varghese, A. Mano, T. Mori and A. Vinu, *Journal of Materials Chemistry*, 2012, **22**, 9831-9840.
121. S. N. Talapaneni, G. P. Mane, A. Mano, C. Anand, D. S. Dhawale, T. Mori and A. Vinu, *ChemSusChem*, 2012, **5**, 700-708.
122. S. N. Talapaneni, J. H. Lee, S. H. Je, O. Buyukcakir, T.-w. Kwon, K. Polychronopoulou, J. W. Choi and A. Coskun, *Advanced Functional Materials*, 2017, **27**, 1604658.
123. G. P. Mane, S. N. Talapaneni, K. S. Lakhi, H. Ilbeygi, U. Ravon, K. Al-Bahily, T. Mori, D.-H. Park and A. Vinu, *Angewandte Chemie International Edition*, 2017, **56**, 8481-8485.
124. S. N. Talapaneni, J. Kim, S. H. Je, O. Buyukcakir, J. Oh and A. Coskun, *Journal of Materials Chemistry A*, 2017, **5**, 12080-12085.
125. K. S. Lakhi, D.-H. Park, K. Al-Bahily, W. Cha, B. Viswanathan, J.-H. Choy and A. Vinu, *Chemical Society Reviews*, 2017, **46**, 72-101.
126. O. Buyukcakir, S. H. Je, S. N. Talapaneni, D. Kim and A. Coskun, *ACS Applied Materials & Interfaces*, 2017, **9**, 7209-7216.
127. K. S. Lakhi, D.-H. Park, S. Joseph, S. N. Talapaneni, U. Ravon, K. Al-Bahily and A. Vinu, *Chemistry – An Asian Journal*, 2017, **12**, 595-604.
128. A. Vinu, K. Ariga, T. Mori, T. Nakanishi, S. Hishita, D. Golberg and Y. Bando, *Advanced Materials*, 2005, **17**, 1648-1652.
129. A. Vinu, *Advanced Functional Materials*, 2008, **18**, 816-827.
130. X. Jin, V. V. Balasubramanian, S. T. Selvan, D. P. Sawant, M. A. Chari, G. Q. Lu and A. Vinu, *Angewandte Chemie International Edition*, 2009, **48**, 7884-7887.
131. D.-H. Park, K. S. Lakhi, K. Ramadass, M.-K. Kim, S. N. Talapaneni, S. Joseph, U. Ravon, K. Al-Bahily and A. Vinu, *Chemistry – A European Journal*, 2017, **23**, 10753-10757.
132. Y. J. Lee, S. N. Talapaneni and A. Coskun, *ACS Applied Materials & Interfaces*, 2017, **9**, 30679-30685.
133. S. N. Talapaneni, G. P. Mane, D.-H. Park, K. S. Lakhi, K. Ramadass, S. Joseph, W. M. Skinner, U. Ravon, K. Al-Bahily and A. Vinu, *Journal of Materials Chemistry A*, 2017, **5**, 18183-18192.
134. K. S. Lakhi, D.-H. Park, G. Singh, S. N. Talapaneni, U. Ravon, K. Al-Bahily and A. Vinu, *Journal of Materials Chemistry A*, 2017, **5**, 16220-16230.
135. X.-h. Li, K. Wan, Q.-b. Liu, J.-h. Piao, Y.-y. Zheng and Z.-x. Liang, *Chinese Journal of Catalysis*, 2016, **37**, 1562-1567.
136. Y. Yang, G. Lan, X. Wang and Y. Li, *Chinese Journal of Catalysis*, 2016, **37**, 1242-1248.
137. A. Chen, Y. Wang, Q. Li, Y. Yu, Y. Li, Y. Zhang, Y. Li, K. Xia and S. Li, *Journal of The Electrochemical Society*, 2016, **163**, A1959-A1964.
138. Y. Kwon, K. Kim and R. Ryoo, *RSC Advances*, 2016, **6**, 43091-43097.
139. H. Chen, Q. Li, N. Teng, D. Long, C. Ma, Y. Wei, J. Wang and L. Ling, *Electrochimica Acta*, 2016, **214**, 231-240.
140. Y. Liu, X. Zhao, G. S. Chauhan and J.-H. Ahn, *Applied Surface Science*, 2016, **380**, 151-158.
141. B. Han, E. J. Lee, W. H. Choi, W. C. Yoo and J. H. Bang, *New Journal of Chemistry*, 2015, **39**, 6178-6185.
142. H. Tang, Y. Zeng, D. Liu, D. Qu, J. Luo, K. Binnemans, D. E. De Vos, J. Fransaer, D. Qu and S.-G. Sun, *Nano Energy*, 2016, **26**, 131-138.
143. L. Cheng, C. Hou, B. Zhang and G. Liu, *RSC Advances*, 2016, **6**, 114361-114373.
144. S. Jiao, J. Du, Z. Du, D. Long, W. Jiang, Z. Pan, Y. Li and X. Zhong, *The Journal of Physical Chemistry Letters*, 2017, **8**, 559-564.
145. J. Balach, T. Jaumann, M. Klose, S. Oswald, J. Eckert and L. Giebeler, *Journal of Power Sources*, 2016, **303**, 317-324.
146. C. Goel, H. Bhunia and P. K. Bajpai, *RSC Advances*, 2015, **5**, 46568-46582.
147. H. Chen, F. Sun, J. Wang, W. Li, W. Qiao, L. Ling and D. Long, *The Journal of Physical Chemistry C*, 2013, **117**, 8318-8328.
148. J. Hu, K. T. Ho, X. U. Zou, W. H. Smyrl, A. Stein and P. Bühlmann, *Analytical Chemistry*, 2015, **87**, 2981-2987.
149. J. Hu, X. U. Zou, A. Stein and P. Bühlmann, *Analytical Chemistry*, 2014, **86**, 7111-7118.
150. K. Sakaushi and M. Antonietti, *Bulletin of the Chemical Society of Japan*, 2014, **88**, 386-398.
151. J. Gong, M. Antonietti and J. Yuan, *Angewandte Chemie International Edition*, 2017, **56**, 7557-7563.
152. H. Wang, S. Min, C. Ma, Z. Liu, W. Zhang, Q. Wang, D. Li, Y. Li, S. Turner, Y. Han, H. Zhu, E. Abou-hamad, M. N. Hedhili, J. Pan, W. Yu, K.-W. Huang, L.-J. Li, J. Yuan, M. Antonietti and T. Wu, *Nature Communications*, 2017, **8**, 13592.
153. S. Mascotto, D. Kuzmicz, D. Wallacher, M. Siebenbürger, D. Clemens, S. Risse, J. Yuan, M. Antonietti and M. Ballauff, *Carbon*, 2015, **82**, 425-435.
154. N. Fechler, T.-P. Fellinger and M. Antonietti, *Advanced Materials*, 2013, **25**, 75-79.
155. T.-P. Fellinger, A. Thomas, J. Yuan and M. Antonietti, *Advanced Materials*, 2013, **25**, 5838-5855.
156. P. Hu, D. Meng, G. Ren, R. Yan and X. Peng, *Applied Materials Today*, 2016, **5**, 1-8.
157. D. Liu, D. Zheng, L. Wang, D. Qu, Z. Xie, J. Lei, L. Guo, B. Deng, L. Xiao and D. Qu, *The Journal of Physical Chemistry C*, 2014, **118**, 2370-2374.
158. M. Chen, L.-L. Shao, Y.-P. Liu, T.-Z. Ren and Z.-Y. Yuan, *Journal of Power Sources*, 2015, **283**, 305-313.
159. D. Liu, C. Zeng, D. Qu, H. Tang, Y. Li, B.-L. Su and D. Qu, *Journal of Power Sources*, 2016, **321**, 143-154.
160. Y. Yang, B. Zhao, P. Tang, Z. Cao, M. Huang and S. Tan, *Carbon*, 2014, **77**, 113-121.
161. B. Nagy, S. Villar-Rodil, J. M. D. Tascón, I. Bakos and K. László, *Microporous and Mesoporous Materials*, 2016, **230**, 135-144.
162. D. Liu, G. Cheng, H. Zhao, C. Zeng, D. Qu, L. Xiao, H. Tang, Z. Deng, Y. Li and B.-L. Su, *Nano Energy*, 2016, **22**, 255-268.
163. R. Liu, L. Pan, L. Wan and D. Wu, *Physical Chemistry Chemical Physics*, 2015, **17**, 4724-4729.
164. L.-N. Han, X. Wei, Q.-C. Zhu, S.-M. Xu, K.-X. Wang and J.-S. Chen, *Journal of Materials Chemistry A*, 2016, **4**, 16698-16705.
165. Y. Chang, F. Hong, J. Liu, M. Xie, Q. Zhang, C. He, H. Niu and J. Liu, *Carbon*, 2015, **87**, 424-433.

166. A. Sánchez-Sánchez, F. Suárez-García, A. Martínez-Alonso and J. M. D. Tascón, *Carbon*, 2014, **70**, 119-129.
167. A. Sánchez-Sánchez, F. Suárez-García, A. Martínez-Alonso and J. M. D. Tascón, *Applied Surface Science*, 2014, **299**, 19-28.
168. C. Weinberger, S. Haffer, T. Wagner and M. Tiemann, *European Journal of Inorganic Chemistry*, 2014, **2014**, 2787-2792.
169. U. Byambasuren, Y. Jeon, D. Altansukh and Y.-G. Shul, *Journal of Solid State Electrochemistry*, 2016, **20**, 645-655.
170. T. Panja, D. Bhattacharjya and J.-S. Yu, *Journal of Materials Chemistry A*, 2015, **3**, 18001-18009.
171. J. Feng, W. Song, L. Sun and L. Xu, *RSC Advances*, 2016, **6**, 110337-110343.
172. Z. Li, J. Liu, C. Xia and F. Li, *ACS Catalysis*, 2013, **3**, 2440-2448.
173. H. Huang, X. Wang, M. Tan, C. Chen, X. Zou, W. Ding and X. Lu, *ChemCatChem*, 2016, **8**, 1485-1489.
174. F. Wang, J. Xu, X. Shao, X. Su, Y. Huang and T. Zhang, *ChemSusChem*, 2016, **9**, 246-251.
175. D. Ye, R. Zhang, Y. Fu, J. Bu, Y. Wang, B. Liu and J. Kong, *Electrochimica Acta*, 2015, **160**, 306-312.
176. C. Ray, S. Dutta, R. Sahoo, A. Roy, Y. Negishi and T. Pal, *Chemistry – An Asian Journal*, 2016, **11**, 1588-1596.
177. R. Balgis, G. M. Anilkumar, S. Sago, T. Ogi and K. Okuyama, *Journal of Power Sources*, 2013, **229**, 58-64.
178. B. Duan, W. Wang, H. Zhao, B. Xu, K. Yuan and Y. Yang, *Journal of The Electrochemical Society*, 2012, **159**, A2092-A2095.
179. X.-H. Yan and B.-Q. Xu, *Journal of Materials Chemistry A*, 2014, **2**, 8617-8622.
180. H.-W. Liang, W. Wei, Z.-S. Wu, X. Feng and K. Müllen, *Journal of the American Chemical Society*, 2013, **135**, 16002-16005.
181. C. You, D. Dang, X. Qiao, G. Wang, W. Fan, R. Chen, Y. Li, X. Li and S. Liao, *Journal of Materials Chemistry A*, 2015, **3**, 23512-23519.
182. A. Kong, X. Zhu, Z. Han, Y. Yu, Y. Zhang, B. Dong and Y. Shan, *ACS Catalysis*, 2014, **4**, 1793-1800.
183. Z. Li, G. Li, L. Jiang, J. Li, G. Sun, C. Xia and F. Li, *Angewandte Chemie International Edition*, 2015, **54**, 1494-1498.
184. C. Deng, H. Zhong, L. Yao, S. Liu, Z. Xu and H. Zhang, *ChemSusChem*, 2014, **7**, 3435-3441.
185. G.-H. An, E.-H. Lee and H.-J. Ahn, *Journal of Alloys and Compounds*, 2016, **682**, 746-752.
186. Y. Yang, L. Jia, B. Hou, D. Li, J. Wang and Y. Sun, *ChemCatChem*, 2014, **6**, 319-327.
187. T. Sun, L. Xu, S. Li, W. Chai, Y. Huang, Y. Yan and J. Chen, *Applied Catalysis B: Environmental*, 2016, **193**, 1-8.
188. T. Maiyalagan, T. O. Alaje and K. Scott, *The Journal of Physical Chemistry C*, 2012, **116**, 2630-2638.
189. G.-H. Wang, Z. Cao, D. Gu, N. Pfänder, A.-C. Swertz, B. Spliethoff, H.-J. Bongard, C. Weidenthaler, W. Schmidt, R. Rinaldi and F. Schüth, *Angewandte Chemie International Edition*, 2016, **55**, 8850-8855.
190. M.-S. Wu, Z.-Z. Ceng, C.-Y. Chen and C. Wang, *Journal of Alloys and Compounds*, 2016, **688**, 342-349.
191. W. Wang, W. Jing, L. Sheng, D. Chai, Y. Kang and Z. Lei, *Applied Catalysis A: General*, 2017, **538**, 123-130.
192. L. Shen, X. Zhang, E. Uchaker, C. Yuan and G. Cao, *Advanced Energy Materials*, 2012, **2**, 691-698.
193. W. Wei, C. Yu, Q. Zhao, X. Qian, G. Li and Y. Wan, *Applied Catalysis B: Environmental*, 2014, **146**, 151-161.
194. M. Chen, X. Shen, K. Chen, Q. Wu, P. Zhang, X. Zhang and G. Diao, *Electrochimica Acta*, 2016, **195**, 94-105.
195. W. Hu, Q. Wang, S. Wu and Y. Huang, *Journal of Materials Chemistry A*, 2016, **4**, 16920-16927.
196. J. Xiao, Y. Xia, C. Hu, J. Xi and S. Wang, *Journal of Materials Chemistry A*, 2017, **5**, 11114-11123.
197. X. Tan, C. Cui, S. Wu, B. Qiu, L. Wang and J. Zhang, *Chemistry – An Asian Journal*, 2017, **12**, 36-40.
198. F. Sun, H. Cheng, J. Chen, N. Zheng, Y. Li and J. Shi, *ACS Nano*, 2016, **10**, 8289-8298.
199. K. Fu, Y. Wang, L. C. Mao, J. H. Jin, S. L. Yang and G. Li, *Electrochimica Acta*, 2016, **215**, 427-434.
200. G. P. Hao, Z. Y. Jin, Q. Sun, X. Q. Zhang, J. T. Zhang and A. H. Lu, *Energy & Environmental Science*, 2013, **6**, 3740-3747.
201. G. Sun, J. Lu, S. Ge, X. Song, J. Yu, M. Yan and J. Huang, *Anal Chim Acta*, 2013, **775**, 85-92.
202. H. B. Ren, J. Y. Zhu, Y. T. Bi, Y. W. Xu and L. Zhang, *Rsc Advances*, 2016, **6**, 89140-89147.
203. L. R. Nan, W. B. Yue and Y. Jiang, *Journal of Materials Chemistry A*, 2015, **3**, 22170-22175.
204. L. R. Nan, Z. T. Fan, W. B. Yue, Q. Dong, L. S. Zhu, L. Yang and L. Z. Fan, *Journal of Materials Chemistry A*, 2016, **4**, 8898-8904.
205. S. W. Zhou, Q. X. Xie, S. H. Wu, X. L. Huang and P. Zhao, *Ionics*, 2017, **23**, 1499-1507.
206. X. S. Zhang, J. L. Jin, P. T. Yan, J. Xu, R. J. Zhang and C. Wu, *Materials Letters*, 2015, **160**, 190-193.
207. X. Jia, C. Zhang, J. Liu, W. Lv, D. W. Wang, Y. Tao, Z. Li, X. Zheng, J. S. Yu and Q. H. Yang, *Nanoscale*, 2016, **8**, 4447-4451.
208. X. Yang, F. Y. Qu, H. Niu, Q. Wang, J. Yan and Z. J. Fan, *Electrochimica Acta*, 2015, **180**, 287-294.
209. K. Ding, Q. Liu, Y. K. Bu, Y. Y. Huang, J. Q. Lv, J. Wu, S. C. Abbas and Y. B. Wang, *RSC Advances*, 2016, **6**, 93318-93324.
210. D. den Boer, G. D. Han and T. M. Swager, *Langmuir*, 2014, **30**, 762-767.
211. L. K. Shrestha, R. G. Shrestha, Y. Yamauchi, J. P. Hill, T. Nishimura, K. Miyazawa, T. Kawai, S. Okada, K. Wakabayashi and K. Ariga, *Angew Chem Int Ed Engl*, 2015, **54**, 951-955.
212. V. I. Berezkin, V. V. Popov and M. V. Tomkovich, *Physics of the Solid State*, 2017, **59**, 620-628.
213. Z. Tan, K. Ni, G. Chen, W. Zeng, Z. Tao, M. Ikram, Q. Zhang, H. Wang, L. Sun, X. Zhu, X. Wu, H. Ji, R. S. Ruoff and Y. Zhu, *Adv Mater*, 2017, **29**, 1603414.
214. M. Benzigar, S. Joseph, H. Ilbeygi, D. H. Park, S. Sarkar, G. Chandra, S. Umapathy, S. Srinivasan, S. Talapaneni and A. Vinu, *Angew Chem Int Ed Engl*, 2018, 57, 569-573.
215. R. Chakravarti, M. L. Kantam, H. Iwai, S. S. Al-deyab, K. Ariga, D.-H. Park, J.-H. Choy, K. S. Lakhi and A. Vinu, *ChemCatChem*, 2014, **6**, 2872-2880.
216. V. Švorčík, Z. Makajová, N. Slepičková Kasálková, Z. Kolská, P. Žáková, J. Karpíšková, I. Stibor and P. Slepička, *Carbon*, 2014, **69**, 361-371.
217. P. Zakova, N. Slepickova Kasalkova, Z. Kolska, J. Leitner, J. Karpiskova, I. Stibor, P. Slepicka and V. Svorcik, *Mater Sci Eng C Mater Biol Appl*, 2016, **60**, 394-401.

218. W. Lu, J. P. Sculley, D. Yuan, R. Krishna, Z. Wei and H.-C. Zhou, *Angewandte Chemie International Edition*, 2012, **51**, 7480-7484.
219. S.-H. Chai, Z.-M. Liu, K. Huang, S. Tan and S. Dai, *Industrial & Engineering Chemistry Research*, 2016, **55**, 7355-7361.
220. L. Yu, N. Brun, K. Sakaushi, J. Eckert and M. M. Titirici, *Carbon*, 2013, **61**, 245-253.
221. M. Gholami, M. R. Talaie and S. F. Aghamiri, *J Taiwan Inst Chem E*, 2016, **59**, 205-209.
222. D. Lee, C. Zhang and H. Gao, *Macromolecular Chemistry and Physics*, 2015, **216**, 489-494.
223. V. Guillerm, L. J. Weselinski, M. Alkordi, M. I. Mohideen, Y. Belmabkhout, A. J. Cairns and M. Eddaoudi, *Chem Commun (Camb)*, 2014, **50**, 1937-1940.
224. M. Hu, J. Reboul, S. Furukawa, N. L. Torad, Q. Ji, P. Srinivasu, K. Ariga, S. Kitagawa and Y. Yamauchi, *Journal of the American Chemical Society*, 2012, **134**, 2864-2867.
225. M. R. Andalibi and H. C. Foley, *International Journal of Hydrogen Energy*, 2016, **41**, 8506-8513.
226. M. R. Andalibi, A. Qajar and H. C. Foley, *The Journal of Physical Chemistry C*, 2015, **119**, 21314-21322.
227. X. Y. Chen, C. Chen, Z. J. Zhang, D. H. Xie and J. W. Liu, *Journal of Materials Chemistry A*, 2013, **1**, 4017-4025.
228. X. Y. Chen, Y. Y. He, H. Song and Z. J. Zhang, *Carbon*, 2014, **72**, 410-420.
229. M. T. Stone and M. Kozlov, *Langmuir*, 2014, **30**, 8046-8055.
230. C. N. Nanev, E. Saridakis and N. E. Chayen, 2017, **7**, 35821.
231. S. Khurshid, E. Saridakis, L. Govada and N. E. Chayen, *Nat. Protocols*, 2014, **9**, 1621-1633.
232. M. Mahesh, K. V. Arivizhivendhan, P. Maharaja, R. Boopathy, V. Hamsavathani and G. Sekaran, *J Mol Catal B-Enzym*, 2016, **133**, 43-54.
233. F. Hippauf, D. Lunow, L. Borchardt, T. Henle and S. Kaskel, *Carbon*, 2014, **77**, 191-198.
234. F. Hippauf, D. Lunow, C. Huettner, W. Nickel, L. Borchardt, T. Henle and S. Kaskel, *Carbon*, 2015, **87**, 309-316.
235. B. Nagy, A. Toth, I. Savina, S. Mikhalovsky, L. Mikhalovska, I. Grillo, E. Geissler and K. Laszlo, *Carbon*, 2016, **106**, 142-151.
236. B. Nagy, A. Toth, I. Savina, S. Mikhalovsky, L. Mikhalovska, E. Geissler and K. Laszlo, *Carbon*, 2017, **112**, 103-110.
237. C. Z. Guo, R. Hu, W. L. Liao, Z. B. Li, L. T. Sun, D. P. Shi, Y. R. Li and C. G. Chen, *Electrochimica Acta*, 2017, **236**, 228-238.
238. S. M. Alatalo, K. P. Qiu, K. Preuss, A. Marinovic, M. Sevilla, M. Sillanpaa, X. Guo and M. M. Titirici, *Carbon*, 2016, **96**, 622-630.
239. Y. M. Lin, Y. S. Zhu, B. S. Zhang, Y. A. Kim, M. Endo and D. S. Su, *Journal of Materials Chemistry A*, 2015, **3**, 21805-21814.
240. L. Zou, Z. S. Lu, Y. H. Huang, Z. E. Long and Y. Qiao, *Journal of Power Sources*, 2017, **359**, 549-555.
241. G. B. Xu, L. W. Yang, Z. Y. Li, X. L. Wei and P. K. Chu, *Journal of Materials Chemistry A*, 2017, **5**, 2749-2758.
242. D. S. T. Martinez, J. P. V. Damasceno, L. S. Franqui, J. Bettini, I. O. Mazali and M. Strauss, *Mater Sci Eng C Mater Biol Appl*, 2017, **78**, 141-150.
243. H. Ma, C. Li, M. Zhang, J.-D. Hong and G. Shi, *J. Mater. Chem. A*, 2017, **5**, 17040-17047.
244. J. L. Figueiredo, *Journal of Materials Chemistry A*, 2013, **1**, 9351-9364.
245. J. Lai, A. Nsabimana, R. Luque and G. Xu, *Joule*, **2**, 76-93.
246. N. A. Travlou, E. Rodriguez-Castellon and T. J. Bandosz, *Carbon*, 2016, **100**, 64-73.
247. N. A. Travlou and T. J. Bandosz, *Carbon*, 2017, **121**, 114-126.
248. N. A. Travlou and T. J. Bandosz, *Adsorption-Journal of the International Adsorption Society*, 2017, **23**, 271-280.
249. L. Cui, J. Wu and H. Ju, *ACS Applied Materials & Interfaces*, 2014, **6**, 16210-16216.
250. Y. Li, M. F. Zhang, X. P. Zhang, G. C. Xie, Z. Q. Su and G. Wei, *Nanomaterials*, 2015, **5**, 1891-1905.
251. L. Jia, G. Lawrence, V. V. Balasubramanian, G. Choi, J.-H. Choy, A. M. Abdullah, A. Elzatahry, K. Ariga and A. Vinu, *Chemistry – A European Journal*, 2015, **21**, 697-703.
252. P. Salazar, V. Rico and A. R. González-Elipe, *Journal of The Electrochemical Society*, 2016, **163**, B704-B709.
253. L. Donero, N. Bouts, A. A. El Mel, B. Le Borgne, E. Gautron, L. Le Brizoual, F. Le Bihan and P. Y. Tessier, *Thin Solid Films*, 2017, **630**, 59-65.
254. H. L. Poh and M. Pumera, *Chemistry – An Asian Journal*, 2012, **7**, 412-416.
255. H. L. Poh, A. Bonanni and M. Pumera, *RSC Advances*, 2012, **2**, 1021-1024.
256. E. Moazzen, H. Ebrahimzadeh, M. M. Amini and O. Sadeghi, *J. Sol-Gel Sci. Technol.*, 2013, **66**, 345-351.
257. N. L. Torad, Y. Li, S. Ishihara, K. Ariga, Y. Kamachi, H.-Y. Lian, H. Hamoudi, Y. Sakka, W. Chaikittisilp, K. C. W. Wu and Y. Yamauchi, *Chem. Lett.*, 2014, **43**, 717-719.
258. Y. Zhang, E. Che, M. Zhang, B. Sun, J. Gao, J. Han and Y. Song, *Int. J. Pharm. (Amsterdam, Neth.)*, 2014, **473**, 375-383.
259. Q.-L. Zhu, N. Tsumori and Q. Xu, *Chem. Sci.*, 2014, **5**, 195-199.
260. C. Feng, Y. Hao, L. Zhang, N. Shang, S. Gao, Z. Wang and C. Wang, *RSC Adv.*, 2015, **5**, 39878-39883.
261. L. F. Velasco, A. Gomis-Berenguer, J. C. Lima and C. O. Ania, *ChemCatChem*, 2015, **7**, 3012-3019.
262. L. Hao, C. Wang, Q. Wu, Z. Li, X. Zang and Z. Wang, *Anal Chem*, 2014, **86**, 12199-12205.
263. W. Wang and D. Yuan, *Sci Rep*, 2014, **4**, 5711.
264. N. Farzin Nejad, E. Shams, M. K. Amini and J. C. Bennett, *Fuel Processing Technology*, 2013, **106**, 376-384.
265. A. Koolivand, A. Badiei, P. Arab and G. M. Ziarani, *Journal of the Iranian Chemical Society*, 2016, **13**, 1315-1324.
266. X. Ma, M. Cao and C. Hu, *RSC Advances*, 2013, **3**, 10396-10402.
267. L. L. Perreault, S. Giret, M. Gagnon, J. Florek, D. Lariviere and F. Kleitz, *ACS Appl Mater Interfaces*, 2017, **9**, 12003-12012.
268. K. Vasanth Kumar and F. Rodríguez-Reinoso, *RSC Advances*, 2012, **2**, 9671-9678.
269. S. Chu, Y. Zhong, R. Cai, Z. Zhang, S. Wei and Z. Shao, *Small*, 2016, **12**, 6724-6734.
270. Y. Qu, Z. Zhang, X. Zhang, G. Ren, Y. Lai, Y. Liu and J. Li, *Carbon*, 2015, **84**, 399-408.
271. Y. Liu, X. Zhao, G. S. Chauhan and J.-H. Ahn, *Applied Surface Science*, 2016, **380**, 151-158.
272. S. F. Wang, Y. Z. Wu, N. Zhang, G. W. He, Q. P. Xin, X. Y. Wu, H. Wu, X. Z. Cao, M. D. Guiver and Z. Y. Jiang, *Energy & Environmental Science*, 2016, **9**, 3107-3112.
273. S. Chu, Y. Cui and N. Liu, *Nat Mater*, 2016, **16**, 16-22.

274. K. S. Lakhi, D. H. Park, G. Singh, S. N. Talapaneni, U. Ravon, K. Al-Bahily and A. Vinu, *Journal of Materials Chemistry A*, 2017, **5**, 16220-16230.
275. G. Singh, I. Y. Kim, K. S. Lakhi, P. Srivastava, R. Naidu and A. Vinu, *Carbon*, 2017, **116**, 448-455.
276. G. Singh, K. S. Lakhi, I. Y. Kim, S. Kim, P. Srivastava, R. Naidu and A. Vinu, *ACS Appl Mater Interfaces*, 2017, **9**, 29782-29793.
277. J. Zhou, W. Su, Y. Sun, S. G. Deng and X. J. Wang, *J Chem Eng Data*, 2016, **61**, 1348-1352.
278. J. W. To, J. He, J. Mei, R. Haghpanah, Z. Chen, T. Kurosawa, S. Chen, W. G. Bae, L. Pan, J. B. Tok, J. Wilcox and Z. Bao, *J Am Chem Soc*, 2016, **138**, 1001-1009.
279. C. H. Choi, S. H. Park and S. I. Woo, *ACS Nano*, 2012, **6**, 7084-7091.
280. Y.-N. Yu, M.-Q. Wang and S.-J. Bao, *Journal of Solid State Electrochemistry*, 2017, **21**, 103-110.
281. E. Zhang, M. Wu, Q. Tang, Q. Gong, S. Sun, J. Qiao and L. Zhang, *RSC Advances*, 2017, **7**, 669-677.
282. F. Jing, M. Chen, Y. Tang, Z. Xu, T. Huang, Y. Su and D. Wu, *Journal of Colloid and Interface Science*, 2017, **492**, 8-14.
283. J.-C. Li, S.-Y. Zhao, P.-X. Hou, R.-P. Fang, C. Liu, J. Liang, J. Luan, X.-Y. Shan and H.-M. Cheng, *Nanoscale*, 2015, **7**, 19201-19206.
284. C. Zhang, B. Wang, X. Shen, J. Liu, X. Kong, S. S. C. Chuang, D. Yang, A. Dong and Z. Peng, *Nano Energy*, 2016, **30**, 503-510.
285. D.-S. Yang, D. Bhattacharjya, M. Y. Song and J.-S. Yu, *Carbon*, 2014, **67**, 736-743.
286. J. Xiao, Y. Xu, Y. Xia, J. Xi and S. Wang, *Nano Energy*, 2016, **24**, 121-129.
287. J. Tang, T. Wang, X. Pan, X. Sun, X. Fan, Y. Guo, H. Xue and J. He, *The Journal of Physical Chemistry C*, 2013, **117**, 16896-16906.
288. T. Zhou, Y. Zhou, R. Ma, Q. Liu, Y. Zhu and J. Wang, *Journal of Materials Chemistry A*, 2017, **5**, 12243-12251.
289. H. Wang, W. Wang, M. Gui, M. Asif, Z. Wang, Y. Yu, J. Xiao and H. Liu, *ACS Applied Materials & Interfaces*, 2017, **9**, 335-344.
290. H. Tan, Y. Li, X. Jiang, J. Tang, Z. Wang, H. Qian, P. Mei, V. Malgras, Y. Bando and Y. Yamauchi, *Nano Energy*, 2017, **36**, 286-294.
291. L. Liu, Z. Niu and J. Chen, *Chemical Society Reviews*, 2016, **45**, 4340-4363.
292. A. Borenstein, O. Hanna, R. Attias, S. Luski, T. Brousse and D. Aurbach, *Journal of Materials Chemistry A*, 2017, **5**, 12653-12672.
293. T. Chen and L. Dai, *Materials Today*, 2013, **16**, 272-280.
294. H. Itoi, H. Nishihara and T. Kyotani, *Langmuir*, 2016, **32**, 11997-12004.
295. A. Berenguer-Murcia, R. R. Ruiz-Rosas, J. Garcia-Aguilar, K. Nueangnoraj, H. Nishihara, E. Morallon, T. Kyotani and D. Cazorla-Amoros, *Physical Chemistry Chemical Physics*, 2013, **15**, 10331-10334.
296. K. Nueangnoraj, H. Nishihara, T. Ishii, N. Yamamoto, H. Itoi, R. Berenguer, R. Ruiz-Rosas, D. Cazorla-Amorós, E. Morallón, M. Ito and T. Kyotani, *Energy Storage Materials*, 2015, **1**, 35-41.
297. J. Linnemann, L. Taudien, M. Klose and L. Giebeler, *Journal of Materials Chemistry A*, 2017, **5**, 18420-18428.
298. J. W. Lee, A. S. Hall, J.-D. Kim and T. E. Mallouk, *Chemistry of Materials*, 2012, **24**, 1158-1164.
299. X. Zhang, J. Luo, P. Tang, X. Ye, X. Peng, H. Tang, S.-G. Sun and J. Fransaer, *Nano Energy*, 2017, **31**, 311-321.
300. J. Zhou, W. Li, Z. Zhang, X. Wu, W. Xing and S. Zhuo, *Electrochimica Acta*, 2013, **89**, 763-770.
301. D. Zhang, L. Zheng, Y. Ma, L. Lei, Q. Li, Y. Li, H. Luo, H. Feng and Y. Hao, *ACS Applied Materials & Interfaces*, 2014, **6**, 2657-2665.
302. R. J. Wang, Y. Xu, T. Zhang and Y. Jiang, *Anal Methods-Uk*, 2015, **7**, 1701-1706.
303. N. Duan, S. J. Wu, S. L. Dai, T. T. Miao, J. Chen and Z. P. Wang, *Microchim Acta*, 2015, **182**, 917-923.
304. J. Shi, C. Chan, Y. Pang, W. Ye, F. Tian, J. Lyu, Y. Zhang and M. Yang, *Biosens Bioelectron*, 2015, **67**, 595-600.

TOC

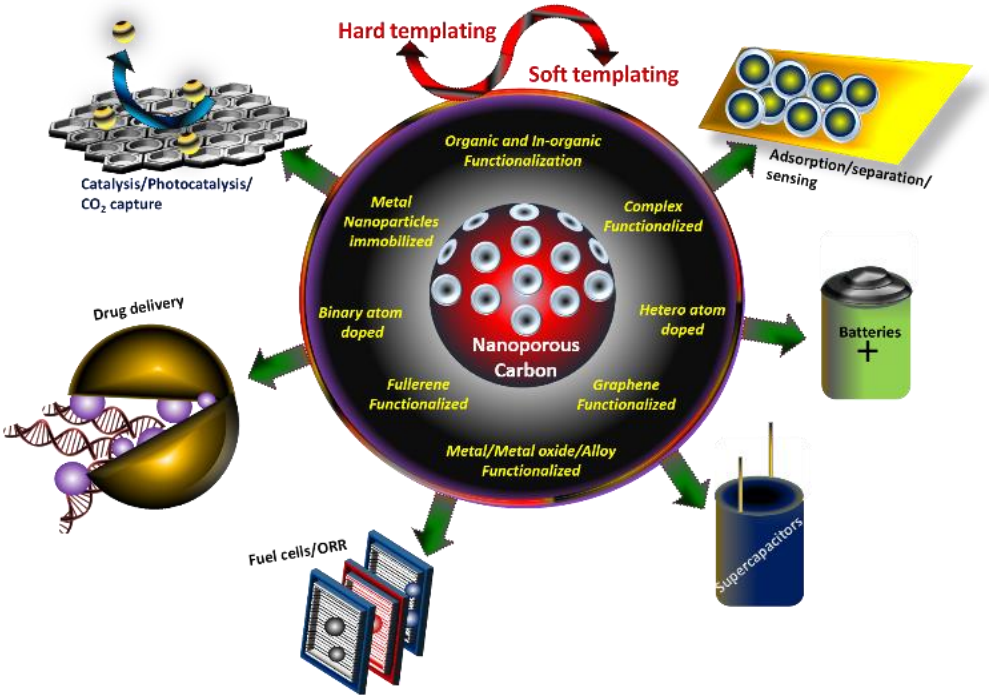

This review provides the recent progress and advances on the design, synthesis and high throughput applications of functionalized micro and mesoporous carbon materials.